공학박사학위논문

확률 통계적 기법을 이용한 다분야 통합 최적설계 공간의 탐색 및 재설정에 관한 연구

Study on Design Space Exploration and Rearrangement Using Stochastic and Statistic Approach for the Multidisciplinary Design Optimization

2012년 8월

서울대학교 대학원

기계항공공학부

전 용 희

확률 통계적 기법을 이용한 다분야 통합 최적설계 공간의 탐색 및 재설정에 관한 연구

Study on Design Space Exploration and Rearrangement Using Stochastic and Statistic Approach for the Multidisciplinary Design Optimization

지도교수 이 동 호

이 논문을 공학박사 학위논문으로 제출함

2012 년 6 월

서울대학교 대학원

기계항공공학부

전 용 희

전용희의 공학박사 학위논문을 인준함

2012 년 8 월

위 원 장 : ______________________

부위원장 : ______________________

위 원 : ______________________

위 원 : ______________________

위 원 : ______________________

To my wife Yeon-Hee

and to my son Jun-Hoo

with all my heart

Abstract

Study on Design Space Exploration and Rearrangement Using Stochastic and Statistic Approach for the Multidisciplinary Design Optimization

Yong-Hee Jeon
School of Mechanical and Aerospace Engineering
Seoul national University

In this study, a stochastic and statistic approach for the systematic design space exploration and rearrangement is proposed. To efficiently investigate the feasibility of the design space, surrogate model and Monte Carlo simulation have been used. With these methods, probability density function, cumulative distribution function and reliability of the design space are calculated to identify the probability of design success. Then, the design space is moved and rearranged into the higher feasible region using Chebyshev inequality and reliability index. First of all, a number of test cases composed of algebraic functions were carried out to investigate the validity of the suggested method. For two exact functions, multidisciplinary feasible and collaborative optimization formulations were performed to verify the utility of proposed methods. As a result, converged design space included the feasible region located outside of the initial design space. Based on these results, the proposed method was applied to the multidisciplinary design optimization of the aircraft wing which also considered collaborative optimization with three subsystems (aerodynamics, structure, and performance). And then, design optimizations were performed for the initial and converged design space separately. Consequently, the feasibility and optimization result of the converged design space were improved in comparison with those of the initial design space. In conclusion, it is verified that the design space exploration and rearrangement method proposed in this study has the capability of searching for the feasible region which is excluded in the initial design space, and can rearrange the design space into the higher feasible design space automatically.

Key Words : Aerodynamic-structural coupled optimization; Aircraft wing; Chebyshev inequality; Collaborative optimization; Design space exploration; Design space rearrangement; Monte-carlo simulation; Reliability index

Student Number : 2001-30442

Table of Contents

Nomenclatures

English Symbols

A	Jacobian matrix
AR	aspect ratio of a wing
C	root airfoil chord length or elastic constitutive matrix
c	speed of sound or vector of regression coefficients
c_0, c_i, c_{ij}	regression coefficients
c_root	maximum camber of a wing root airfoil
c_tip	maximum camber of a wing tip airfoil
E, F, G	inviscid flux vectors
e	total specific energy
F	cumulative distribution function or objective function
f	response surface model or probability density function
G	the c.d.f. of a standard normal distribution
g_i	i-th constraint function
J	transformed Jacobian
K	element stiffness matrix
M	Mach number
n_t	number of regression coefficients
n_c	number of candidate data points
n_s	number of sample data points
n_v	number of design variables
p	pressure or probability

Q	conservative variable vector
q	heat flux
R	residual vector
Re	Reynolds number
S	mesh area (volume) or wing area
t	time
tr	taper ratio of a wing
t_root	thickness ratio of a wing root airfoil
t_tip	thickness ratio of a wing tip airfoil
(U,V,W)	contravariant velocities
(u,v,w)	velocities
w	weighting factor
X	vector of design variables or matrix of data point set or random variable
$x_i^{(p)}, x_j^{(p)}$	design variables
y	observed response
(x,y,z)	Cartesian coordinates

Greek Symbols

α	angle of attack
β	implicit residual smoothing coefficient
γ	specific heat ratio
ε	strain or error
η	mean of normal distribution

θ	linear twist angle of a wing
λ	spectral radius
μ	mean or expected value
μ_x	temporary mean of the feasible region
ρ	density
σ	standard deviation
(ξ, η, ζ)	generalized curvilinear coordinates
Λ	eigenvalue of Jacobian matrix or sweep angle
Ω	probability space

Mathematical Symbol

∇	gradient
Δ	increment
$\nabla\Delta$	second difference operator

Subscript

∞	freestream values

Superscript

baseline	baseline value
n	n^{th} time step
T	transpose of matrix

List of Figures

List of Tables

Chapter 1. Introduction

1.1 Motivations

In the last few decades, there are remarkable advancement of computational capability and numerical analysis techniques such as computational fluid dynamics (CFD), computational structural mechanics (CSM) and numerical optimization methodology. It makes drastic change of the traditional design process that depends on designer's experience and insight. In traditional design process, designer must make a lot of decisions and corrections to obtain appropriate results on the sequential and repetitive 'trial and error' procedure as in Fig. 1.1. By the reason of above demerit, numerical design optimization technique based on mathematical theory has quickly replaced traditional design process. Numerical optimization technique offers a logical approach to design automation, and enables engineers to optimize large and complex system. To design more practical and complex system that includes a number of mutually interact disciplines, multidisciplinary analysis and design optimization must be considered. Multidisciplinary design optimization (MDO) can be described as "*a methodology for the design of systems where the interaction between several disciplines must be considered, and where the designer is free to significantly affect the system performance on more than one discipline*."[1]

For the complex engineering system, life-cycle of the system can be defined by a number of discrete phases from conceptual design to the retirement. While each design phase has an individual and considerable effect on the design product, early design phase has the most leverage. It is clear that the rapid accumulation of the knowledge and information about the given design problem can reduce the design cost and can keep high level of the design degree of freedom (DOF) from the outset to manufacture phase as shown in Fig. 1.2. In a word, the decisions of early design phase have great influence on the direction of the whole design process, performance and efficiency of the design results [2, 3]. Therefore, the more careful consideration must be given on the early phase of complex system design problem. However, there exist only a few information and knowledge about the given design problem at the initial design phase. Even though some information is gathered with various methods, it is still insufficient to grasp the characteristics of the design problem. Therefore, wide scope of the design problem, which includes various objectives, constraints, and design variables, should be carefully considered and explored to understand the design problem. For the lack of information and knowledge about the given design problem, the designer defines initial design space based on one's own intuition or experience, and searches for a feasible design solution within the initially defined design space in most design problems [4]. However, this design space has the infeasible region together with a few pieces of the feasible region in the majority of cases. As the number of design variables and constraints increases, the feasible region tends to decrease and it becomes more difficult to define the valid design space that is physically reasonable and guarantee the success of the optimization and the existence of the global optimum. Especially in a complicated design problem like multidisciplinary design optimization or multilevel design optimization, this difficulty may be more severe.

In this study, an aircraft wing optimization coupled with aerodynamics, structure, and performance is carried out to validate proposed method. Its complexity is higher than that of the design optimization problem based on single discipline analysis. If some information and knowledge for these three disciplines are insufficient, it is difficult to define the reasonable design space in the initial design stage. Hence, efficient and logical design space exploration and arrangement method are greatly required to carry out the multidisciplinary design optimization of aircraft wing.

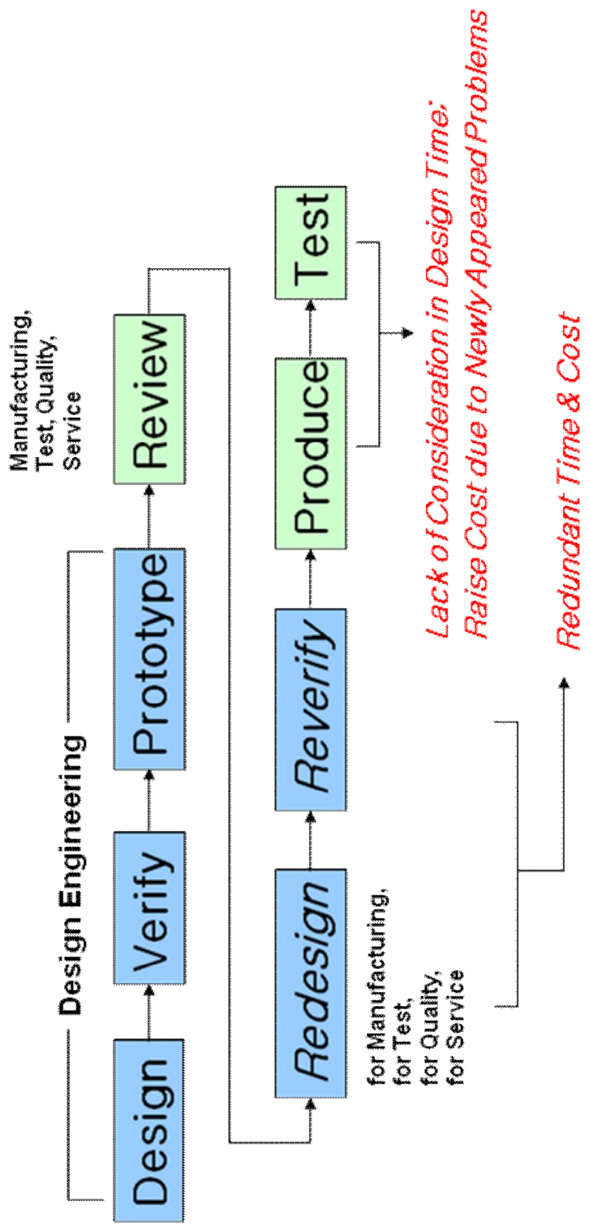

Fig. 1.1 Sequential design process

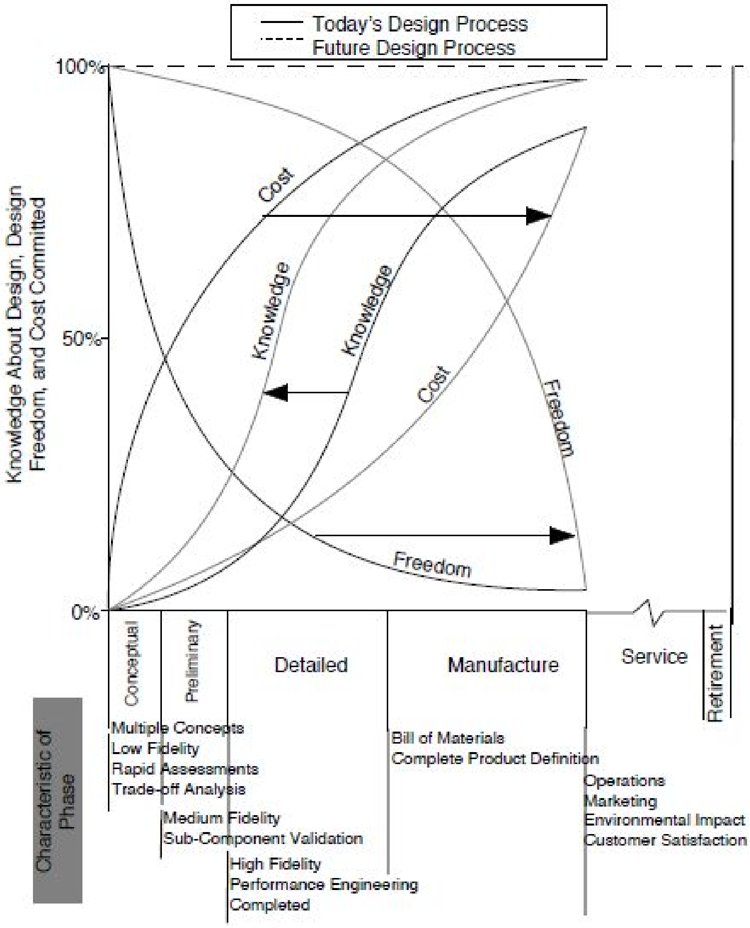

Fig. 1.2 Life-cycle design stages [3]

1.2 Literature Survey

Over the last several decades, various design methods such as the inverse design method and the direct numerical optimization method have been applied to diverse design problems for the airfoil and aircraft wing.

Among those established methods, the inverse design method has been widely used as an efficient design method. Inverse design on the aerodynamic configurations of the transonic airfoil and wing were also implemented based on various governing equations and algorithms [5-12]. However, distributions of the target pressure must be described by designer before the inverse design starts. It is very difficult for each designer, and also has great influence on the design results. To specify the optimal target distribution automatically, some numerical optimization methods were adopted [13-17]. However, results of the inverse design are thoroughly limited by its target pressure distribution and it is very difficult to find and to guarantee the global optimum. Then, direct numerical optimization methods based on mathematical theory have quickly replaced inverse design methods as aerodynamic shape optimization method. Direct numerical optimization methods couple the numerical analysis codes and a numerical optimization algorithm to minimize or maximize the objective function and satisfy the geometric and performance constraints. Among numerous direct numerical optimization methods, the gradient-based optimization algorithms have been widely utilized for conventional direct numerical optimization [18-20]. For the first time, this type of design procedure was introduced by Hicks and Henne to the design of three-dimensional configuration [18]. Jameson et al. and Reuther et al. applied direct optimization method with an adjoint variable method for sensitivity analysis to an aerodynamic configuration of the airplanes [19, 20]. Although the gradient-based optimization algorithm is one of the most efficient optimization algorithms, it cannot ensure the global optimum. Hence, global optimum search algorithms such as genetic algorithm (GA) have been used for the direct numerical optimization [21-26]. In recent years, multidisciplinary analysis and design optimization to the complex three-dimensional wing and aircraft configuration have been carried out intensely [27-39]. It was successfully applied to various applications like aeroelastic analyses and optimization of transonic transport wing, MDO of a supersonic fighter wing, high speed civil transport (HSCT) configurations, and so on.

For the reason of computational efficiency and design cost, various mathematical modeling of systems, approximation concepts, and decomposition techniques have been developed for MDO problems. According to the decomposition method, MDO formulation can be divided into single-level and multi-level approaches. In single-level approach, only one design optimizer exists, and each discipline just takes charge of analysis. It can be categorized as three types roughly: multidisciplinary feasible (MDF), individual disciplinary feasible (IDF), and all-at-once (AAO) approach [40]. In multi-level approach, a number of optimizers also exist to decide the design variables on each subspace and system level. Each subspace optimizer decides and controls its design variables which are assigned by the system optimizer, and then the system optimizer coordinates whole subspace design variables and results to merge into one: concurrent subspace optimization (CSSO), collaborative optimization (CO) and bi-level integrated system synthesis (BLISS) [41-43].

In addition to those studies, a number of approaches have been researched to efficiently explore the design space and to find the global optimum using stochastic criteria and approximation models [44-55]. DIRECT (*di*viding *rec*tangles) method which based on Lipschitz optimization method for finding the global optimum of a multivariate function subject to simple bounds was proposed by Jones et. al. [44] This method was modified to consider parallel load balancing and to reduce the computational time of the design space exploration by Baker et. al. [45], and it was applied to the multidisciplinary design of a high speed civil transport (HSCT). Sevant et. al. used sequential response surfaces to optimize the flying wing [46]. With this method, the design space was sequentially approximated and modified to find the global optimum. With approximation models and merit functions, Chung et. al. [47] exploited the aerodynamic optimization of the small business jet, which includes the noisy design space. Using proposed method can avoid the local optima and predict global optima in fixed design space. Sasena et. al. proposed efficient global optimization (EGO) for constrained global optimization [48]. Kriging model and variance-reducing criteria were used to reduce the root mean square error of the resulting meta-model, and DIRECT algorithm was adopted to find the optimum of the infill sampling criteria. Using these algorithms, the constrained global optimum on a highly nonlinear design surface can be found efficiently and rapid design space exploration can be done. In addition, a large number of probabilistic design approach have been researched to efficiently explore the design space and to produce robust optimum using stochastic criteria and approximation models [49-55]. However, the design space exploration and rearrangement results of above methods are limited within the initial design space in most cases. Because it is hard for them to make the feasible region laying outside of the initial design space included into the rearranged design space, it is impossible to search for better solutions which exist in the outside of the initial design space. Thus, to improve the feasibility, cautious and detailed exploration of the design space must be carried out by including the feasible region laying the outside of the initial design space. For the sake of this purpose, Jeon *et al.*[56-58] presented rearranging method of the design space using Monte Carlo Simulation (MCS) and Chebyshev inequality, and this method has a capability of searching for the outside of the initial design space. However, they have some limits to adopt various types of MDO problem. Hence, systematic and automatic design space rearrangement method is still required.

1.3 Dissertation Objectives and Outline

For the complex system design, especially in case of MDO, it is more difficult to define appropriate design space at the initial design phase. However in the majority of cases, established design methods cannot define the adequate design space if there are not enough knowledge and information about the given design problem. To overcome above drawback, efficient design space exploration method is highly required to rapidly grasp the characteristic of given problem. Moreover, logical and systematic design space rearrangement method is also required to define proper design space automatically.

Therefore this study will propose the systematic design space exploration and rearrangement method using statistic and stochastic approaches. This method is applied to the design optimization problem of the exact function with two variables, and from this problem, it will be confirmed that this method has a capability of including the feasible region laying the outside of the initial design space. In addition, in spite of no feasible region in the initial design space, it will be presented that the design space can have a feasible region from rearrangement of the design space. Finally, the proposed method will be applied to the MDO of the aircraft wing, and its utility for the practical MDO problem will be examined.

Chapter 2. Numerical Analysis

To verify the utility of proposed design space exploration and rearrangement method on diverse design cases, supersonic fighter and transonic transport wing is considered in this study. Therefore, two types of aeroelastic analysis codes have been used according to application case.

2.1 High-Fidelity Aeroelastic Analysis

2.1.1 Aerodynamic Analysis

2.1.1.1 Governing Equation: Three Dimensional Euler Equation

The design range of supersonic fighter wing interested in this study is from the transonic speed to the supersonic speed, therefore the aerodynamic analysis code should be robust and accurate to take account of this wide range. A high fidelity CFD algorithm modeling the three-dimensional Euler equation is used to calculate the transonic and supersonic aerodynamic properties of the supersonic fighter wing.

The three-dimensional Euler Equations can be written in the non-dimensionalized, conservative form as follows:

$$\frac{\partial Q}{\partial t}+\frac{\partial E}{\partial x}+\frac{\partial F}{\partial y}+\frac{\partial G}{\partial Z}=0 \tag{2.1}$$

$$Q = \begin{pmatrix} \rho \\ \rho u \\ \rho v \\ \rho w \\ \rho e \end{pmatrix}, E = \begin{pmatrix} \rho u \\ \rho u^2 + p \\ \rho uv \\ \rho uw \\ (\rho e + p)u \end{pmatrix}, F = \begin{pmatrix} \rho v \\ \rho uv \\ \rho v^2 + p \\ \rho vw \\ (\rho e + p)v \end{pmatrix}, G = \begin{pmatrix} \rho w \\ \rho uw \\ \rho vw \\ \rho w^2 + p \\ (\rho e + p)w \end{pmatrix} \tag{2.2}$$

Where, Q is the conservative variable vector and E, F, G are flux vectors. ρ is the density and u, v, w are the velocity components in the direction of x, y, z-axis. e is the total specific energy and the pressure, p is defined as:

$$p = \rho(\gamma - 1)\left\{e - \frac{1}{2}\left(u^2 + v^2 + w^2\right)\right\} \tag{2.3}$$

Where, γ is the specific heat ratio. All geometrical dimensions are normalized with the root chord length C; the density is normalized with the free stream value ρ_∞; the velocity components are normalized with the free stream speed of sound, c_∞; and the pressure p is normalized with the free stream value $\rho_\infty c_\infty{}^2$; the total specific energy, e is normalized by $c_\infty{}^2$; the time, t is normalized by C / c_∞.

Eq. (2.1) can be transformed from Cartesian coordinates (x, y, z) into curvilinear coordinates (ξ, η, ζ) as follows:

$$\tau = t, \quad \xi = \xi(x, y, z), \quad \eta = \eta(x, y, z), \quad \zeta = \zeta(x, y, z) \tag{2.4}$$

The Jacobian of transformation and metrics are expressed as follows:

$$
\begin{aligned}
&J^{-1} = x_\xi y_\eta z_\zeta + x_\eta y_\zeta z_\xi + x_\zeta y_\xi z_\eta - x_\xi y_\zeta z_\eta - x_\eta y_\xi z_\zeta - x_\zeta y_\eta z_\xi = Volume \\
&\xi_x = J\left(y_\eta z_\zeta - y_\zeta z_\eta\right), \quad \xi_y = J\left(z_\eta x_\zeta - z_\zeta x_\eta\right), \quad \xi_z = J\left(x_\eta y_\zeta - x_\zeta y_\eta\right) \\
&\eta_x = J\left(y_\zeta z_\xi - y_\xi z_\zeta\right), \quad \eta_y = J\left(z_\zeta x_\xi - z_\xi x_\zeta\right), \quad \eta_z = J\left(x_\zeta y_\xi - x_\xi y_\zeta\right) \\
&\zeta_x = J\left(y_\xi z_\eta - y_\eta z_\xi\right), \quad \zeta_y = J\left(z_\xi x_\eta - z_\eta x_\xi\right), \quad \zeta_z = J\left(x_\xi y_\eta - x_\eta y_\xi\right)
\end{aligned}
\tag{2.5}
$$

The resulting transformed equation is presented as follows:

$$
\frac{\partial \hat{Q}}{\partial \tau} + \frac{\partial \hat{E}}{\partial \xi} + \frac{\partial \hat{F}}{\partial \eta} + \frac{\partial \hat{G}}{\partial \zeta} = 0 \tag{2.6}
$$

$$
\hat{E} = \frac{1}{J}\begin{pmatrix} \rho U \\ \rho u U + \xi_x p \\ \rho v U + \xi_y p \\ \rho w U + \xi_z p \\ (\rho e + p)U \end{pmatrix}, \quad \hat{F} = \frac{1}{J}\begin{pmatrix} \rho V \\ \rho u V + \eta_x p \\ \rho v V + \eta_y p \\ \rho w V + \eta_z p \\ (\rho e + p)V \end{pmatrix}, \quad \hat{G} = \frac{1}{J}\begin{pmatrix} \rho W \\ \rho u W + \zeta_x p \\ \rho v W + \zeta_y p \\ \rho w W + \zeta_z p \\ (\rho e + p)W \end{pmatrix} \tag{2.7}
$$

U, *V* and *W* represent the contravariant velocities.

$$
\begin{aligned}
U &= \xi_x u + \xi_y v + \xi_z w \\
V &= \eta_x u + \eta_y v + \eta_z w \\
W &= \zeta_x u + \zeta_y v + \zeta_z w
\end{aligned}
\tag{2.8}
$$

2.1.1.2 Spatial Discretization

Finite volume method (FVM) is relatively independent on the quality of grid system and stable at the discontinuity of the flow. Therefore, FVM is applied to discretize the computational domain with structured grid system in this study. If the divergence theorem is applied to the integral form of the Eq. (2.1), the resulting equation is:

$$\frac{1}{J}\frac{\partial}{\partial t}\iiint_{cv} QdS + \iint_{A}\left[\frac{\partial \hat{E}}{\partial \xi}\vec{i} + \frac{\partial \hat{F}}{\partial \eta}\vec{j} + \frac{\partial \hat{G}}{\partial \zeta}\vec{k}\right]\cdot \vec{n}dA = 0 \tag{2.9}$$

Applying this relation to a single cell element, and using the mid-point rule, it can be discretized as:

$$\frac{1}{J}\frac{\partial \hat{Q}_{i,j,k}}{\partial \tau} + \hat{E}_{i+\frac{1}{2},j,k} - \hat{E}_{i-\frac{1}{2},j,k} + \hat{F}_{i,j+\frac{1}{2},k} - \hat{F}_{i,j-\frac{1}{2},k} + \hat{G}_{i,j,k+\frac{1}{2}} - \hat{G}_{i,j,k-\frac{1}{2}} = 0 \tag{2.10}$$

In Eq. (2.10), $\hat{Q}$ must be interpreted as a cell-averaged value. Setting $\Delta\xi = \Delta\eta = \Delta\zeta = 1$, then J^{-1} can be interpreted as a cell volume. Other terms are defined in Eq. (2.7). This relation is called semi-discrete, since the time variable remains continuous.

To capture stationary discontinuities without oscillations, an upwind method is used. In this study, Van Leer's flux vector splitting was employed to calculate the Jacobian matrix, and Roe's flux difference splitting to solve the flux vector.

The flux vector splitting methods of Van Leer [59, 60] is based on a directional discretization of the flux derivatives. The flux vector is split as:

$$E = E^{+} + E^{-} \tag{2.11}$$

where, E^{+} has positive eigenvalue and E^{-} has negative eigenvalue. Van Leer's flux vector can be written for the generalized coordinate (ξ, η) as in the Eq. (2.12)

$$\overline{M} \geq 1, \quad \begin{cases} \hat{E}^{+} = \hat{E} \\ \hat{E}^{-} = 0 \end{cases}$$

$$\overline{M} \leq -1, \quad \begin{cases} \hat{E}^{+} = 0 \\ \hat{E}^{-} = \hat{E} \end{cases}$$

$$\left|\overline{M}\right| < 1, \quad \hat{E}^{\pm} = \begin{bmatrix} f_1^{\pm} \\ f_1^{\pm}\left[n_x \dfrac{(-\bar{u} \pm 2c)}{\gamma} + u\right] \\ f_1^{\pm}\left[n_y \dfrac{(-\bar{u} \pm 2c)}{\gamma} + v\right] \\ f_1^{\pm}\left[\dfrac{1}{(\gamma^2 - 1)}\{(\gamma - 1)\bar{u}(-\bar{u} \pm 2c) + 2c^2\} + \dfrac{1}{2}q^2\right] \end{bmatrix} \tag{2.12}$$

$$where, \quad f_1^{\pm} = \pm\frac{c\rho}{4}[\overline{M} \pm 1]^2 \frac{|\nabla\xi|}{J}, \quad \bar{u} = n_x u + n_y v, \quad \overline{M} = \frac{\bar{u}}{c} \tag{2.13}$$

n_x, n_y is the x, y components of the normal vector of ξ-constant cell boundary, respectively and given as $n_x = \xi_x / |\nabla\xi|$ and $n_y = \xi_y / |\nabla\xi|$.

Roe's approximate Riemann solver [61] is adopted to calculate the numerical flux at the cell interface because it is simple to use and shows good shock resolution in one-dimensional cases. Roe's scheme can be clarified by considering the following linearized equation.

$$\frac{\partial Q}{\partial t} + A(Q_L, Q_R)\frac{\partial Q}{\partial x} = 0 \tag{2.14}$$

The numerical flux at the cell interface is:

$$\hat{E}_{i+\frac{1}{2}} = \frac{1}{2}[\hat{E}(Q^R_{i+\frac{1}{2}}) + \hat{E}(Q^L_{i+\frac{1}{2}}) - |A_{i+\frac{1}{2}}|(Q^R_{i+\frac{1}{2}} - Q^L_{i+\frac{1}{2}})] \tag{2.15}$$

Where, A is a Jacobian matrix based on Roe's averaging which leads to as follows:

$$\begin{aligned}
\tilde{\rho} &= \sqrt{\rho_R \rho_L} \\
\tilde{u} &= \frac{u_R\sqrt{\rho_R} + u_L\sqrt{\rho_L}}{\sqrt{\rho_R} + \sqrt{\rho_L}} \\
\tilde{v} &= \frac{v_R\sqrt{\rho_R} + v_L\sqrt{\rho_L}}{\sqrt{\rho_R} + \sqrt{\rho_L}} \\
\tilde{h} &= \frac{h_R\sqrt{\rho_R} + h_L\sqrt{\rho_L}}{\sqrt{\rho_R} + \sqrt{\rho_L}}
\end{aligned} \tag{2.16}$$

The flux difference can be obtained in the following manner

$$|A|(Q^R - Q^L) = |\Delta E|_1 + |\Delta E|_2 + |\Delta E|_3 + |\Delta E|_4 \tag{2.17}$$

$$|\Delta E|_1 = |\Lambda_1|(\Delta\rho - \frac{\Delta p}{\bar{c}^2})\begin{bmatrix} 1 \\ u \\ v \\ \frac{q^2}{2} \end{bmatrix} , \quad |\Delta E|_2 = |\Lambda_2|\rho\begin{bmatrix} 0 \\ \Delta u - \eta_x \Delta u \\ \Delta v - \eta_x \Delta u \\ \Delta(\frac{q^2}{2}) - u\Delta u \end{bmatrix}$$

$$|\Delta E|_{3,4} = |\Lambda_{3,4}|(\frac{\Delta p \pm \overline{\rho c}\Delta U}{2\bar{c}^2})\begin{bmatrix} 1 \\ u \pm \eta_x c \\ v \pm \eta_x c \\ H + cu \end{bmatrix} \tag{2.18}$$

where Λ is the eigenvalues of Jacobian matrix based on Roe's averaging, and is given in the Eq. (2.19). ε in Eq. (2.20) is a small positive number.

$$\begin{aligned} \Lambda_1 &= \tilde{u}\frac{|\nabla\xi|}{J} \\ \Lambda_2 &= \Lambda_1 \\ \Lambda_3 &= (\tilde{u} + \tilde{c})\frac{|\nabla\xi|}{J} \\ \Lambda_4 &= (\tilde{u} - \tilde{c})\frac{|\nabla\xi|}{J} \end{aligned} \tag{2.19}$$

$$|\Lambda| = \begin{cases} |\Lambda| & |\Lambda| \geq \varepsilon \\ \dfrac{\Lambda^2 + \varepsilon^2}{2\varepsilon} & |\Lambda| < \varepsilon \end{cases} \tag{2.20}$$

To increase the order of spatial accuracy, Q_R and Q_L are computed by monotone upstream-centered scheme for conservation law (MUSCL) scheme. Primitive variables are used to calculate the slope, since using the conservative variables gives slightly dissipative results for some problems [62]. The MUSCL scheme is used with Van Albada limiter as follows [63]:

$$
\begin{aligned}
&Q^{-}_{i+1/2} = Q_i + 0.25\phi s\,[(1-\chi s)\Delta_- + (1+\chi s)\Delta_+]_i \\
&Q^{+}_{i+1/2} = Q_{i+1} - 0.25\phi s\,[(1+\chi s)\Delta_- + (1-\chi s)\Delta_+]_{i+1} \\
&\Delta_+ = Q_{i+1} - Q_i, \quad \Delta_- = Q_i - Q_{i-1} \\
&s = \frac{2\Delta_+\Delta_- + \varepsilon}{\Delta_+{}^2 + \Delta_-{}^2 + \varepsilon}, \quad \varepsilon = 1.0\times10^{-6}
\end{aligned}
\qquad (2.21)
$$

The spatial accuracy is determined by the values of ϕ and χ.

$\phi = 0$: 1st order upwind

$\phi = 1$, χ = -1 : 2nd order fully upwind

$\phi = 1$, χ = 1/3 : 3rd order upwind biased approximation

2.1.1.3 Time Integration

Among the varied time integration techniques, Beam-Warming's AF-ADI (Approximate Factorization - Alternating Direction Implicit) scheme is employed for time integration.

The time integration scheme adopted here is backward Euler time integration and given by

$$
\begin{aligned}
&\frac{1}{J}\frac{\Delta\hat{Q}}{\Delta t} + D_\xi \hat{E}^{n+1} + D_\eta \hat{F}^{n+1} + D_\zeta \hat{G}^{n+1} = 0 \\
&\Delta Q = Q^{n+1} - Q^n
\end{aligned}
$$

(2.22)

Here, $\hat{E}^{n+1}$, $\hat{F}^{n+1}$ and $\hat{G}^{n+1}$ are unknown values at the n+1 time step. Eq. (2.22) is linearized by using a Taylor series expansion.

$$
\begin{aligned}
&\hat{E}^{n+1} = \hat{E}^{n} + \hat{A}^{n}\,(Q^{n+1} - Q^{n}) + O(\Delta t^{2}) \approx \hat{E}^{n} + \hat{A}^{n}\Delta Q \\
&\hat{F}^{n+1} = \hat{F}^{n} + \hat{B}^{n}\,(Q^{n+1} - Q^{n}) + O(\Delta t^{2}) \approx \hat{F}^{n} + \hat{B}^{n}\Delta Q \\
&\hat{G}^{n+1} = \hat{G}^{n} + \hat{C}^{n}\,(Q^{n+1} - Q^{n}) + O(\Delta t^{2}) \approx \hat{G}^{n} + \hat{C}^{n}\Delta Q \\
&\hat{A} = \frac{\partial \hat{E}}{\partial Q} \quad ,\hat{B} = \frac{\partial \hat{F}}{\partial Q} \quad ,\hat{C} = \frac{\partial \hat{G}}{\partial Q}
\end{aligned}
\tag{2.23}
$$

By substituting Eq. (2.23) into Eq. (2.22), Eq. (2.22) can be expressed as follows:

$$
\left[\frac{I}{J\Delta t} + D_{\xi}^{-}\hat{A} + D_{\eta}^{-}\hat{B} + D_{\zeta}^{-}\hat{C}\right]\Delta Q = -\left[D_{\xi}\hat{E} + D_{\eta}\hat{F} + D_{\zeta}\hat{G}\right] \tag{2.24}
$$

Applying the 1st order upwind scheme to the left hand side of Eq. (2.24), the resulting equation is as follows:

$$
\begin{aligned}
&\left[\frac{I}{J\Delta t} + D_{\xi}^{-}\hat{A}^{+} + D_{\xi}^{+}\hat{A}^{-} + D_{\eta}^{-}\hat{B}^{+} + D_{\eta}^{+}\hat{B}^{-} + D_{\zeta}^{-}\hat{C}^{+} + D_{\zeta}^{+}\hat{C}^{-}\right]\Delta Q = -R^{n}{}_{i,j,k} \\
&R^{n}{}_{i,j,k} = \left[\hat{E}^{+}(Q^{L}) + \hat{E}^{-}(Q^{R})\right]_{i+1/2,j,k} - \left[\hat{E}^{+}(Q^{L}) + \hat{E}^{-}(Q^{R})\right]_{i-1/2,j,k} \\
&\qquad + \left[\hat{F}^{+}(Q^{L}) + \hat{F}^{-}(Q^{R})\right]_{i,j+1/2,k} - \left[\hat{F}^{+}(Q^{L}) + \hat{F}^{-}(Q^{R})\right]_{i,j-1/2,k} \\
&\qquad + \left[\hat{G}^{+}(Q^{L}) + \hat{G}^{-}(Q^{R})\right]_{i,j,k+1/2} - \left[\hat{G}^{+}(Q^{L}) + \hat{G}^{-}(Q^{R})\right]_{i,j,k-1/2}
\end{aligned}
\tag{2.25}
$$

AF-ADI scheme finds the inverse matrix by dividing the block diagonal matrix into three tri-diagonal matrices. Eq. (2.25) is rearranged by applying AF-ADI scheme as follows:

$$
\begin{aligned}
&X\ Sweep: \left[\frac{I}{J\Delta t} + D_\xi^- \hat{A}^+ + D_\xi^+ \hat{A}^- \right] \Delta Q^{**} = -R^n \\
&Y\ Sweep: \left[\frac{I}{J\Delta t} + D_\eta^- \hat{B}^+ + D_\eta^+ \hat{B}^- \right] \Delta Q^{*} = \frac{I}{J\Delta t} \Delta Q^{**} \\
&Z\ Sweep: \left[\frac{I}{J\Delta t} + D_\zeta^- \hat{C}^+ + D_\zeta^+ \hat{C}^- \right] \Delta Q = \frac{I}{J\Delta t} \Delta Q^{*} \\
&Q^{n+1} = Q^n + \Delta Q
\end{aligned}
\tag{2.26}
$$

To accelerate the steady state solution, local time step method is used for each cell's individual time step. Furthermore, Saw tooth cycle multi-grid scheme [64, 65] and implicit residual smoothing [66] scheme are also adopted to accelerate convergence of analysis and to stabilize analysis code.

2.1.1.4 Grid System and Validation

As shown in Fig. 2.1, (O-H) type wing mesh is used for aerodynamic analysis. The O-type airfoil grid is generated by the transfinite Interpolation technique and is expended toward spanwise direction to produce the wing mesh of O-H type grid topology. Total number of mesh size is (121×33×33).

In order to validate the accuracy of the developed numerical analysis code, the transonic flow field around the ONERA M6 wing was evaluated and compared with the experimental data of Schmitt et al [67]. Fig. 2.2 shows the pressure contours on the upper surface of the ONERA M6 wing and compares

C_p distribution between the computed surface pressure distribution and the experimental data for two different spanwise locations.

2.1.2 Structural Analysis

To build detailed structural model of the wing, each parts of the wing structure those are spar, rib and skin have been modeled individually. Nine-node shell mixed finite element has been used to facilitate the structural modeling of the wing component. To connect the structural analysis code and the aerodynamic analysis code, automatic mesh generation algorithm using non-uniform bi-cubic spline composite surface method is used to transform aerodynamic mesh to finite element mesh. VMT method is adopted to transfer aerodynamic force to the structural analysis code. Minimum size of structural component has been determined to bear ultimate loading condition and the buckling of upper surface.

2.1.2.1 Nine-node Shell Mixed Finite Element and Drilling DOF

Nine-node shell mixed finite element is utilized for the structural analysis in this study. The element has three translational degrees of freedom (DOF) and two rotational DOF per node as shown in Fig. 2.3, and therefore each element has 45 DOF. The element is constructed on the basis of the Hellinger-Reissner principle with the assumed displacement field as well as the independently assumed strain field, which lead to the equilibrium Eq. (2.27) and the compatibility Eq. (2.28).

$$\int_V \delta \overline{E}^T CEdV - \delta W = 0 \tag{2.27}$$

$$\int_V \delta E^T C(\overline{E} - E) dV = 0 \tag{2.28}$$

where $\overline{E}$ and $\delta\overline{E}$ are the displacement dependent strain vector and its virtual strain vector, respectively, E and δE are the independent strain vector and its virtual strain vector, respectively, C is the elastic constitutive matrix, δW is the virtual work done due to external load, and V is the volume of integration.

To improve the element performance by reducing the locking effect and suppressing the spurious modes, the assumed strain field of the present element is defined as Eq. (2.29) with 38 independent parameters. Because these parameters are eliminated in element level, additional computation time is negligible.

$$\begin{aligned}
\varepsilon_{xx} &= \alpha_1 + \alpha_2\xi + \alpha_3\eta + \alpha_4\xi\eta + \alpha_5\zeta + \alpha_6\xi\zeta \\
&\quad + \alpha_7\eta\zeta + \alpha_8\xi\eta\zeta + \alpha_{33}\xi\eta^2 + \alpha_{37}\xi\eta^2\zeta \\
\varepsilon_{yy} &= \alpha_9 + \alpha_{10}\xi + \alpha_{11}\eta + \alpha_{12}\xi\eta + \alpha_{13}\zeta + \alpha_{14}\xi\zeta \\
&\quad + \alpha_{15}\eta\zeta + \alpha_{16}\xi\eta\zeta + \alpha_{34}\xi^2\eta + \alpha_{38}\xi^2\eta\zeta \\
\varepsilon_{xy} &= \alpha_{17} + \alpha_{18}\xi + \alpha_{19}\eta + \alpha_{20}\xi\eta + \alpha_{21}\zeta + \alpha_{22}\xi\zeta \\
&\quad + \alpha_{23}\eta\zeta + \alpha_{24}\xi\eta\zeta \\
\varepsilon_{yz} &= \alpha_{25} + \alpha_{26}\xi + \alpha_{27}\eta + \alpha_{28}\xi\eta + \alpha_{35}\xi^2\eta \\
\varepsilon_{zx} &= \alpha_{29} + \alpha_{30}\xi + \alpha_{31}\eta + \alpha_{32}\xi\eta + \alpha_{36}\xi\eta^2
\end{aligned} \tag{2.29}$$

In spite of three translational DOF and two rotational DOF per node, normal direction of the surface may not be continuous for the modeling of complicated structures such as wing boxes. Because the rotational deformation of discontinuous surface cannot be expressed with only two rotational DOFs per node, “drilling degrees of freedom” is adopted to the elements [68], as shown in Eq. (2.30).

$$K^e q^e = \begin{bmatrix} \underset{45\times45}{K_0} & \underset{45\times9}{0} \\ \underset{9\times45}{0} & \underset{9\times9}{K_d} \end{bmatrix} \begin{Bmatrix} u_i \\ v_i \\ w_i \\ \theta_{xi} \\ \theta_{yi} \\ \theta_{zi} \end{Bmatrix} \tag{2.30}$$

where K_0 is the element stiffness matrix of nine-node shell mixed element without the drilling DOF, and K_d is the element stiffness matrix associated with the drilling DOF.

2.1.2.2 Validation of Nine-node Shell Mixed Finite Element

The performance of the element is validated with cut-out hemisphere subjected to alternating point load as shown in Fig. 2.4. Cut-out hemisphere is representative test problem for validation of shell element. Since hemisphere has a doubly curved configuration, it is important to model curved surface and to avoid a membrane locking simultaneously. The geometry and material properties of the hemisphere are shown in Fig.2.4, also. Both ends of hemisphere are under free condition. A pinched hemisphere, with two inward and out ward forces 90° apart can be modeled using symmetry boundary conditions on one quadrant.

The radial displacement at the loading point is normalized by the result of Simo et. al. [69]. Fig 2.5 shows normalized displacement at the loading point vs. mesh size. The results indicate that the element has good accuracy as well as convergence characteristics for structural analysis

2.1.2.3 Modeling of Wing Structure

To combine CFD with CSM, the automatic mesh generation algorithm is adopted to construct CSM mesh with the wing surface information obtained from CFD mesh. Non-uniform bi-cubic spline composite surface method is used to transform CFD mesh to CSM mesh. The leading edge flap and the trailing edge flap are not considered due to their negligible contribution to wing stiffness as shown in Fig. 2.6.

2.1.2.4 CFD and CSM Connection Scheme

In this study, “VMT (V:shear force, M:moment, T:torque) method” is adopted for transformation. VMT transforms aerodynamic forces to structural nodal forces maintaining shear force, moment, and torque equilibriums. The wing is divided into several parts for multi-VMT method as shown in Fig. 2.7.

Since the major deformation of the wing is due to bending and torsional behavior, it is assumed that the geometry of airfoil is not changed during deformation. Therefore, only the translations and rotations of airfoil are considered to create a deformed CFD mesh.

The deformation can be described by the translation of the trailing edge and the rotation around the trailing edge. The deformed shape of wing in span direction is determined by the new location of airfoil due to translations and rotations with the second order spline interpolation of the airfoil sections [70].

2.1.2.5 Sizing of Structural Component by Ultimate Loading Condition

Before multidisciplinary design starts, minimum size of structural component should be determined to bear expected ultimate loading condition. DaDT (Durability and Damage Tolerance) allowable method is used for spar, rib, and lower skin which are subjected to tension forces. Secondly, the minimum size of the structural component is determined to withstand the buckling. The buckling load of the upper skin is obtained by the analysis of an idealized equivalent rectangular panel.

In this study, four parameters which are upper and lower wing skin's thickness at the root and tip are selected as the structural design variables. Those are most important design parameters because the largest compressive and tensile stresses are induced on those regions.

2.1.3 Aeroelastic Analysis

The structural deformation of the wing changes the distribution of the aerodynamic force on the wing surface and this altered aerodynamic force distribution has a reverse influence on the structural deformation (Fig. 2.8).

For the static aeroelastic analyses, there are two CFD/CSM analysis code coupling method. First one is loose coupling method. First of all, aerodynamic analysis is performed to obtain converged aerodynamic force distributions, and then it is transformed the structural forces and transferred to FEM code. After FEM analysis, deformation information is transferred to the grid generation module and updates the aerodynamic and structure grid. With regenerated mesh, next iteration of the static aeroelastic analysis is repeated until it converges (Fig. 2.9). However, this method requires about 4-7 times aeroelastic analysis iteration and it is very time-consuming and inefficient.

To overcome above problem, tight coupling method is introduced. During the iteration of the flow solver, the FEM solver is called and executed per every specified number of iteration, and then renews aerodynamic and structural meshes. The static aeroelastic analysis is performed until the flow solver is converged. This method requires only 30% to 50% additional time for the CFD calculation and it’s very efficient compared with the loose coupling method.

To validate the adequacy of the tight coupling method, the displacements of the wing tip are calculated by both methods and compared in table 2.1 and Fig. 2.10. The main wing of T-50, the baseline wing of the optimization, is used for this calculation and Mach number is 0.9. The leading edge flap is rotated downward by 10° and the angle of attack is 10°.

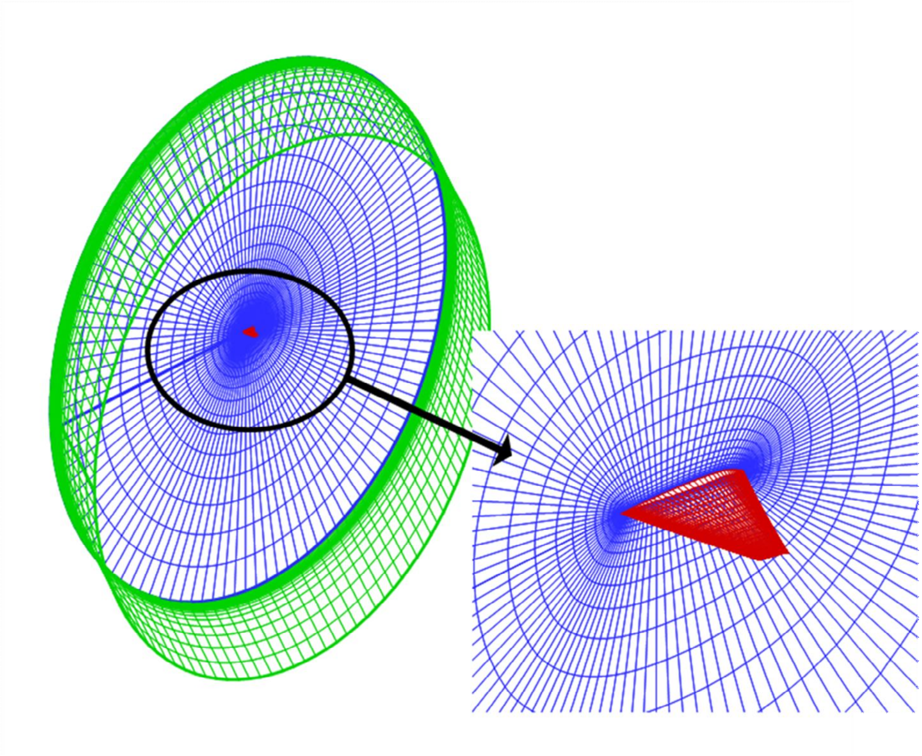

Fig. 2.1 O-H type grid system (121×33×33)

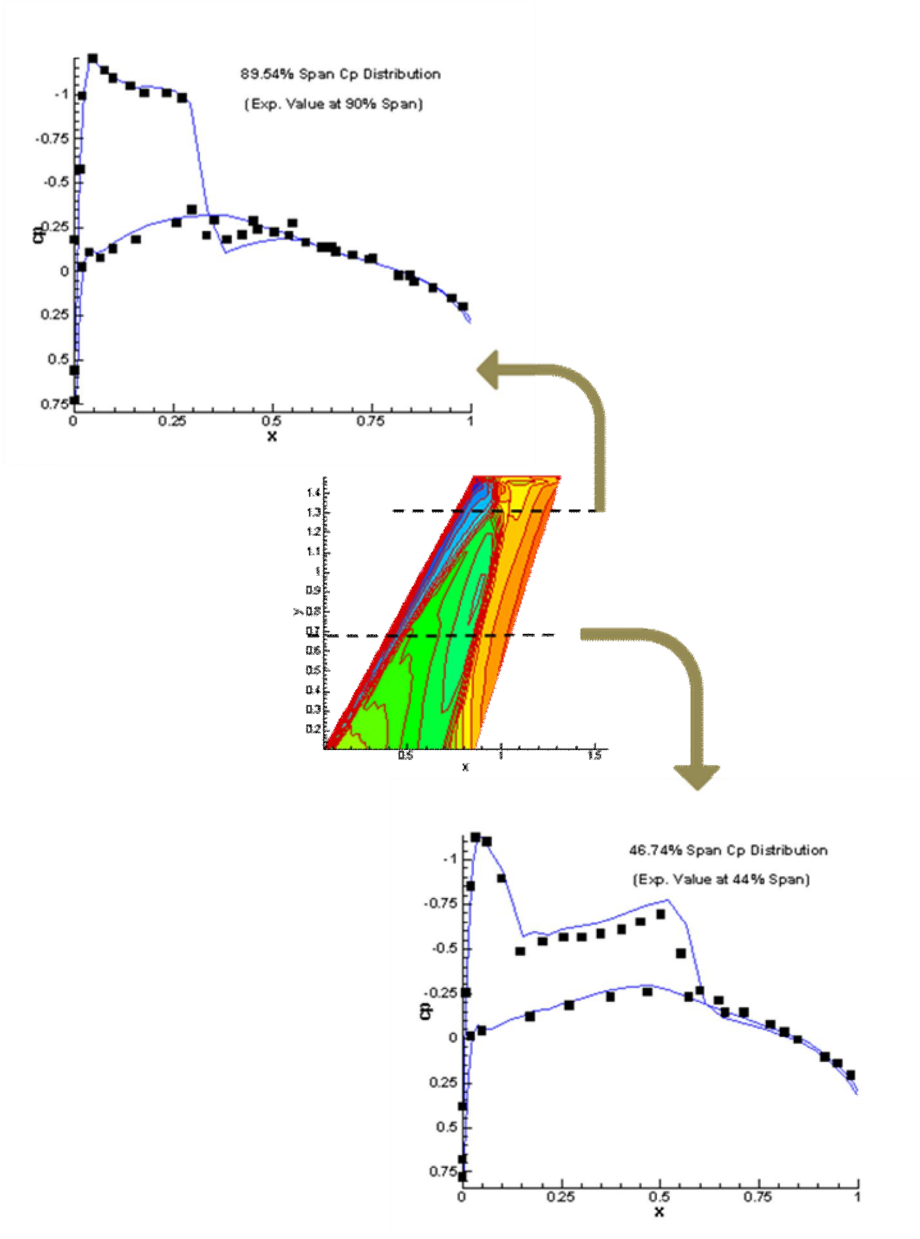

Fig. 2.2 Pressure contour on the upper surface and comparison of the measured and computed surface pressure coefficients of the ONERA M6 (M_∞=0.84, α=3.06°, Re=1.1×10^7)

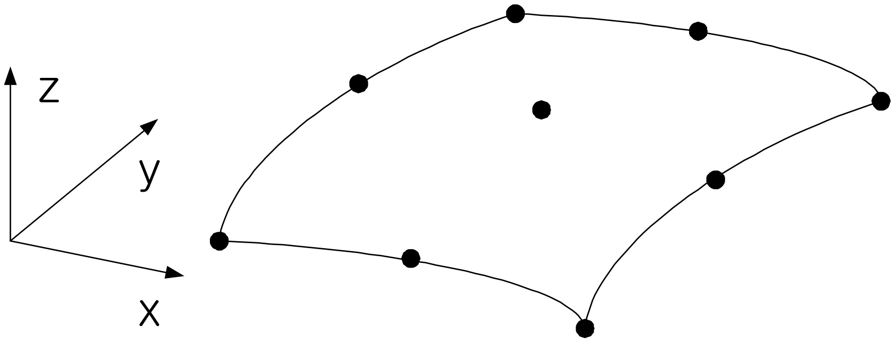

Fig. 2.3 Nine-node shell mixed element [37]

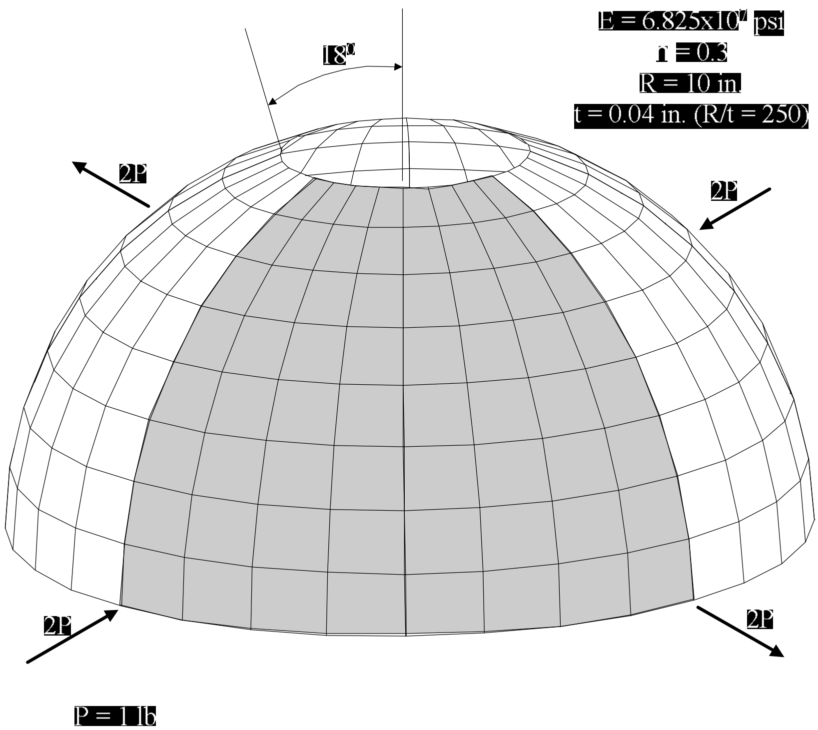

Fig. 2.4 Cut-out hemisphere problem

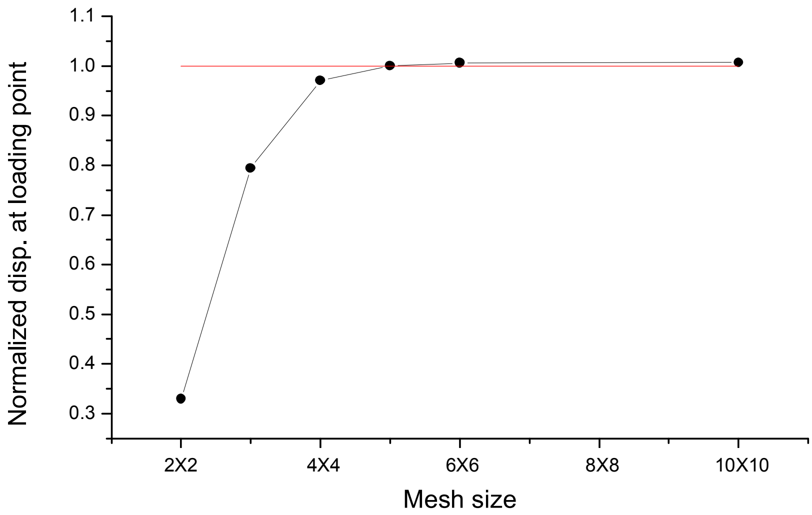

Fig. 2.5 Cut-out hemisphere problem result

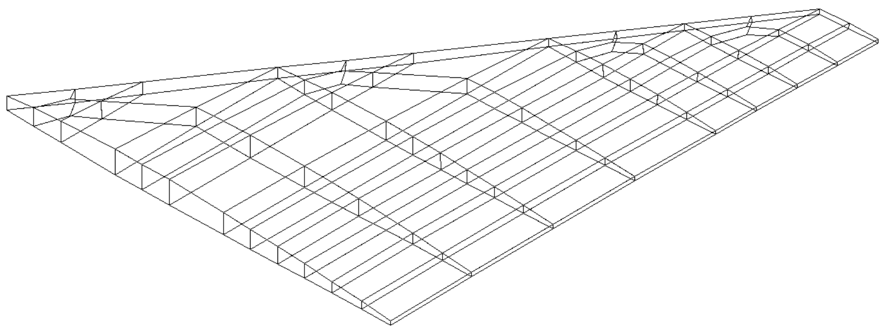

Fig. 2.6 CSM model of the fighter wing [37]

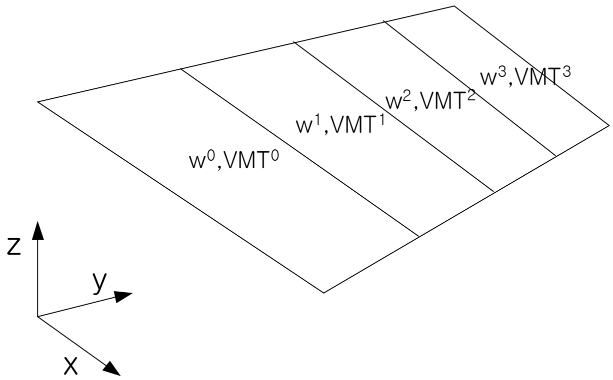

Fig. 2.7 Multi-VMT method [37]

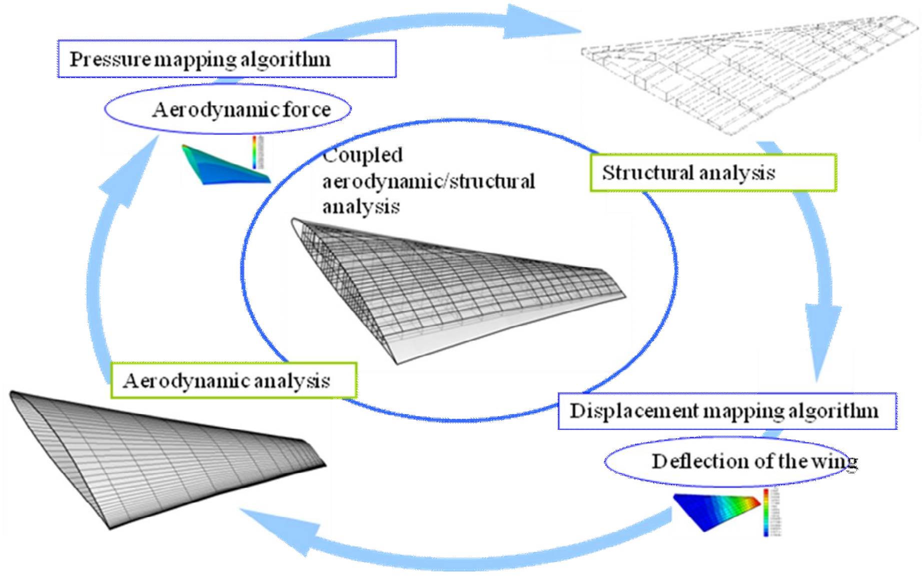

Fig.2.8 The Schematic of aeroelastic analysis between CFD and CSM

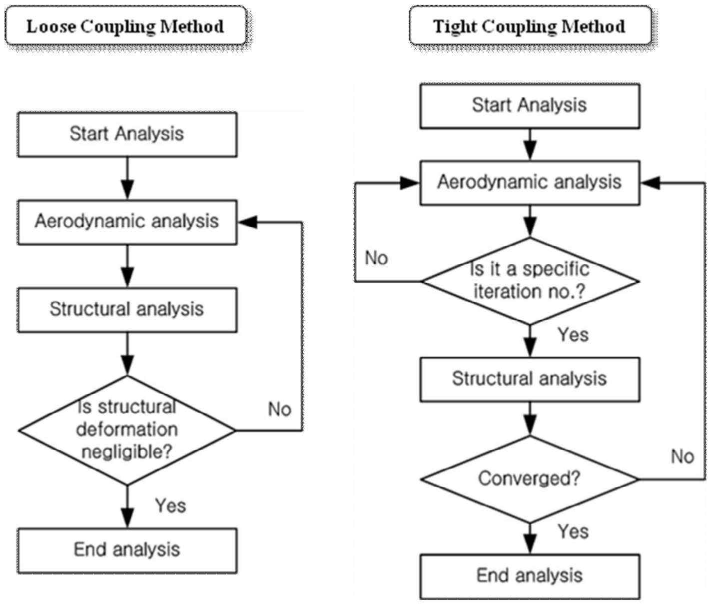

Fig. 2.9 Coupling methods of aeroelastic analysis

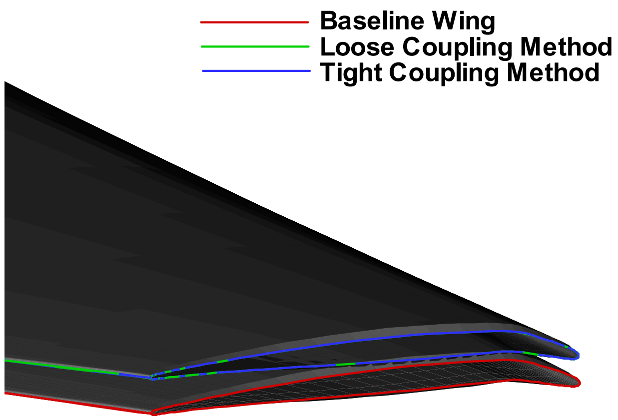

Fig. 2.10 Comparison of the aeroelastic deformations of the wing between loose and tight coupling method

Table 2.1 Comparison of aeroelastic displacement of wing tip by each method

Analysis Method	Loose Coupling	Tight Coupling
Displacement (inch)	2.16701232	2.1676974

2.2 Low-Fidelity Aeroelastic Analysis

In addition to high-fidelity aeroelastic analysis code for the supersonic fighter wing, low-fidelity aeroelastic analysis code for the transonic transport wing has been adopted to consider varied paradigm of MDO problem. In this study, *CO* which is representative multi-level design method is applied to the wing design for a commercial aircraft of DC-9, considering aerodynamics, structure, and performance disciplines.

For disciplinary analyses of the aircraft wing, vortex lattice method (*VLM*) is used for aerodynamic analysis and Wing-box modeling for structural analysis. Fig. 2.11 shows each simplified analysis model and grid systems. Each analysis module is decomposed along aerodynamic and structural disciplines. Weissinger method is applied as a *VLM*, in which aerodynamic force is computed from the planar geometry of the lift surface created by the superposition of vortex filaments, and trapezoidal vortex ring is distributed on the lift surface to consider the effect of mean camber line of the wing section. To consider the compressibility, Prandtl-Glauert rule is used, under the assumption of small disturbance. Induced drag, skin-friction drag, profile drag and wave drag are considered as to compute total drag. Induced drag is computed by Treffz Plane analysis, profile drag by empirical equation and wave drag by Crest-Critical Mach number method. Besides, the wing structure is modeled by 20 segments in a direction of span. Based on the fact that the leading edge and the trailing edge take a little role in transferring the load from the wing to the fuselage, the wing-box endures main load applied to the wing. Upper and lower skin, spar and rib consist of the wing-box. More details and validation of analysis code are given in Ref. [71, 72].

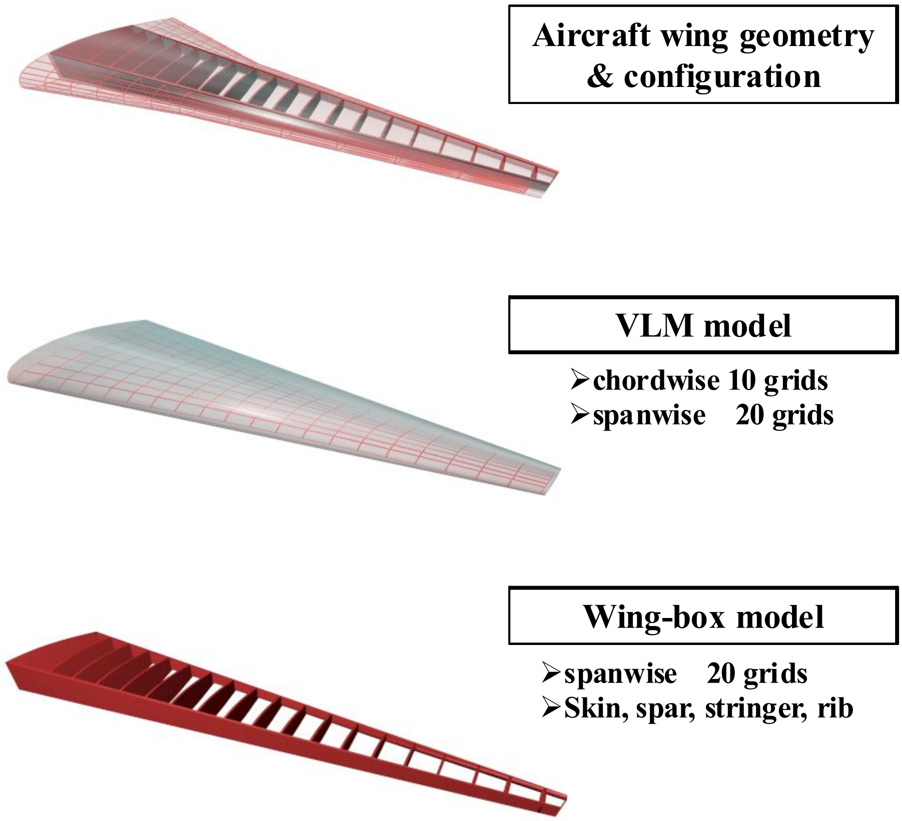

Fig. 2.11 VLM model and wing-box model aircraft wing [71]

Chapter 3. Stochastic Approaches for the DSE and Rearrangement

In this study, establishment of the systematic design space exploration (DSE) and rearrangement method is main objective. To achieve this goal, surrogate model is used to consider the efficiency of the MDO and DSE. Monte-carlo simulation (MCS) is also adopted to investigate the probabilistic quality and quantity of the whole design space. Probabilistic values of the design space obtained with surrogate model and MCS are used for rearrangement of the design space. Detailed description about stochastic approaches used in this study is following.

3.1 Surrogate Model

In a large percentage of cases, the MDO problem has a number of disciplines which are strongly coupled each other. For that reason, relatively huge amount of calculation time is required then single discipline analysis. Therefore, efficiency of analysis is the key point for appropriate MDO framework. To resolve the crux of analysis efficiency, surrogate models frequently replace the analysis code in the most part of MDO problem. Second order polynomial regression model of response surface method (RSM) and artificial neural network (ANN) is used to replace the analysis module in this study.

3.1.1 Response Surface methodology

Response Surface Methodology (RSM) is a collection of statistical and mathematical technique useful for developing, improving, and optimization process. RSM uses Design of Experiments (DOE) techniques, regression analysis, and Analysis of Variance (ANOVA) collectively [73].

RSM is widely used for an efficient tool of design/control since it is expected to have following advantages over other direct optimization methods.

- Compared with other optimization methods, it can be simply implemented.
- It smoothes out the high frequency noise of the objective function and is thus expected to find a solution near the global optimum.
- Various objectives and constraints can be attempted in the design process without additional numerical computations.
- It can be effectively applied to MDO problems with many objectives and constraints.
- It does not require a modification in analysis codes.

However there are some drawbacks to RSM. The range of the design parameters highly affects the fitting capabilities of the RS models. The wide range may increase the prediction error such that the predicted performances cannot be exactly obtained. RSM has also a limitation on the number of the design parameters because the computation time for the construction of the

RS models is proportional to the square of the number of the design parameters.

The response surface model is usually assumed as a second order polynomial as Fig. 3.1, which can be written for n_v design variables as follows:

$$y^{(p)} = c_0 + \sum_{1 \le i \le n_v} c_i x_i^{(p)} + \sum_{1 \le i \le j \le n_v} c_{ij} x_i^{(p)} x_j^{(p)} + \varepsilon , \quad p = 1,\ldots,n \tag{3.1}$$

where $y^{(p)}$ is the response; $x_i^{(p)}$ and $x_j^{(p)}$ are the n_v design variables; c_0, c_i and c_{ij} are unknown coefficients; and ε is an error. The second order model of Eq. (3.1) has $n_t = (n_v + 1)(n_v + 2)/2$ regression coefficients. For n_s sample data points, Eq. (3.1) can be written in a matrix form as

$$\{y\} = [X]\{c\} + \{\varepsilon\} \tag{3.2}$$

where vector $\{y\}$ has n_s dimensions, and the matrix $[X]$ is a $[n_s \times n_t]$ matrix. We can determine the vector of regression coefficients $\{c\}$ using the method of least squares so that L_2 norm of the error vector $\{\varepsilon\}$ is minimized. The least square estimator is defined as

$$\begin{aligned} L \equiv \sum_{i=1}^{k} \varepsilon_i^2 &= \{\varepsilon\}^T \{\varepsilon\} = (\{y\} - [X]\{c\})^T (\{y\} - [X]\{c\}) \\ &= \{y\}^T \{y\} - 2\{c\}^T [X]^T \{y\} + \{c\}^T [X]^T [X]\{c\} \end{aligned} \tag{3.3}$$

The least square estimator must satisfy zero as following,

$$\left\{\frac{\partial L}{\partial c}\right\} = -2[X]^T\{y\} + 2[X]^T[X]\{c\} = \{0\} \tag{3.4}$$

Thus, the regression coefficients $\{c\}$ is determined as,

$$\{c\} = \left([X]^T[X]\right)^{-1}[X]^T\{y\} \tag{3.5}$$

3.1.2 Artificial Neural Network

ANN model in this study consists of three layers – input, output and hidden layers as shown in Fig. 3.2. The transfer function, $S(x)$ connecting information of between neurons in layers is a sigmoid function such as Eq. (3.6).

$$S(x) = \frac{1}{1+e^{-x}} \tag{3.6}$$

Neurons in the hidden and in the output layers are calculated as Eq. (3.7) and (3.8).

$$H_j = S_{Hidden}\left(c_j + \sum_i a_{ij} X_i\right) \Rightarrow \mathrm{H} = \omega_{\mathrm{Hidden}}\mathrm{X} \tag{3.7}$$

$$Y_k = S_{Outout}\left(d_k + \sum_j b_{jk} H_j\right) \Rightarrow \mathrm{Y} = \omega_{\mathrm{Outout}}\mathrm{H} \tag{3.8}$$

Where, **X** is the input variables vector, **Y** is the output variables vector and **H** is the vector of the hidden nodes. The *a*, *b*, *c*, *d* and $\boldsymbol{\omega}$ mean weights of neurons. Using above equations, the correlation of input variables (design variables or flow condition; **X**) and output variables (unknown variables of the reduced order model; **Y**) is replaced with weights of ANN ($\boldsymbol{\omega}_{\mathbf{Hidden}}$, $\boldsymbol{\omega}_{\mathbf{Outout}}$).

Because output variables can be variously formulated as cross and power terms of input variables, it is difficult to determine the form of output variables as polynomial expressions. ANN transmits the linear combination of input variables to a hidden layer by a transfer function, and then the linear combination of values in a hidden layer is propagated to an output layer. That is, ANN itself can select terms that represent output variables due to its structure as mentioned before. The weight of ANN obtained from a series of this procedure determines whether input variables are mutually independent or not.

Levenberg-Marquardt algorithm is a variation of Newton's method that was designed for minimizing functions that are sums of squares of other nonlinear functions. This is very well suited to neural network training where the performance index is the mean squared error. This algorithm finds an optimum by searching along direction that a gradient descends through sensitivity information and a modified Hessian matrix [74].

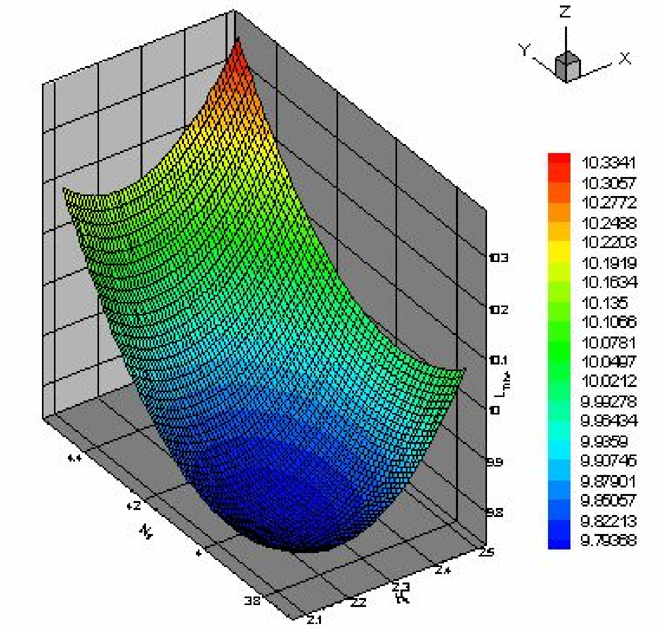

Fig. 3.1 Second order polynomial response surface model

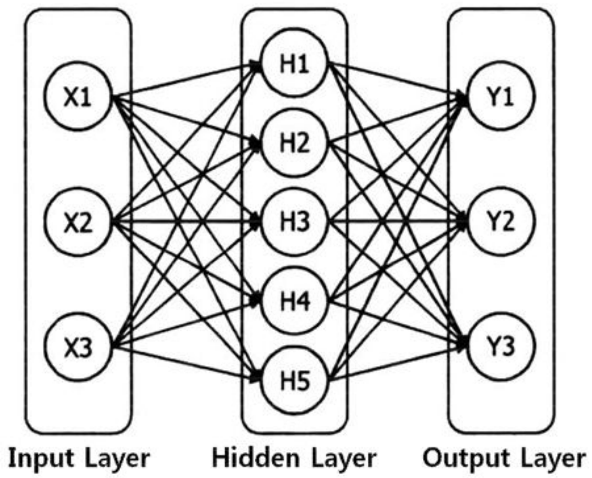

Fig. 3.2 Three-layer artificial neural network (ANN) model

3.2 Design of Experiment (DOE)

Design of experiment (DOE) is the design by information-gathering exercise in the design space that is the region where design variables exist. The simplest way to improve surrogate model accuracy is screening experiment points as much as possible. Full factorial design extracts a large number of experiment points to reproduce a real design space more accurately. 2k and 3k full factorial design is the most widely used, and they extract 2^n and 3^n number of combinations of n design variables. However, as n becomes large the evaluation of both 2^n and 3^n full factorial design becomes impractical. A full factorial design is used for ten or fewer design variables.

In order to reduce the number of the required numerical experiments, another DOE known as central composite design (CCD) may be used. In CCD a 2^n full factorial experimental design is employed along with $2n$ “star” design points and one or more “center” design points. A three variables CCD is shown in Fig. 3.3.

In this experimental design, the star points lie outside the boundary created by 2^n full factorial design points. The distance from the star points to the center of the CCD typically varies from 1.0 to $\sqrt{n}$. Using the response data from $2^n + 2n + 1$ experiments specified by a CCD, a quadratic response surfaces may be constructed. As with 2^n and 3^n full factorial designs, the number of required CCD experiments also becomes impractical as n becomes large.

Therefore, D-Optimal design is more frequently used for the large number of design variables. D-Optimal experimental designs provide an attractive method for creating experimental designs inside an irregularly shaped design space. In addition, D-Optimal experimental designs require fewer than $2^n + 2n + 1$ response values needed for central-composite experimental designs. A sample D-Optimal design is shown in Fig. 3.3.

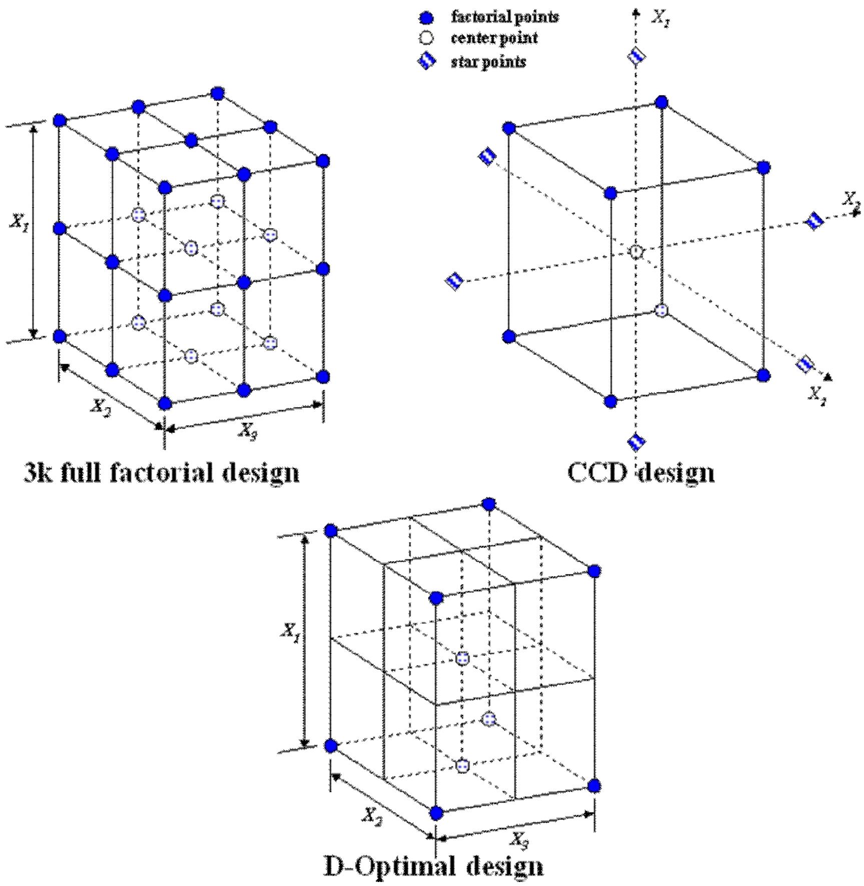

Fig. 3.3 Comparison of three variables DOE results

3.3 Analysis of Variance (ANOVA)

After estimating the coefficients in the response surface (RS) model, analysis of variance and regression analysis produce a measure of uncertainty in the coefficients. This uncertainty estimation is provided by *t-static* defined as:

$$t = \frac{c_{j-1}}{\sqrt{\hat{\sigma}^2 (X^T X)^{-1}_{jj}}}, \qquad j = 1, \ldots, n_t \tag{3.9}$$

Where $\hat{\sigma}^2$ is the estimation of variance. Coefficients with low values for the *t-static* are not accurately predicted. Allowing poorly estimated terms to remain in the RS model may reduce the prediction accuracy of the model.

One of important statistical parameters is the *coefficient of determination*, R^2, which provides a summary statistic that measures how well the regression equation fits the data. It is given as,

$$R^2 = \frac{SSR}{SSTO} = 1 - \frac{SSE}{SSTO} \tag{3.10}$$

Where, *SSTO* means the *total sum of squares* and *SSE* is *error sum of squares*.

However, a large value of R^2 does not necessarily imply that the regression model is a good one. Adding a variable to the model will always increase R^2, regardless of whether the additional variable is statistically significant or not. Thus it is possible for models that have large value of R^2 to yield poor predictions of new observations of the estimates of the mean response. Because R^2 always increases as we add terms to the model, some regression model builders prefer to use an adjusted R^2 statistic defined as,

$$R^2{}_{adj} = 1 - \frac{SSE/(n_s - n_{rc})}{SSTO/(n_s - 1)} = 1 - \left(\frac{n_s - 1}{n_s - n_{rc}}\right)(1 - R^2) \qquad (3.11)$$

Where SSE is the error sum of squares and SYY is the total sum squares. Typical values of R_{adj}^2 are from 0.9 to 1.0 when the observed response values are accurately predicted.

3.4 Monte-Carlo Simulation (MCS)

In this study, rapid collection of the whole design space information is important so that Monte-Carlo simulation (MCS) should be performed to an approximated model. In case of the function composed of algebraic expression, it is not a big issue, but solving the partial differential equation (PDE) like Euler equations, it could take from several times to a few days to get a single output. Therefore, if it is not an algebraic expression, it is efficient to construct surrogated model, e.g. 2nd order polynomial or neural network. By performing the MCS to the constructed approximate models, the ratio of occupation of the feasible region in the design space (probability of success; POS) and reliability index ($\boldsymbol{k}$) of the each sample are calculated. MCS is also applied to evaluating the distribution of the objective functions and the constraints. Because required time of function evaluation is reduced with surrogate model, about 2^{20} (about one million) number of the sample points are used for accuracy of the MCS. Sample points are randomly generated with the uniform distribution and the standard normal distribution.

3.5 Calculate the probability of success

Joint probability formulation is needed to evaluate the probability that satisfies simultaneously the distribution of the joint random variables. Typically, it was used to two formulations that the joint probability model and the empirical probability function. This density function is an analytical probability model that represents the joint distribution from given corresponding means and standard deviations and represented by:

$$
\begin{aligned}
f_{XY}(x,y) = & \frac{1}{2\pi\sigma_X\sigma_Y\sqrt{1-\rho^2}}\exp\{\frac{1}{2\rho^2-2}[(\frac{x-\mu_X}{\sigma_X})^2 \\
& -2\rho(\frac{x-\mu_X}{\sigma_X})(\frac{y-\mu_Y}{\sigma_Y})+(\frac{y-\mu_Y}{\sigma_Y})^2]\}
\end{aligned}
\tag{3.12}
$$

Where, for random variables X and Y, μ_X and μ_Y are the means, σ_X and σ_Y are the standard deviations, and ρ is correlation coefficient. Limited information is only required for this model, which guarantees the flexibility for the application. However, in the case of aircraft design that is complex system with many design variables, it is difficult to obtain correlation coefficient. If the number of the random variables is n, correlation coefficient should be calculated as many as the combination selecting r among n ($1 < r \leq n$).

$$
\sum_{r=2}^{n} {}_nC_r = \sum_{r=1}^{n} {}_nC_r - n = 2^n - n \tag{3.13}
$$

On the other hand, the empirical distribution function is based on empirically collected data samples. Since this model is not needed the correlation coefficient, it is more useful than the analytic model. In addition to, the empirical model has the most accurate joint distribution prediction, because it does not rely on any approximation methods to generate the criterion statistics needed.

The empirical function is depend on sample data and is not concerned about the distribution of random variables. If sample data is enough, then the joint distribution can be predicted accurately. But if too many, much time is spent in the design process.

The joint probability mass function is defined by

$$f(x_1, x_2, \cdots, x_m) = \frac{1}{n}\sum_{i=1}^{n} I((a_{i1}, a_{i2}, \cdots, a_{im}) = (x_1, x_2, \cdots, x_m))$$
$$I((a_{i1}, a_{i2}, \cdots, a_{im}) = (x_1, x_2, \cdots, x_m)) = \begin{cases} 1 & for(a_{i1} \le x_1, a_{i2} \le x_2, \cdots, a_{in} \le x_n) \\ 0 & otherwise \end{cases}$$

(3.14)

Where, a_i is the sample values derived from a sampling method such as MCS and x_i is random variables.

The joint probability distribution function is similarly given by

$$f(x_1, x_2, \cdots, x_m) = \frac{1}{n}\sum_{i=1}^{n} I(a_{i1} \le x_1, a_{i2} \le x_2, \cdots, a_{in} \le x_n)$$

$$I(a_{i1} \le x_1, a_{i2} \le x_2, \cdots, a_{in} \le x_n) = \begin{cases} 1 & for(a_{i1} \le x_1, a_{i2} \le x_2, \cdots, a_{in} \le x_n) \\ 0 & otherwise \end{cases}$$

(3.15)

In this paper, a_i is predicted values of the objective function from MCS and x_i is 1 in the case of satisfying all constraints and 0 otherwise.

The joint probability of success is the probability that all constraints is satisfied and is defined by

$$probability\ of\ success = \frac{1}{M}\sum_{j=1}^{M} I(Z_{j\min} \le Z_j \le Z_{j\max}) \tag{3.16}$$

for the empirical distribution function with M = number of samples,

$$probability\ of\ success = \int_{Z_{\min}}^{Z_{\max}} f(Z)dZ \tag{3.17}$$

for the joint probability model. Generally, as the probability of success is higher, the feasible region is larger.

Fig. 3.4 is shown geometrically the probability of success with two objective functions [75]. It is decided by overlapping high humps in the interested region and the ring is the same probability.

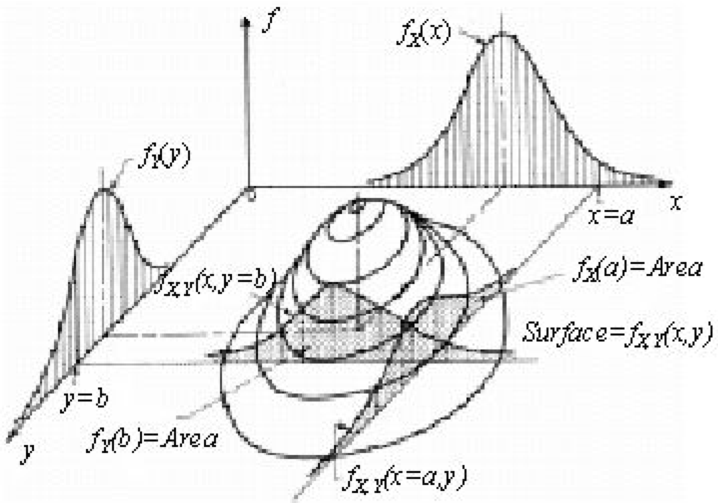

Fig. 3.4 Joint and marginal probability density function of continuous criteria

X and *Y* [75]

3.6 Chebyshev Inequality Condition

For the MDO problem, there are not enough information and knowledge about the given design problem at the initial design phase, in most cases. In the worst case, designer cannot define suitable range of design variables at the initial design phase due to above reason. As a result, there can be no feasible region within the design space. Therefore, initial design space which has no feasible region or has just tiny feasible region should be rearranged into the proper design space to include feasible region for the success of design.

Chebyshev inequality condition is applied to the modification of the design space in order to improve the feasibility of the design space. Chebyshev inequality condition can be written as:

$$P\{|x-\mu| \le \varepsilon\} \ge 1-\frac{\sigma^2}{\varepsilon^2} \tag{3.18}$$

Where μ is the mean value, σ is the standard deviation of the random variable x and ε is arbitrary positive range. If x has normal distribution and ε equals 2σ, the probability can be calculated as:

$$P\{|x-\eta| \le 2\sigma\} = 2G(2)-1 = 0.9545 \tag{3.19}$$

In a word, the probability that x exists inside the interval (-2σ, 2σ) is about 95%. However, if the distribution of the random variable is unknown, adjusted Chebyshev inequality condition for the uniform distributed random variables is used. For the uniform distributed random variables, the probability that x exists inside the interval (-3σ, 3σ) is at least 8/9. If the mean and standard deviation values of the design variables which exist on the feasible design space can be obtained, designer can rearrange the design space into the improved feasible region using Chebyshev inequality condition as in Fig. 3.5.

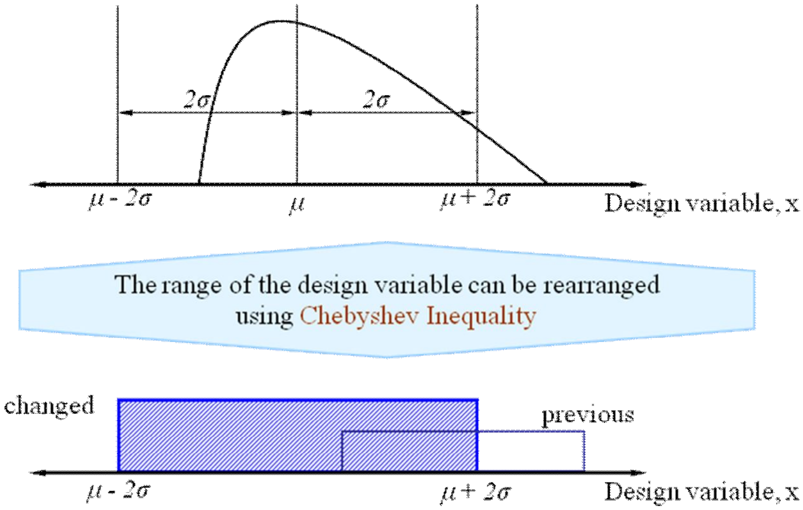

Fig. 3.5 Chebyshev inequality condition and rearranged design space

3.7 Reliability Index

POS is calculated by the number of the samples which satisfy all the given constraints through spraying about one million samples into the design space. If the feasible region is very small or even it does not exist, several millions of samples are not enough to find the feasible region from the design space exactly. However reliability index based method proposed in this study can search the feasible design space efficiently, even though there is no feasible region within the initial design space. The reliability index at the sampled point defined as Eq. (3.20) is calculated by using the Monte Carlo simulation and surrogate model. Even though the feasible region cannot be found exactly, approximate location of the feasible region can be inferred with reliability index.

$$k_i = -\frac{g_i}{\sigma_{g_i}} \quad , \quad i = 1, \cdots, m \tag{3.20}$$

In above equation, g_i means i-th constraint, σ_{gi} means deviation of g_i and m means the number of constraints. Each g_i value at sampled design point can be easily evaluated via Monte-Carlo simulation using surrogate model. If g_i is negative, it satisfies the constraint and σ_{gi} shows the variation of g_i caused by disturbance of input. Therefore, the reliability index (k_i) at the sampled point physically means the distance of the sampled point from the boundary of g_i. In short, if k_i of a sampled point is positive, it satisfies constraint g_i and as the value of k_i is larger, the sample is farther from the boundary of g_i. On the contrary, if k_i is negative, it does not satisfy g_i and as the value of k_i is smaller, the sample exists farther from the region which satisfies g_i. From k_i which has these characteristics, each sample should choose the minimum k_i value as a representative so that it can be estimated whether the sample exists in the feasible region or not.

Using the decided reliability index, temporary mean μ_x should be chosen as shown in Eq. (3.21). This means that the input value which has the largest k value among the reliability indexes (k) of each sample is taken as the mean (μ_x) of the feasible region and at the same time, choosing the largest k among critical k values.

$$\mu_x = \underset{x \in \{input\ of\ MCS\ sample\}}{\arg\max} \left(\min\ k_i \right) \quad , \quad i = 1, \cdots, m \tag{3.21}$$

As shown in Fig. 3.6 (a), if the design space includes the feasible region completely, the mean of the feasible region, the mean of the input and the mean from the reliability index are close together. However, as shown in Fig. 3.6 (b), if the design space does not cover the real feasible region, the mean of the input could show some difference with the mean of the real feasible region whereas the mean defined in Eq. (3.21) could approach to the mean of the real feasible region. Therefore, deciding the mean as shown in Eq. (3.21) is more efficient way to search the real feasible region than just using the input mean.

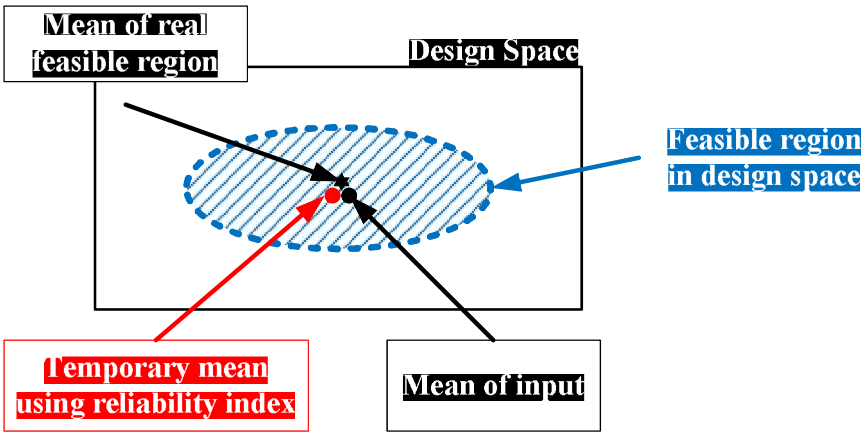

(a) The design space exactly includes feasible region.

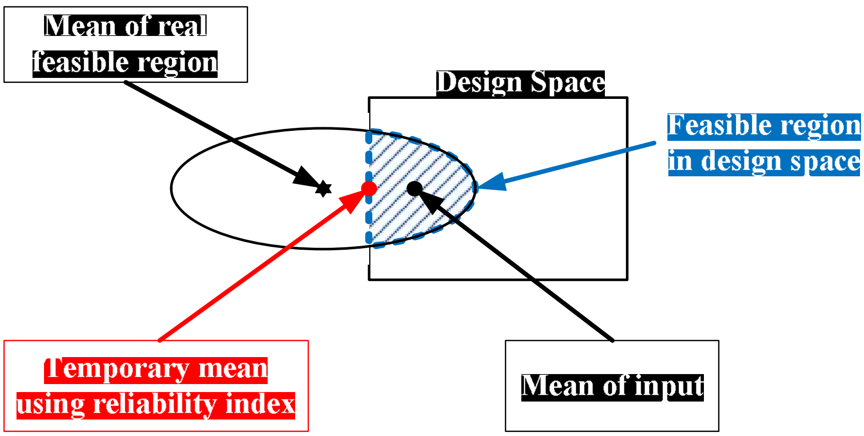

(b) The design space does not exactly include feasible region.

Fig. 3.6 Mean of input and temporary mean from reliability index with respect to the design space.

Chapter 4. Design Space Exploration and Rearrangement Results and Discussion

In this chapter, design space exploration method using surrogate model and MCS will be proposed. Using surrogate model and MCS, probabilistic quantities and qualities of the design space and all variables are efficiently investigated. With these probabilistic data from DSE, feasibility of the design space is investigated and then rearranges the design space into the updated space which has higher feasibility. To update design variable range, Chebyshev inequality condition and reliability index (RI) is adopted to determined new design space.

This method is applied to the design optimization problem of the exact function with two variables, and from this problem, it will be confirmed that this method has a capability of including the feasible region laying the outside of the initial design space. Finally, the proposed method will be applied to the design optimization problem coupled disciplines of aerodynamics, structure, and performance, and from these results, it will be showed that this method can search for better solution than an optimum in the initial design space

4.1 DSE and Rearrangement of the Design space to Improve the Feasibility with Chebyshev Inequality

DSE and rearrangement procedure using Chebyshev inequality is shown in Fig. 4.1. At the very first, define the problem and the initial range of design space, and then surrogate model of the defined problem is constructed to consider the efficiency of evaluation during whole design process. Then Monte-Carlo simulation (MCS) is implemented to obtain the probabilistic quantities and qualities of the design space with constructed surrogate model. Through the Monte-Carlo simulation, probabilistic and statistic quantities of the design space such as probability of success (POS), reliability index value, mean or deviation of design variables can be calculated. In the case of Chebyshev inequality based method, convergence check procedure is directly done using calculated POS and mean values of the present design space. If the present design space satisfies convergent criteria, rearrangement iteration finishes instantly and optimization process will start. On the other hand, rearrangement procedure based on Chebyshev inequality condition will be performed to update the whole design variables range with calculated mean and deviation value of the current feasible region, and then next iteration will start for updated design space. Through a number of iteration, the design space steadily converges into the higher feasible region.

4.1.1 Test Functions

For the validation of the proposed design space exploration and rearrangement method, Goldstein function and Branin function are selected. These functions are the representative test functions for the MDO problem which have nonlinear characteristics and multiple local optima and global optimum simultaneously. For the validation of proposed method, test functions are subjected to relatively simple constraints to remove the absence of feasible region on the design space. Moreover, these simple constraint functions make design problem into the closed form.

4.1.1.1 Goldstein Function

Goldstein function which has two variables (x_1, x_2) and four local optima was selected as test function, and two constraint functions (g_1, g_2) was considered as following.

$$\begin{aligned}
f = &\{1+(x_1+x_2+1)^2(19-14(x_1+x_2)+3(x_1+x_2)^2)\} \\
&\{30+(2x_1-3y_1+1)^2(18-16(2x_1-3y_1)+3(2x_1-3y_1)^2)\}, \\
&(where,\ y_1 = x_1+x_2) \\
g_1 &= 0.5(x_1+1.4)^2 + x_2 < 0 \\
g_2 &= (x_1-0.2)^2 + x_2 - 1.5 < 0
\end{aligned} \tag{4.1}$$

Goldstein function has the global optimum value at (0,-1) located in the feasible design space, and three local optima exist simultaneously as shown in Fig. 4.2.

Among those local optima, a local optima exists on the feasible region at (-0.6, -0.4) as shown in Fig. 4.3. Therefore, optimum value of the initial design space is $f(-0.6, -0.4)^* = 30$.

To perform DSE and rearrangement using Chebyshev inequality, the initial design space has been defined as shown in table 4.1. POS of the initial design space is about 2.53%. After eight iterations, the converged design space includes whole feasible region as in Fig. 4.3. During the iteration, each variables mean and POS have been changed as in Fig. 4.4 and POS has been increased up to 15.26%.

4.1.1.2 Branin Function

Branin function has two variables (x_1, x_2) and three optima at ($-\pi$, 12.275), (π , 2.275) and (9.42478, 2.475) with $f(x_1, x_2)$=0.397887. Two constraint functions (g_1, g_2) have been considered as following.

$$
\begin{aligned}
f(x_1, x_2) &= \left(x_2 - \frac{5.1}{4\pi^2} x_1^2 + \frac{5}{\pi} x_1 - 6 \right)^2 + 10\left(1 - \frac{1}{8\pi}\right)\cos(x_1) + 10 \\
g_1(x_1, x_2) &= \frac{1}{5}(x_1 - 3)^2 + 6 + x_2 \leq 0 \\
g_2(x_1, x_2) &= \frac{2}{7}(x_1 - 5)^2 - x_2 \leq 0
\end{aligned}
\tag{4.2}
$$

Branin function has three optima and their values are equal, but only one optima locates on the feasible region at (π , 2.275) as shown in Fig. 4.5.

The initial design space has been defined as shown in table 4.2. POS of the initial design space is about 6.01%, and optimum of the initial design space is $f(2, 4)^{*} \approx 6.4482$.

After nine iterations, converged design space includes whole feasible region like the Goldstein function case (Fig. 4.6). During the iteration, each variables mean and POS have been changed as in Fig. 4.7 and POS has been increased up to 30.43%. Besides, the optimum of the converged design space is $f(\pi, 2.275)^{*} \approx 0.3979$ that is one of the three optima.

4.1.1.3 Collaborative Optimization (CO) of Goldstein Function with Chebyshev Inequality Condition

Collaborative optimization (CO) is a multi-level decomposed optimization methodology for a large-scale MDO. CO is known to have computational and organizational advantages. Its decomposed architecture removes a necessity of direct communication among disciplines, and guarantees their autonomy. CO decomposes the design problem into system level and subsystem level as shown in Fig. 4.8.

In case of CO, definition of design optimization problem is shown in Fig. 4.9 and the relation of variables among the system and the subsystems are arranged in table 4.3. As shown in Fig. 4.9 and table 4.3, by adding algebraic formula $y_1=x_1+x_2$, an interdisciplinary variable is generated, which an output of a subsystem is the input of the other subsystem.

To exploit Chebyshev inequality based method, initial range was defined from -1 to 1 for all design variables. Result of CO is shown on the Z-space in

Fig. 4.10. In this case, the global optimum has been included within the initial design space and the converged design space at the same time.

In this case, converged space covered whole feasible space also. In table 4.4, CO result of the Goldstein function has been described. Through the iteration, POS has been increased from 0.32% to 34.94% in Z-space and the global optimum has been found at (0, -1) in both of them. Consequently, it is confirmed that the proposed method can be applied to the CO appropriately.

4.1.2 MDO of the Aircraft Wing

4.1.2.1 Aero-structural Optimization of the Supersonic Fighter Wing with High Fidelity Analysis

The proposed method has been applied to the aero-structural multidisciplinary optimization of the supersonic fighter wing. Since the aerodynamics is coupled with structure and constraints are complicatedly connected to each other, it is one of the most representative MDO problems which correspond with real aircraft wing design. Three-dimensional Euler code in aerodynamic analysis and nine-node shell mixed FEM code in structural analysis are used. Sweep angle, aspect ratio, twist, reference area and taper ratio of the wing which are defined the wing platform, thickness of root lower skin, tip lower skin, root upper skin and tip upper skin are selected as the design variables (See Fig.4.11 and table 4.5). Lift, drag, lift to drag ratio, area of the wing and the displacement of the wing tip are selected as constraint functions. Lift, lift to drag ratio and wing area must be larger than the baseline, but drag and the displacement of the wing tip must be smaller than the baseline.

$$
\begin{aligned}
&\text{Objective} \;\; : \text{maximize}(L/D) \\
&\text{Subject to} : Lift > Lift_{baseline}, \quad L/D > L/D_{baseline}, \\
&\qquad\qquad\quad Wing\ Area > Wing\ Area_{baseline}, \quad Drag < Drag_{baseline}, \\
&\qquad\qquad\quad \Delta Tip\ displacement < 0.05 \times (Tip\ displacement_{baseline})
\end{aligned}
\tag{4.3}
$$

Since the number of design variables is more than previous examples, we calculated the probability of success from 10^7 sample points uniformly distributed. In the initial design space, the probability of success is 0.00195%. After 8 iterations, the probability of success is converged with same procedure as the previous example. The probability of success is increased by 30.93% in the changed design space and history of the POS is represented in Fig. 4.12. At the initial design space, the probability distribution of each design variable shows irregular distribution as shown in Fig. 4.13, whereas regulated probability distributions are represented in Fig. 4.14 at the converged design space. Fig. 4.15 and 4.16 represent the ranges of both initial and final design variables and optimized wing planforms at each design space. Compared to initial design space, the ranges of sweep angle, aspect ratio, twist and area are reduced, but others are expanded to outside of the initial design space in Fig. 4.15.

To compare the C_p distributions of the optimized wing, the initial design space optimal wing has relatively wider negative C_p region on the upper surface than the optimized wing of the converged design space as shown in Fig. 4.17. Moreover, the optimized aspect ratio of the initial design space is bigger about 8.2% than the optimized aspect ratio of the converged design space (see table 4.6). Along the spanwise direction, C_p distributions are compared in Fig. 4.18. Each airfoil sections are located on the root, 25% and 85% of the span. For the optimized wing cases, there is no significant change of the C_p distribution from first airfoil section to third airfoil section. But the C_p distributions of the baseline wing show considerable change as the distance from the wing root increases. C_p distribution of the third airfoil section shows drastic pressure rise on the upper surface. It causes loss of the aerodynamic performance of the baseline wing. Consequently, optimized wings have a tendency to avoid such drastic pressure change, and then their leading edge sweep angles have been changed to get larger sweep back angle.

Hence, optimized lift to drag ratio of the initial design space has more improved results than the converged design space. As in table 4.6, lift to drag ratio maximized in each design space is increased to 27.76% at the initial design space and to 18.40% at the converged design space with respect to the baseline, but the initial design space result seriously violated the tip displacement constraint. In fact, the probability of success is too low at the initial design space, and it means that the initial space has no feasible regions. Fig. 4.19 and 4.20 show the probability density function and cumulative distribution function of lift to drag ratio. Same as previous examples, the increase of the probability can be verified from 48.81% to 95.0%.

According to presented results, the proposed probabilistic approach to improve the feasibility of the design space can be successfully applied to the aerodynamic-structural multidisciplinary design optimization of the wing. And it produced better optimized solutions in the converged design space than in the initial design space.

4.1.2.2 Aero-structural Optimization of the Transonic Wing with Low Fidelity Analysis

The proposed method is applied to the aero-structural multidisciplinary optimization of the transonic wing. Vortex Lattice Method (VLM) code in aerodynamic analysis and wing-box model in structural analysis are used. Semi-span, taper ratio, leading edge sweep angle, t/c at root and t/c at tip of the wing are selected as the design variables, which are in table 4.7 and Fig. 4.21 Lift to drag ratio, lift, drag, weight and area of the wing are selected as objective function and constraints. Lift to drag ratio, lift and wing area must be larger than the baseline, but drag and weight must be smaller than the baseline.

$$\begin{aligned}
&\text{Objective} && : \text{maximize}(L/D) \\
&\text{Subject to} && : L/D > L/D_{baseline}, \quad Lift > Lift_{baseline}, \\
& && \quad Wing\ Area > Wing\ Area_{baseline}, \quad Drag < Drag_{baseline}, \\
& && \quad Weight < Weight_{baseline}
\end{aligned} \tag{4.4}$$

Because only 42 points are success out of 2^{20} (about 1,000,000) points, the probability of success in the initial design space is 0.0042% and probability distribution of each design variables are represented in Fig. 4.22. Chebyshev inequality condition is used to modify the initial design space. Because the distribution of design variables in case of success is unknown, modify the boundaries of design variables using 3σ to contain 89% of the feasible region. The probability of success in the changed design space is grown up to 4.2442%. And the distribution of design variables is approach to normal distribution. So we modify the design space using 2σ to maintain nearly constant ranges of the design variables and to contain 95% out of the range of success. This process is repeated until the increase of POS is less than 1%. The POS in the converged design space is grown up to 18.8853%, and the distributions of design variables in converged space are represented in Fig. 4.23. Fig. 4.24 represents the ranges of both initial and final design variables. Compared to initial random design space, the ranges of semi-span, t/c(root), and L.E. Sweep are reduced, but taper ratio and t/c(tip) are expanded. Fig. 4.25 shows optimized wing planforms in initial design space and converged design space.

To investigate the POS of objective function, Fig. 4.26 and Fig. 4.27 represent the probability density function and cumulative distribution function of lift to drag ratio. In Fig. 4.26, most values of the objective function are on the infeasible region at the initial design space, but at the converged design space, most values of the objective function move to the feasible region. In Fig. 4.27, the probability of success in initial space, 32.38%, is dramatically increase in converged space, 73.83%, by rearranging of the design space.

When the problem maximizing lift to drag ratio is solved in the initial and converged design space, the optimal point is different in each case. If the converged design space shrinks into the initial space, the optimal point is almost the same. But, if the converged design space is extended to the outside of the initial space, it can be verified that the optimal point is located at the new space. In addition, it can be verified that optimized lift to drag ratio of the initial and converged design space is improved with respect to the base line design by 7.34 %, 10.88 % each. This means the altered design space includes a proper optimal point but the initial design space doesn't. (See table 4.8)

4.1.2.3 CO of the Transonic Wing with Low Fidelity Analysis

In this study, CO is applied to the wing design for a commercial aircraft of DC-9, considering aerodynamics, structure, and performance disciplines

To exploit multidisciplinary design optimization of transonic aircraft wing, the design formulation is specified as following. In this study, the design objective is maximization of the flight range:

$$Range = \frac{V}{SFC} \cdot \frac{L}{D} \cdot \ln\left(\frac{W_i}{W_f}\right) \tag{4.5}$$

Eq. (4.5), Brequet range equation, includes lift to drag ratio (*L/D*) represented the aerodynamic performance and weights (W_i, W_f) estimated from the structure analysis. Because cruise velocity (*V*), specific fuel consumption (*SFC*) and the initial aircraft weight (W_i) are constant, *L/D* has to be increased and the aircraft weight after finishing its mission (W_f) must be decreased to maximize range. While range is maximized, six constraints as follows should be satisfied.

$$\begin{aligned}
&L/D > L/D_{baseline} \\
&C_D < C_{D,baseline} \\
&Area > Area_{baseline} \\
&W_{wing} < W_{wing,baseline} \\
&W_{fuel} < W_{fuel,baseline} \\
&\left|\Delta d_{tip}\right| < 0.05 d_{tip,baseline}
\end{aligned} \tag{4.6}$$

The initial design variables rage is described in table 4.9. The initial value of each design variable is determined based on DC-9 specification. For this problem, the flight condition should be like following. The aircraft cruises at 7,620 m (25,000ft) above the ground with Mach number 0.75. Angle of attack is considered to be zero and take-off gross weight is 49,000 kg (108,000 lb). Definition of design optimization problem is shown in Fig. 4.28, and all system variables are depicted in table 4.10.

As a result, POS of design space has been increased from 0.13% to 38.0% and optimum result of the converged design space represents 12.4% improved range than baseline wing (see table 4.11 and 12). The converged design space has been rearranged into the varied direction for each design variable as in Fig. 4.29. Especially, converged design spaces of taper ratio and thickness to chord ratio at root have been moved right or left side of the initial design space. And also, converged design space optimum exists out of the initial design space. Moreover in Fig. 4.30, PDF of lift to drag ratio shows improved POS from 49.8% to 77.3%.

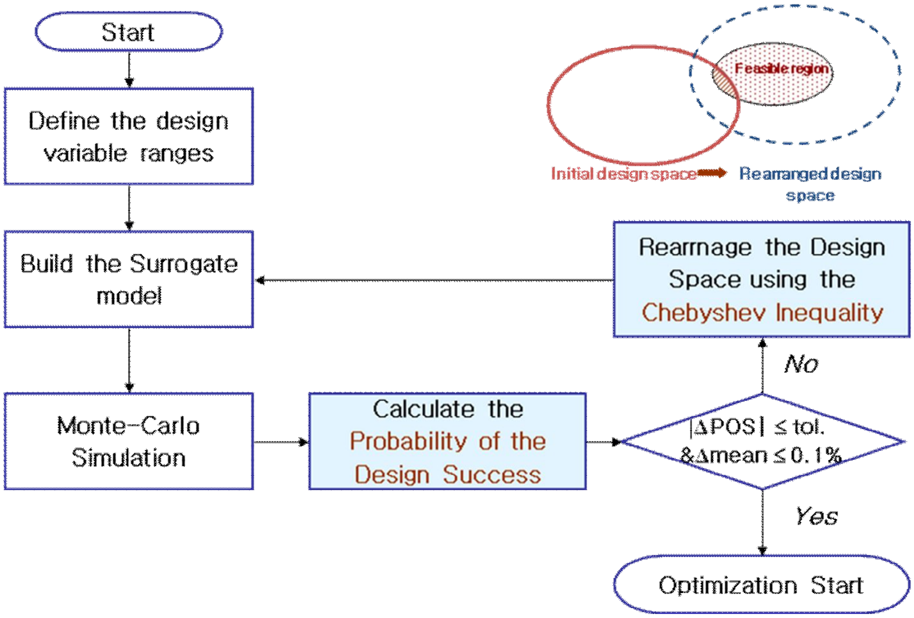

Fig. 4.1 DSE and rearrangement of the design space with Chebyshev Inequality

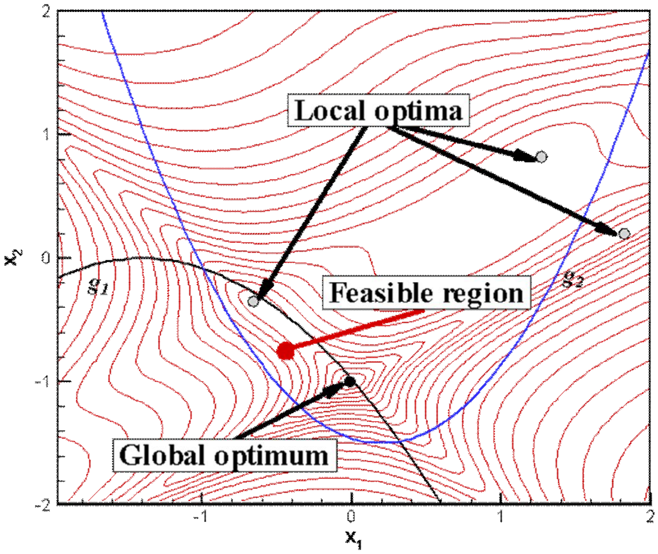

Fig. 4.2 Goldstein function and constraints

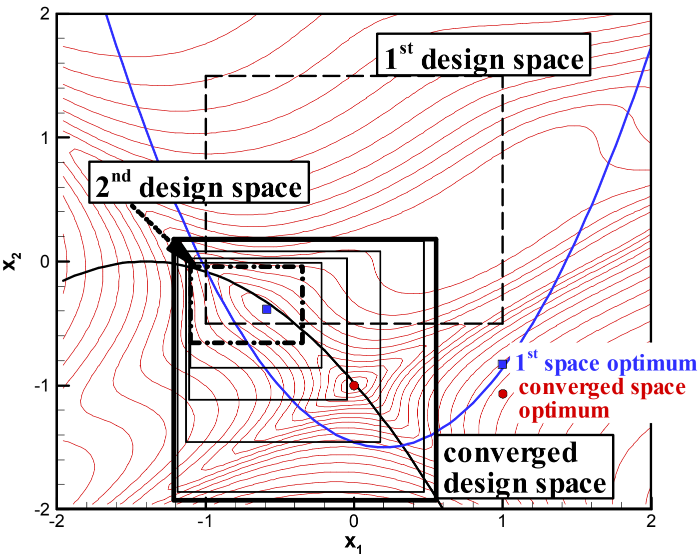

Fig. 4.3 Result of Goldstein function with Chebyshev inequality

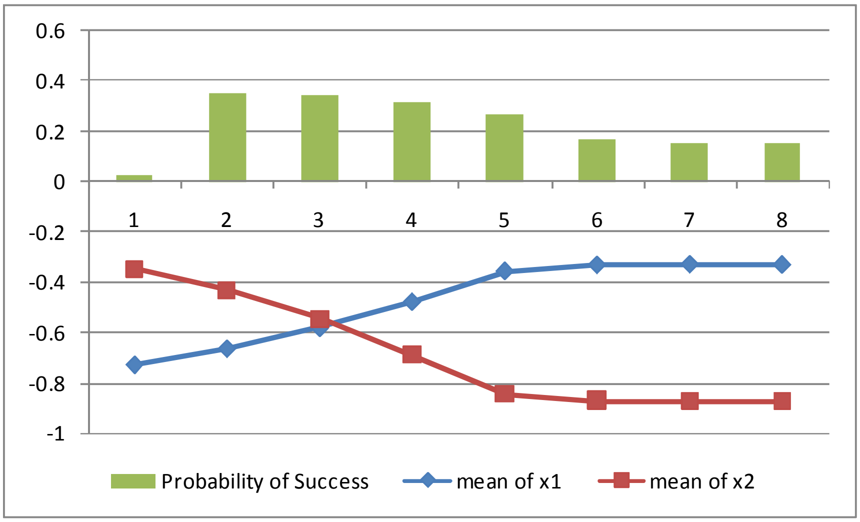

Fig. 4.4 Convergence history of Goldstein function

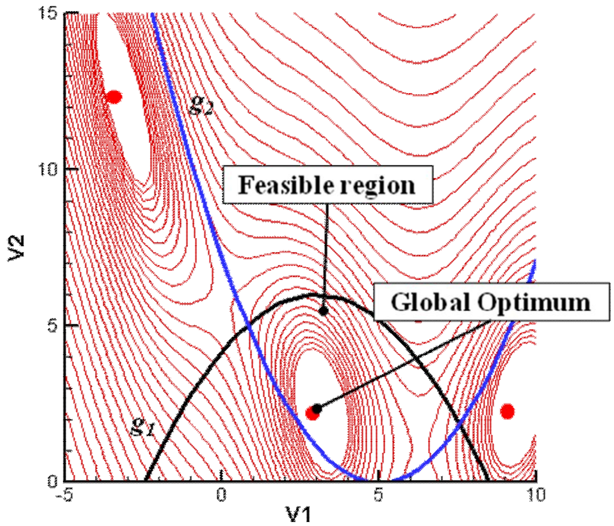

Fig. 4.5 Branin function and constraints

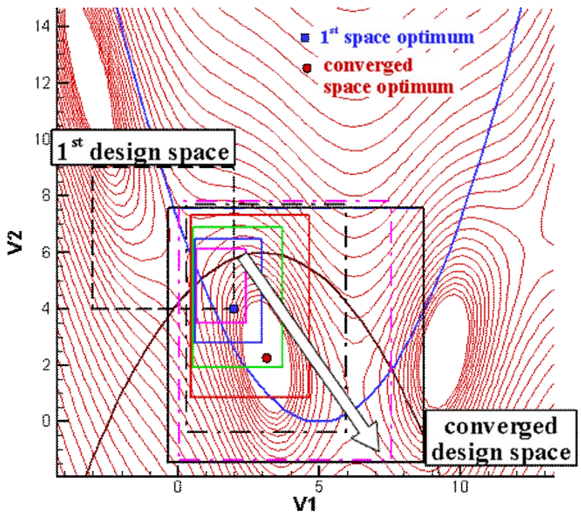

Fig. 4.6 Result of Branin function with Chebyshev inequality

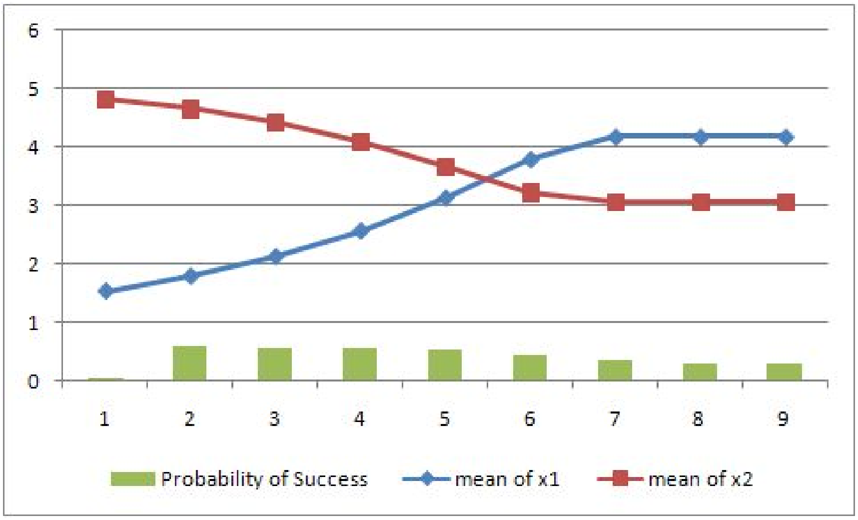

Fig. 4.7 Convergence history of Branin function

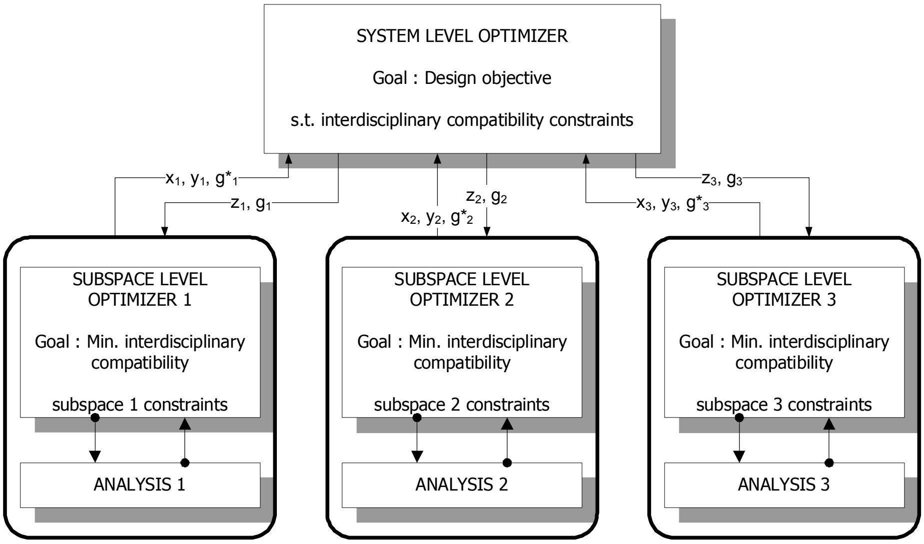

Fig. 4.8 Collaborative Optimization (CO) architecture

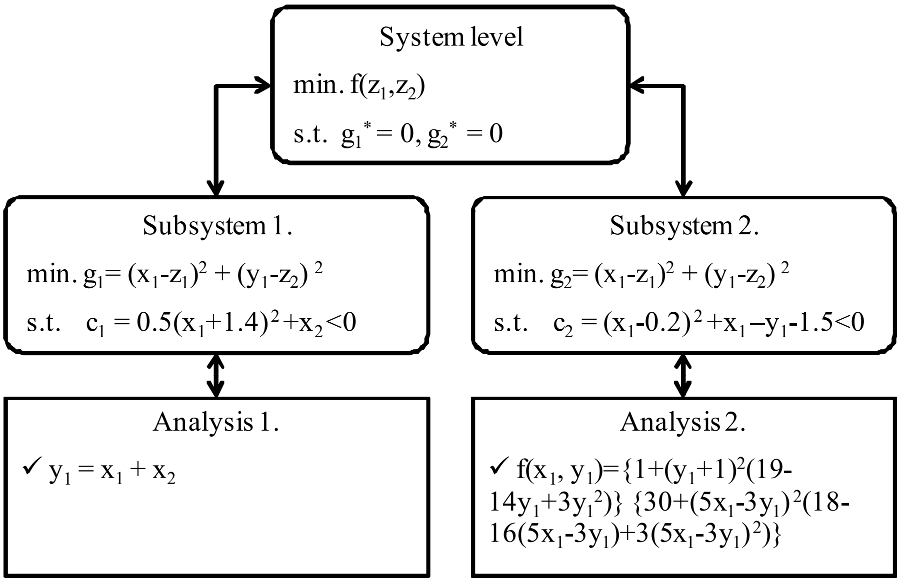

Fig.4.9 CO formulation of Goldstein function

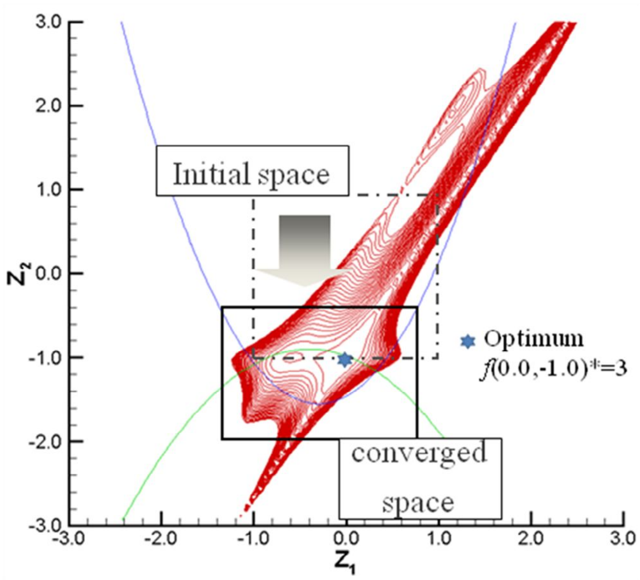

Fig. 4.10 Result of CO for Goldstein function

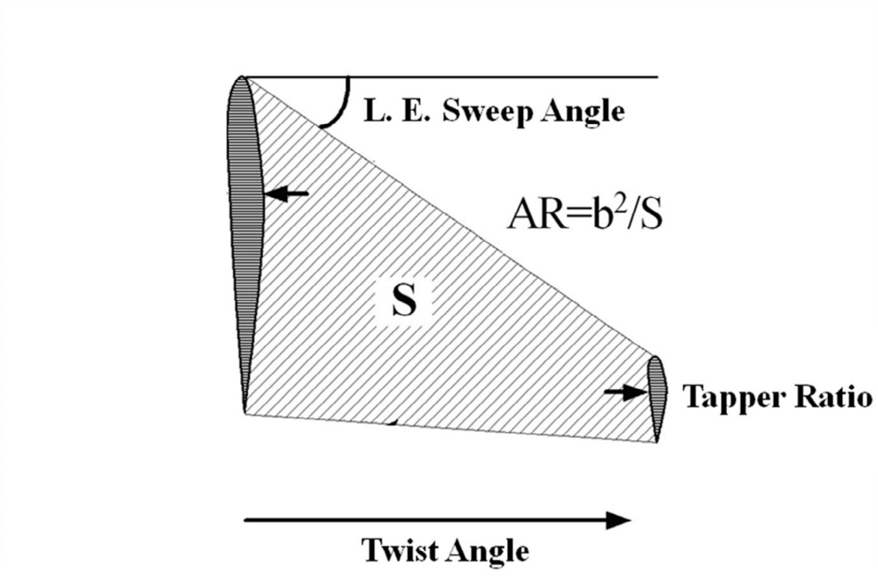

Fig. 4.11 Aerodynamic design variables of the supersonic wing

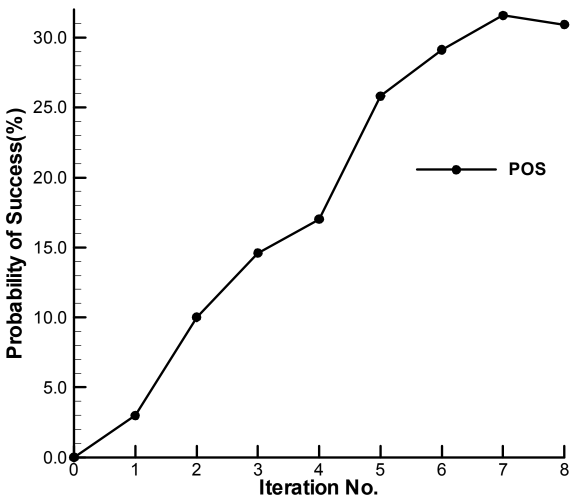

Fig. 4.12 POS history via iterations (M_{∞}=0.87)

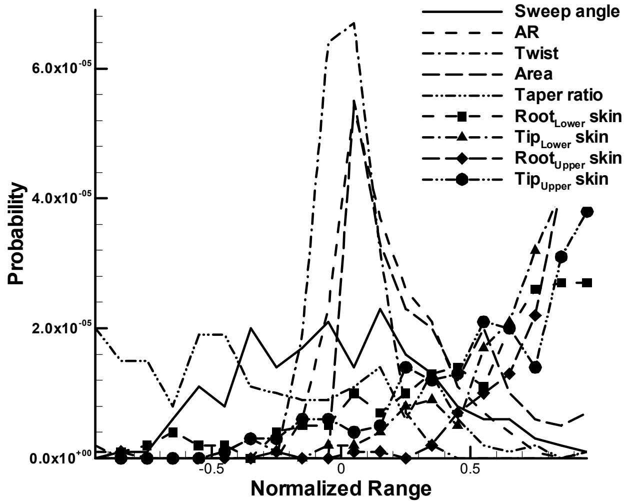

Fig. 4.13 Probability distribution of the initial design variables

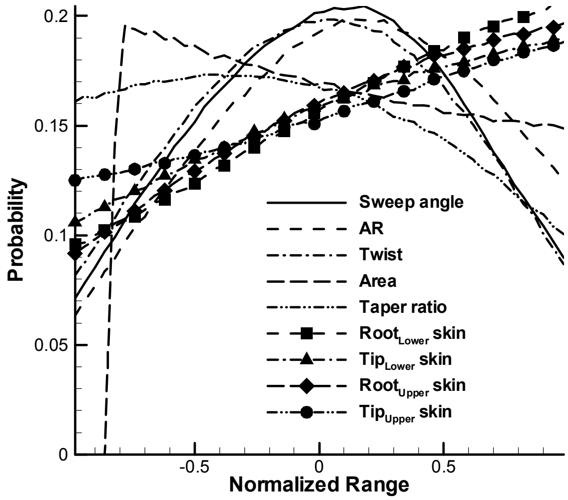

Fig. 4.14 Probability distribution of the converged design variables

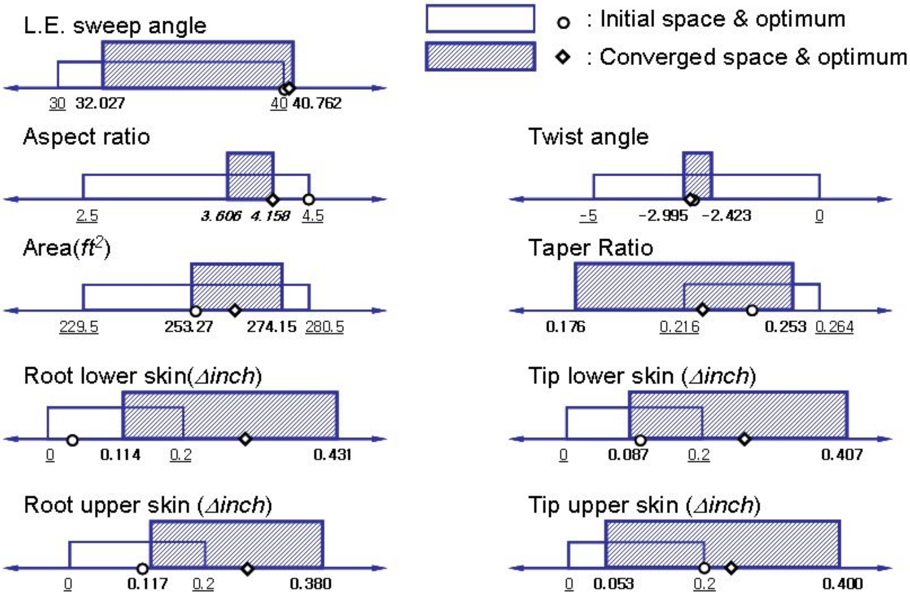

Fig. 4.15 Comparison of the design space and optimum (M_∞=0.87)

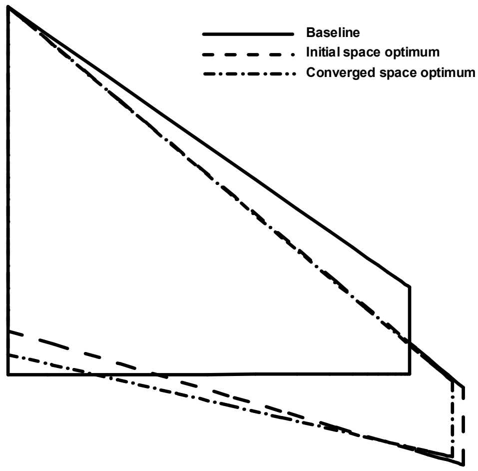

Fig. 4.16 Comparison of the supersonic wing planform (M_∞=0.87)

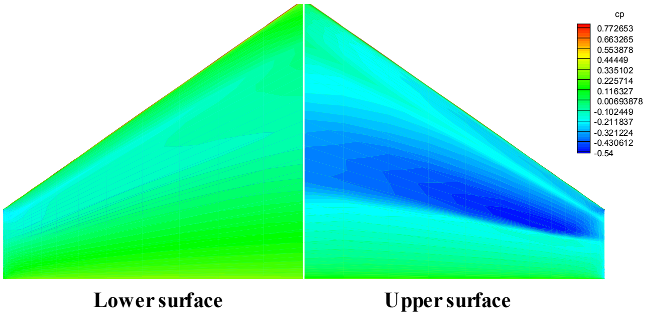

a) Baseline Wing

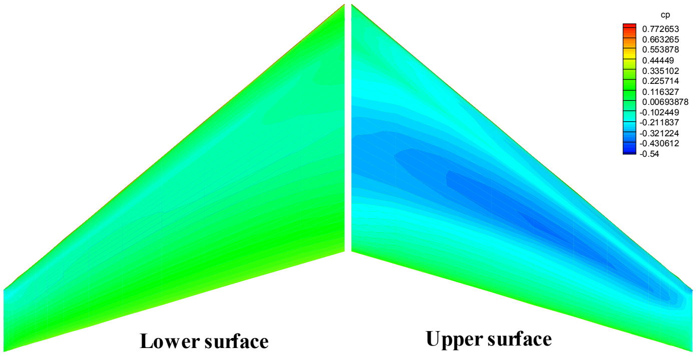

b) Initial design space optimum wing

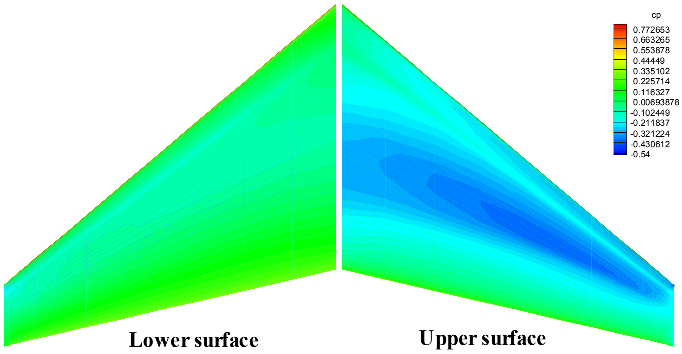

c) Converged design space optimum wing

Fig. 4.17 Cp distributions of the supersonic wing (left=lower surface / right=upper surface, M_∞=0.87)

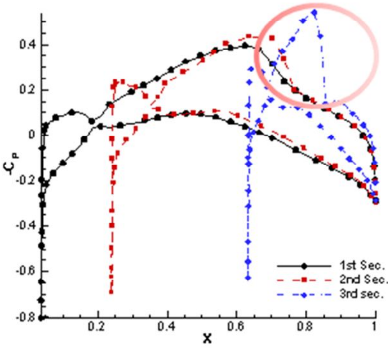

a) Baseline wing

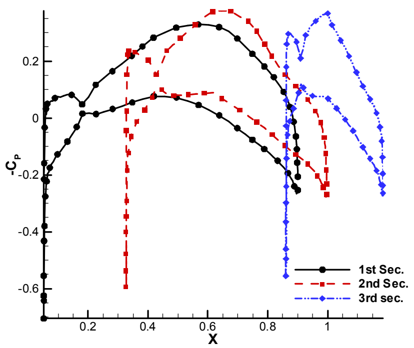

b) Optimized Wing at the initial design space

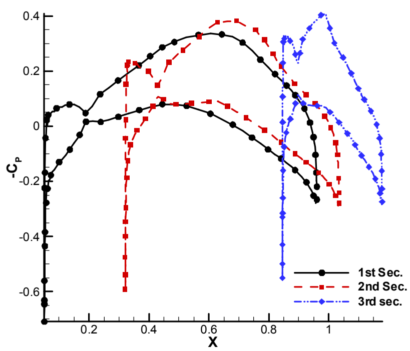

c) Optimum wing at the converged space

Fig. 4.18 Cp distributions along the wing span (1^{st} sec.= root, 2^{nd} sec.= 25%, 3^{rd} sec.= 85% of span)

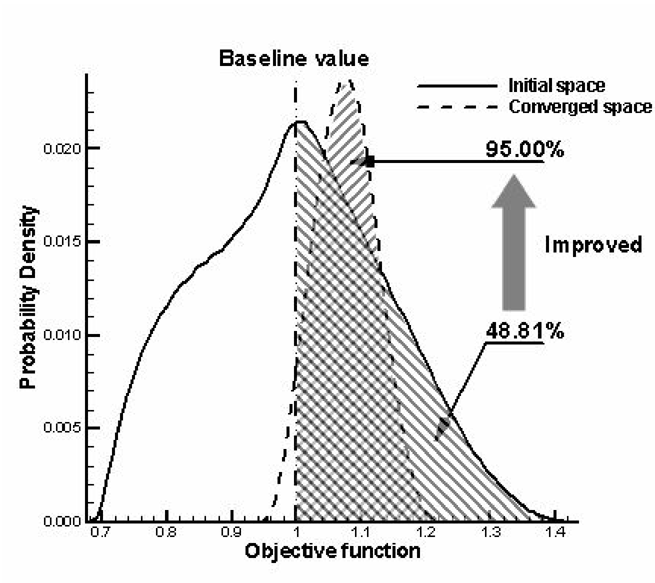

Fig. 4.19 PDF of the lift to drag ratio (M_∞=0.87)

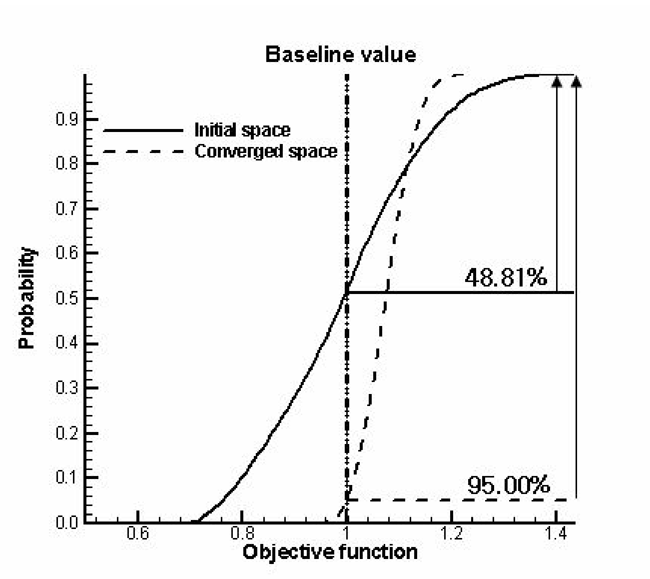

Fig. 4.20 CDF of the lift to drag ratio (M_∞=0.87)

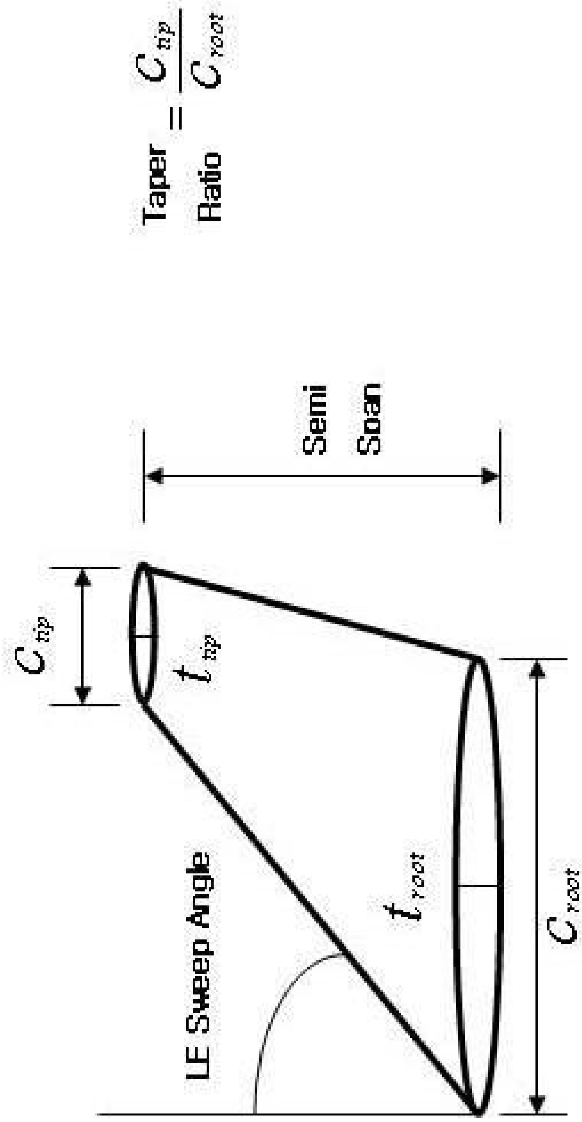

Fig. 4.21 Transonic wing geometry and design variables

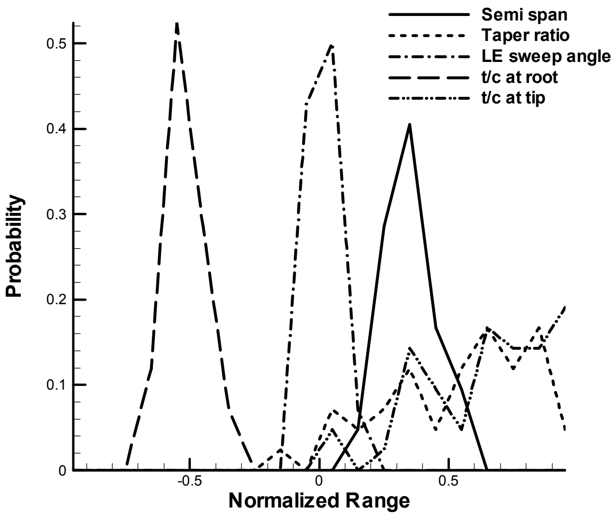

Fig. 4.22 Probability distribution of the initial design variables

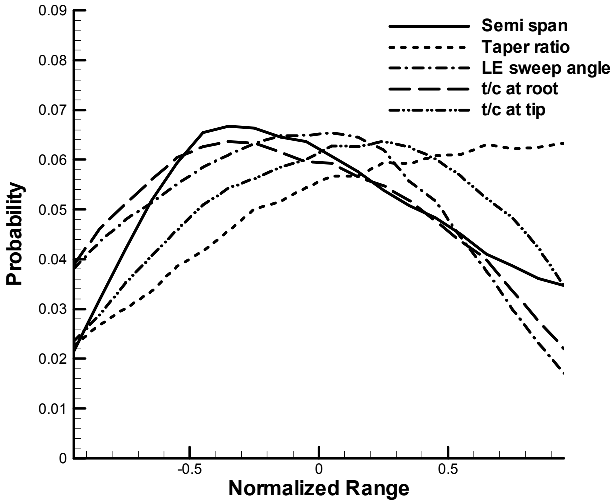

Fig. 4.23 Probability distribution of the converged design variables

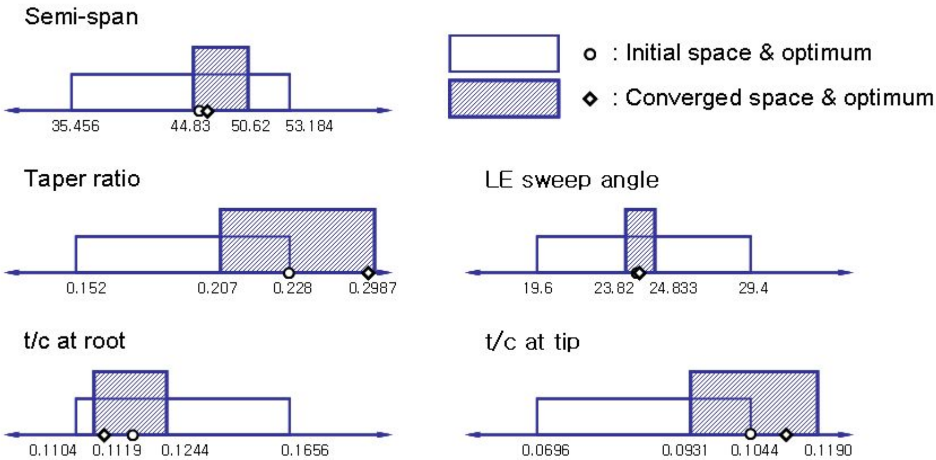

Fig. 4.24 Comparison of the design space (M_∞=0.75)

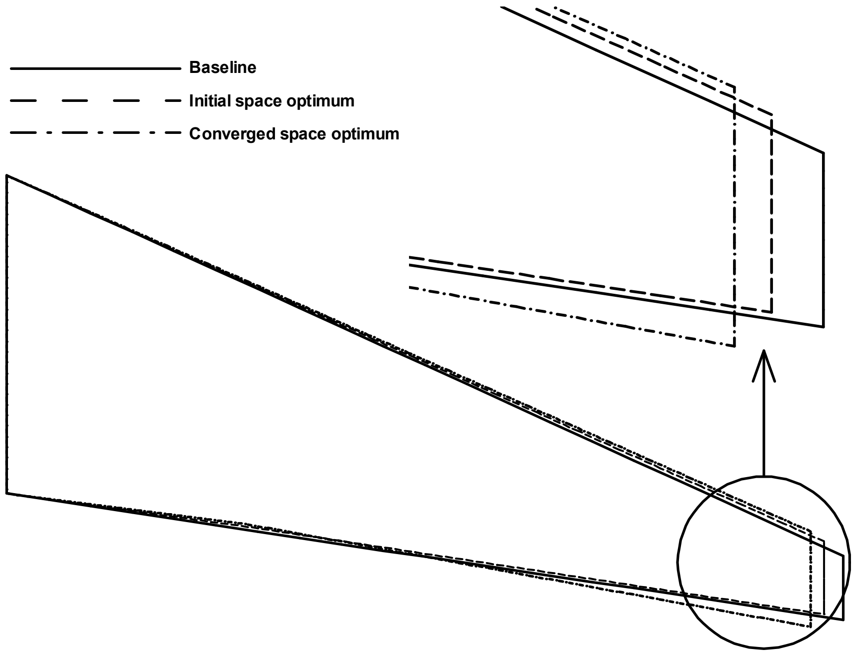

Fig. 4.25 Comparison of the transonic wing planform

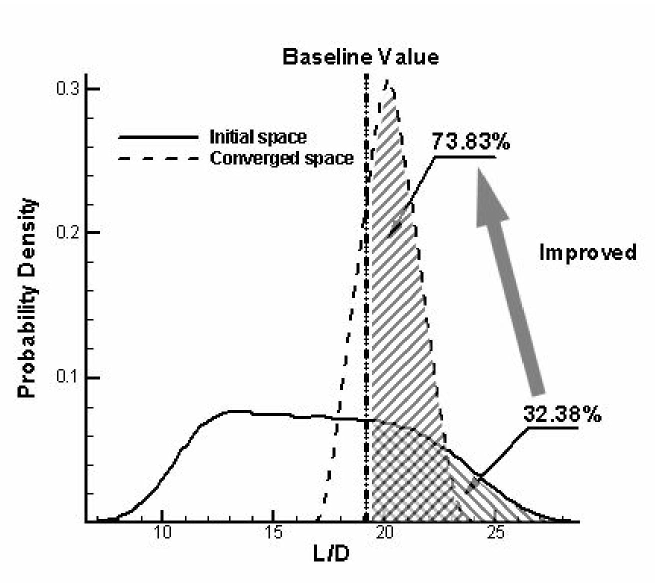

Fig. 4.26 PDF of lift to drag ratio (M_∞=0.75)

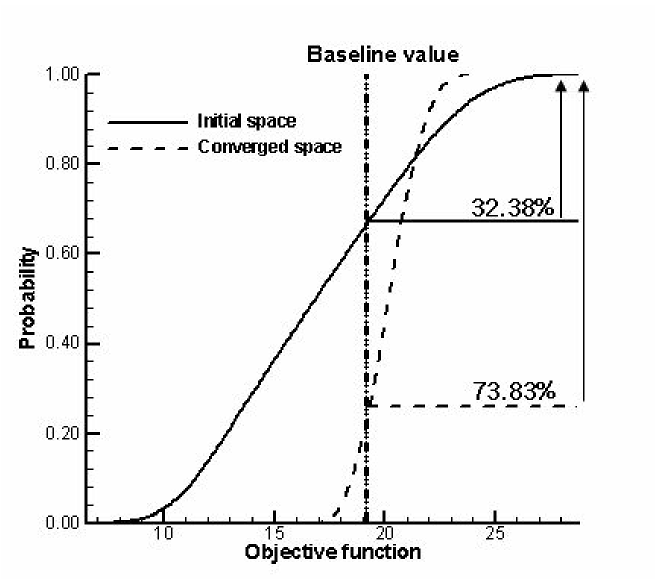

Fig. 4.27 CDF of lift to drag ratio (M_∞=0.75)

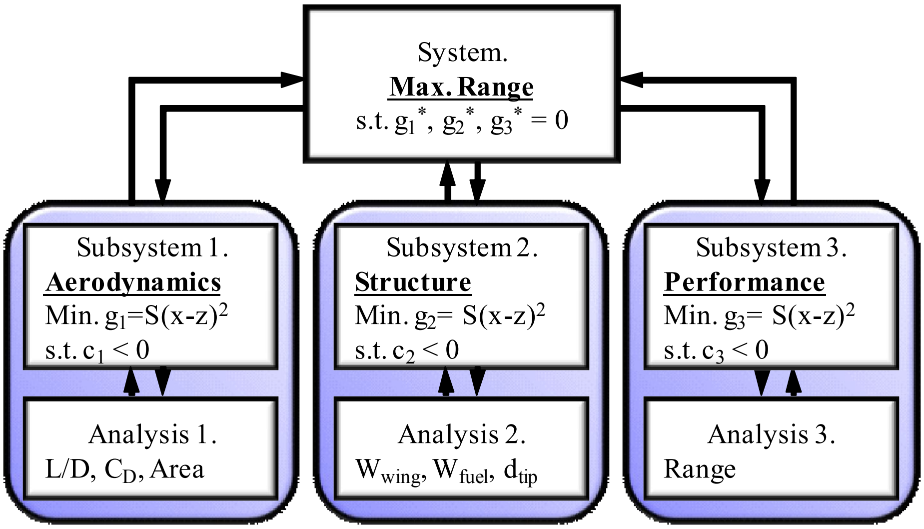

Fig.4.28 The structure of CO for wing design problem

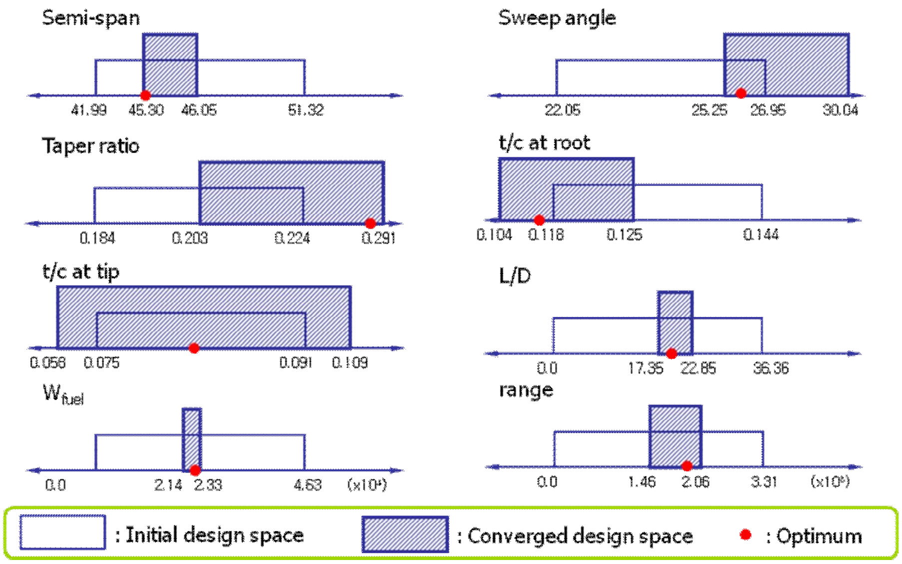

Fig. 4.29 Comparison of the design space (CO, M_∞=0.75)

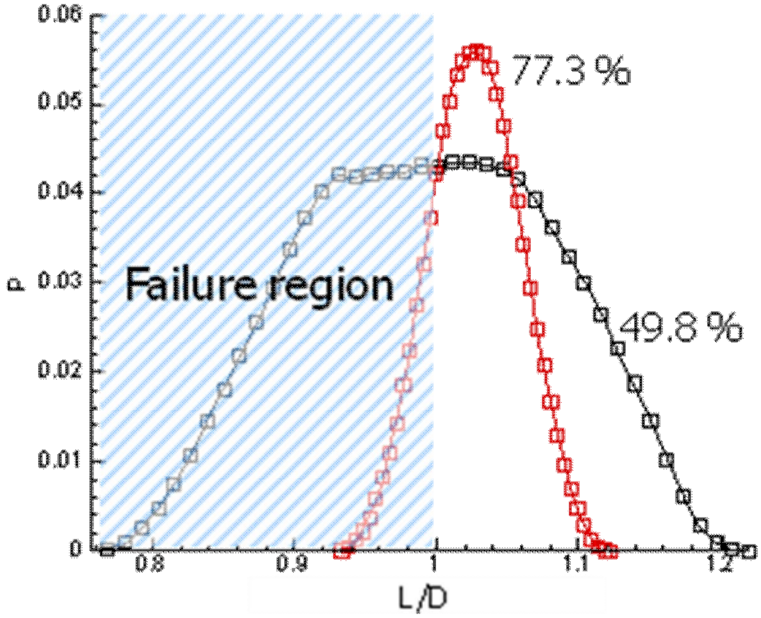

Fig. 4.30 PDF of lift to drag ratio (CO, M_∞=0.75)

Table 4.1 Design space and POS of the Goldstein function

	X1	X2	Optimum	POS(%)
Initial space	(-1~1)	(-0.5~1.5)	$f(-0.6,-0.4)^*$ $=30.0$	2.5298
Converged space	(-1.21~0.55)	(-1.92~0.18)	$f(0,1)^*$ $=3.0$	15.2562

Table 4.2 Design space and POS of the Branin function

	X1	X2	Optimum	POS(%)
Initial space	(-3~2)	(4~9)	$f(2,4)^*$ $=6.4482$	6.0865
Converged space	(-0.348~8.711)	(-1.457~7.565)	$f(\pi,2.275)^*$ $=0.3979$	30.4336

Table 4.3 Summary of the input & output variables

	X_1	X_2		F
System	z_1	n/a	z_2	n/a
Subsystem 1	x_1	x_2	y_1	n/a
Subsystem 2	x_1	n/a	y_1	f

Table 4.4 Design space and POS of the CO (Goldstein function)

	Z_1	Z_2	Optimum	POS(%)
Initial space	(-1.00 ~1.00)	(-1.00 ~1.00)	$f(0,-1)^*=3$	0.3160
Converged space	(-1.4876 ~0.8269)	(-2.0270 ~-0.4037)	$f(0,-1)^*=3$	34.9440

Table 4.5 Range of design variables at initial design space (M_∞=0.87)

Design Variables		Lower limit	Baseline	Upper limit
L.E. sweep angle (°)	Initial	30	35	40
	Converged	32.027		40.762
Aspect ratio	Initial	2.5	3	4.5
	Converged	3.606		4.158
Twist angle (°)	Initial	-5	-2.5	0
	Converged	-2.995		-2.423
Wing area (ft^2)	Initial	229.5	255	280.5
	Converged	253.27		274.15
Taper ratio	Initial	0.2162	0.2402	0.2642
	Converged	0.176		0.253
$Root_{Lower\ Skin}$ Thickness (inch)	Initial	0	0.1	0.2
	Converged	0.114		0.431
$Tip_{Lower\ Skin}$ Thickness (inch)	Initial	0	0.1	0.2
	Converged	0.087		0.407
$Root_{Upper\ Skin}$ Thickness (inch)	Initial	0	0.1	0.2
	Converged	0.117		0.380
$Tip_{Upper\ Skin}$ Thickness (inch)	Initial	0	0.1	0.2
	Converged	0.053		0.400

Table 4.6 Results of optimization (M_∞=0.87)

Design variables & Objective function	Baseline	Initial space optimum	Converged space optimum
L.E. sweep angle (°)	35	40	40.19
Aspect ratio	3.5	4.5	4.158
Twist angle (°)	-2.5	-2.84	-2.83
Wing area (ft^2)	255	255.02	262.88
Taper ratio	0.2402	0.2415	0.2219
$Root_{Lower\ Skin}$ Thickness (inch)	0.1	0.0353	0.2896
$Tip_{Lower\ Skin}$ Thickness (inch)	0.1	0.1164	0.2638
$Root_{Upper\ Skin}$ Thickness (inch)	0.1	0.1186	0.2622
$Tip_{Upper\ Skin}$ Thickness (inch)	0.1	0.2000	0.2406
L/D	37.79	48.28	44.75
ΔL/D(%)		**27.76**	**18.40**
Tip Displacement	**6.158e-002**	**1.113e-001**	**6.403e-002**

Table 4.7 Initial and converged design space (M_∞=0.75)

Design variables		Lower limit	Baseline	Upper limit
Semi span	Initial space	35.456	46.655	53.184
	Converged space	44.830		50.620
Taper ratio	Initial space	0.152	0.2	0.228
	Converged space	0.207		0.299
L.E. sweep angle	Initial space	19.6	24.5	29.4
	Converged space	23.820		24.833
t/c at root	Initial space	0.1104	0.1310	0.1656
	Converged space	0.1119		0.1244
t/c at tip	Initial space	0.0696	0.0830	0.1044
	Converged space	0.0931		0.1190

Table 4.8 Result of optimization (M_∞=0.75)

Design variables & Objective function	Baseline	Initial design space optimum	Converged design space optimum
semi-span (ft)	46.6550	45.5841	44.8299
Taper ratio	0.2	0.228	0.2987
sweep angle (deg)	24.5	24.1784	23.9414
t/c at root	0.131	0.1186	0.1125
t/c at tip	0.083	0.1044	0.1112
L/D	19.3620	20.7843	21.4693
ΔL/D (%)		**7.34**	**10.88**

Table 4.9 Range of design variables

Design Variables	Min.	Baseline	Max.
Span (ft)	41.989	46.655	51.320
Sweep angle (deg)	22.050	24.500	26.950
Taper ratio	0.184	0.204	0.224
t/c at wing root	0.118	0.131	0.144
t/c at wing tip	0.075	0.083	0.091

Table 4.10 Summary of variables for CO

	system	sub 1.	sub 2.	sub 3.
span	Z1	X1	X1	n/a
sweep	Z2	X2	X2	n/a
taper ratio	Z3	X3	X3	n/a
t/c root	Z4	X4	X4	n/a
t/c tip	Z5	X5	X5	n/a
L/D	Z6	Y1	n/a	X1
C_D	n/a	Y2	n/a	n/a
Area	n/a	Y3	n/a	n/a
W_{wing}	n/a	n/a	Y1	n/a
W_{fuel}	Z7	n/a	Y2	X2
d_{tip}	n/a	n/a	Y3	n/a
Range	F	n/a	n/a	Y1

Table 4.11 Comparison of initial & converged design spaces

	Initial space	Converged space
span	41.989 ~ 51.320	45.363 ~ 46.054
sweep	22.050 ~ 26.950	25.250 ~ 30.044
taper ratio	0.184 ~ 0.224	0.233 ~ 0.291
t/c root	0.118 ~ 0.144	0.104 ~ 0.125
t/c tip	0.075 ~ 0.091	0.058 ~ 0.109
L/D	0.000 ~ 36.361	17.355 ~ 22.851
W_{fuel} (10^4)	0.000 ~ 4.626	2.137 ~ 2.333
feasibility	0.1272 %	38.3769 %

Table 4.12 Comparison of the optimum values

	Initial space	Converged space
span	46.258	45.325
sweep	23.462	25.723
taper ratio	0.224	0.282
t/c root	0.124	0.110
t/c tip	0.089	0.084
Range	1768.8	1862.4
	6.8 %	12.4 %

4.2 DSE and Rearrangement of the Design space to Improve the Feasibility with Reliability Index

Earlier proposed design space rearrangement method based on Chebyshev inequality condition is performed along with solid line procedure as shown in Fig. 4.31. This early proposed method is relatively simple iterative algorithm, but probabilistic evaluation and rearrangement of the design space can be successively done by using Chebyshev inequality. Even though probabilistic distributions of the design variables are absolutely unknown, Chebyshev inequality condition for uniform distributed random variables provides reasonable basis for the rearrangement of the design space. However, if the feasible region doesn't exist within the initial design space, mean and deviation values of the feasible region cannot exist. As a result, Chebyshev inequality cannot be applied. Furthermore, if there exists very small feasible region within the initial design space, iteration number will increase unnecessarily to find converged design space. To overcome these problems, reliability index which includes geometric information among the whole design points and constraint functions has been introduced. In Fig. 4.31, hatched box shows replaced procedure to obtain mean and deviation using the reliability index based approach. Even though feasible region does not exist within the design space, mean and deviation value of the design variables could be evaluated and determined efficiently with newly proposed method.

4.2.1 Test Functions

To compare reliability index (RI) based method to Chebyshev inequality (CI) based method, same test functions those are Goldstein function and Branin function are adopted with same problem. In addition, additional test case to validate the ability of RI based method is exploited starting on the unfeasible region: Chebyshev inequality based method cannot perform DSE and rearrangement.

4.2.1.1 Goldstein function

- **Start on feasible region**

The design optimization problem was performed using the both formal design space defining method and the RI based method in this study concerned with the initial design space setting x_1 and x_2 into (-1, 1) and (-0.5, 1.5). Fig. 4.32 shows the procedure of automatic rearrangement of the design space and it is identified that the RI based method includes more feasible region than the CI based method does when observing the 2nd design space.

As explained in numerical approach, the former method uses only information of the feasible region in the design space and the newly proposed method uses approximate information of global feasible region so that the position of the center (mean value) of the new method is more close to the center of the whole feasible region. Therefore, the 2nd design space is defined that the new method includes more feasible region comparing with the CI based method.

In Fig. 4.33, the five iterations are required to converge and the RI based method is more efficient about 30%. POS is also increased from 2.53% to

14.10% (table 4.13). Since both proposed methods are subjected to the same constraint function and have same objective, same number of function evaluations has been required for single sampling point in both methods. At every rearrangement iteration loop, same number of total sampling points has been used to carry out Monte-Carlo simulation, so total number of function evaluations per iteration is equal. Hence, additional algebraic calculations to obtain reliability index and temporary mean are required to newly proposed method. But it is relatively small and negligible in comparison with function evaluation via Monte-Carlo simulation.

So to speak, it is confirmed that the design space which contains the entire feasible region is automatically rearranged with relatively low computation than CI based method. While optimization is performed in the initial design space, only the local minimum $f(-0.6,-0.4) = 30$ is found but in the converged design space which contains the global optimum $f(0,-1) = 3$, higher quality of optimal solution can be acquired.

■ **Start on infeasible region**

This case is the same design optimization problem but only the initial design space is different as setting x_1 and x_2 into 0 ~ 1(table 4.14). Because there is no feasible region in this space, automatic rearrangement of the design space is impossible with the CI based method. However, in the RI based method, rearrangement of the design space is possible because of the reliability index which reveals information of the whole feasible region. As shown in Fig. 4.34, the RI based method has information that the position of the whole feasible region in the initial design space is located in the lower left so that movement to the 2^{nd} design space is possible. For this reason, even though the designer defines the wrong design space due to the lack of knowledge or due to the mistake, the RI based method proposed in this study can automatically rearrange the design space.

Fig. 4.35 shows the feasibility (%) of the design space for this case and shows the similar iteration number with above case. Moreover, there was no optimum in the initial design space but in the converged design space, it is found that two optima $f(0,-1) = 3$ and $f(-0.6, -0.4) = 30$ exist

4.2.1.2 Branin Function

- **Start on feasible region**

This case is also same problem with CI base method. Comparing with CI based method, it has been converged into almost same design space as shown in Fig. 4.36 and table 4.15 and required iteration numbers decrease about 30% (see Fig. 4.37)

- **Start on infeasible region**

Starting design space of this case is ($-5<x1<0$, $5<x2<10$) and it is infeasible region (see Fig. 4.38). Just like Goldstein function case, RI based method can find converged space which has same improved POS and design variables range with starting on feasible region case, as described in table 4.16.

Furthermore, location and variable range of the starting design space is not a problem for RI based method as shown in Fig. 4.39. All test cases converged same design space, regardless of starting location (see table 4. 17).

According to the above results, it is confirmed that RI based method is useful and robust for DSE and rearrangement of the design space.

4.2.1.3 Collaborative Optimization (CO) of Goldstein Function with Reliability Index

- **<u>Start on feasible region</u>**

In case of CO, definition of design optimization problem is same as section 4.1.1.3. The initial design space is summarized in table 4.18. If the range of the interdisciplinary variable z_2 (y_1) is specified like in the table 4.18, the range of y_1 in the subsystem 1 becomes to -2 ~ 2. Because it includes the initial specified range -1 ~ 1, both the system and the subsystems have the common region and CO can be performed without any trouble to find the optimal solution. However, the design space does not contain the entire feasible region therefore; there is possibility that a higher quality of optimum solution could exist in the feasible region outside of the design space.

Fig. 4.40 shows the result of performing design space exploration in the z-space which consists of the system variable. Comparing with the former MDF result(sec 4.1.1.1 and 4.2.1.1), it is confirmed that the design space of this case is specified as a larger one. The reason is estimated that the system does not deal with x_1, x_2 variables directly but indirectly as z_1, z_2 ($y_1=x_1+x_2$) variables. As a result, the design space is converged to a larger one than the x_1 and x_2 of former case.

Fig. 4.41 shows the feasibility (%) of the design space of this case and total 7 iterations were performed. It needs a little more iterations than the former examples of RI based method for Goldstein function and this is because the system does not use feasible region information directly but presume the feasible region from information of subsystem design space. Also, high feasibility close to 0.6 is caused by regarding the common design space of the subsystems as the feasible region.

■ **Start on infeasible region**

In this case, there is no feasible region in the initial design space and the range of the design variables (z_1, z_2, x_2) is varied from 1 to 2 (table 4.19). There is no common space between the interdisciplinary variables (y_1) and z_2 because y_1 is 2 ~ 4 in this range. Therefore, it is impossible to perform CO. However, if the design space is rearranged by the proposed method in this work, the design optimization can be executed properly due to existence of the common space between y_1 and z_2.

Fig. 4.42 shows the procedure of design space automatic rearrangement of this case. Just like above case, it is found that the design space includes the whole feasible region. Total 17 iterations have been performed in this procedure. Because the initial design space does not include any feasible region, about 7 iterations were consumed to find this feasible region. (Fig. 4.43)

Comparing with results of section 4.2.1.1, it took more iteration to find the feasible region and this is also caused by the lack of direct information from the feasible region. By adding the procedure of exploring the feasible region, the range of z_1 variable presumed largely and consequently, the larger design space is defined than above case and the feasibility is confirmed as a low value 0.35.

4.2.2 CO of the Transonic Wing with Low Fidelity Analysis Using RI Based Method

This section's CO problem is under same condition with section 4.1.2.3. To consider the efficiency of design procedure, artificial neural network (ANN) model has been constructed. In this study, ANN model consists of three layers – input, output and hidden layers.

Since single analysis of this study requires relatively short time than other CFD analysis code based on Euler or Navier-Stokes governing equations, 5^5 experimental points have been used for training of ANN model to obtain improved result. ANOVA results of the constructed model are shown in table 4.20. As shown in table 4.20, maximum root mean square error (RMSE) is less than 0.02415 and minimum R^2 is more than 0.995. According to above result, constructed model ensures reliable prediction of the objective and constraint functions. Moreover, sensitivity of the defined design variables to the objective and constraints function is shown in Fig. 4.44. It is clear that the Semi-span length is the most effect on the whole response, but t/c at tip is the least. Even so, it can be confirmed that L/D and W_{fuel} increase or decrease according to the change of t/c at tip. As stated above, defined design variables are adequate for aircraft wing design problem. SQP method that is one of the widely used gradient based optimization method has been applied to efficiently find optimal solution.

Fig. 4.45 shows the converged design space by the proposed method. White rectangles are the initial design space, and hatched rectangles mean the converged one. Circles on horizontal axis indicate optimum point in the converged design space. The design space of semi-span, W_{fuel}, L/D, and range are shrunk comparing with the initial design space, and those of taper ratio and t/c at tip are extended. The design space of the sweep angle and t/c at root are moved toward upper bound and lower bound of the initial design space, respectively. With above results, flexibility and degree of freedom to rearrange the design space of the proposed method can be verified. In general, as rearrangement iteration progressed, other design space exploration and rearrangement method moved toward biased direction. Table 4.21 summarizes optimal points obtained in the initial and the converged design space. The objective function, range is improved by 4.6% in the initial design space, but by 8.2% in the converged design space. However, due to the instable characteristic of CO, W_{fuel} increases by 2.0% in the initial design space and 3.8% in the converged design space. Since each discipline is absolutely disconnected on subsystem level, matching condition must be introduced on system level optimization. So, equality constraint necessarily required on system level and it is very difficult to directly concern for most gradient based optimization algorithm. Hence, converts equality constraint to separated inequality constraints and deals with them. On this process, there is the potential that the opposite tolerances of separated inequality conditions produce unpredictable error and accumulate it. Even though optimal result violates W_{fuel} constraint, its amount is relatively small as compared with improvement of objective function. Considering instable characteristic of CO, this result can be acceptable.

From these results, it can be confirmed that have the ratio of infeasible region in the initial design space is more than those in the converged design space for semi-span, W_{fuel}, L/D, and range. In case of t/c at root, optimal point is laying on the outside of the initial design space, and the design space obtained from this proposed method offers the opportunity searching for better solution than optimum in the initial design space.

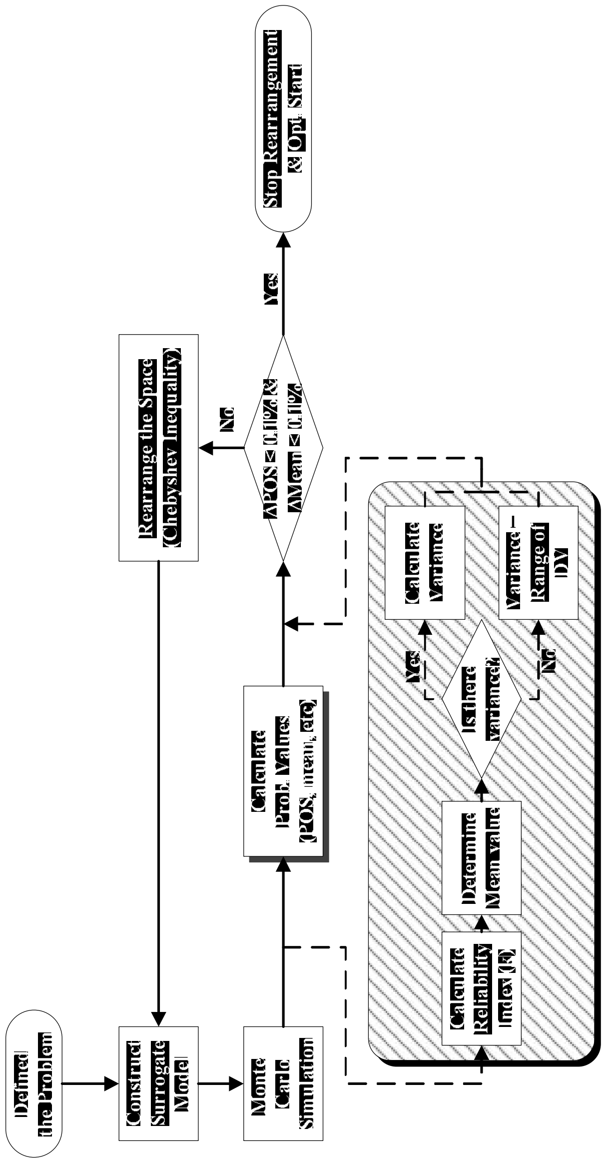

Fig. 4.31 Flow chart of the automatic design space rearrangement method

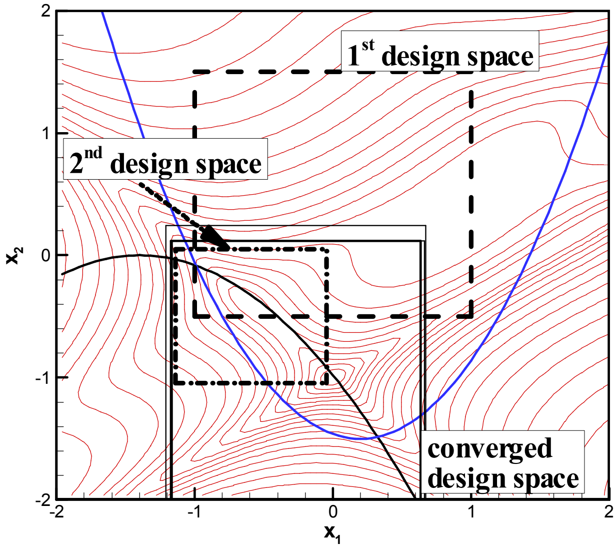

Fig. 4.32 Result of Goldstein function with RI

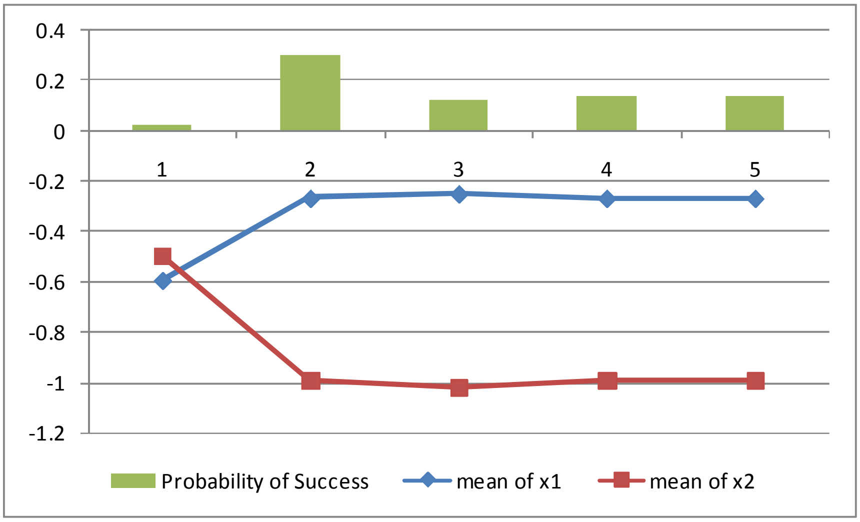

Fig. 4.33 Convergence history of Goldstein function with RI

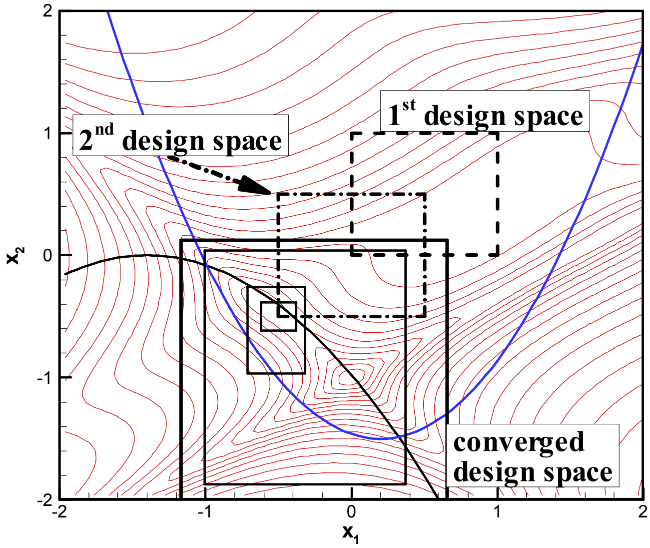

Fig. 4.34 The procedure of automatic rearrangement of the design space with RI based method

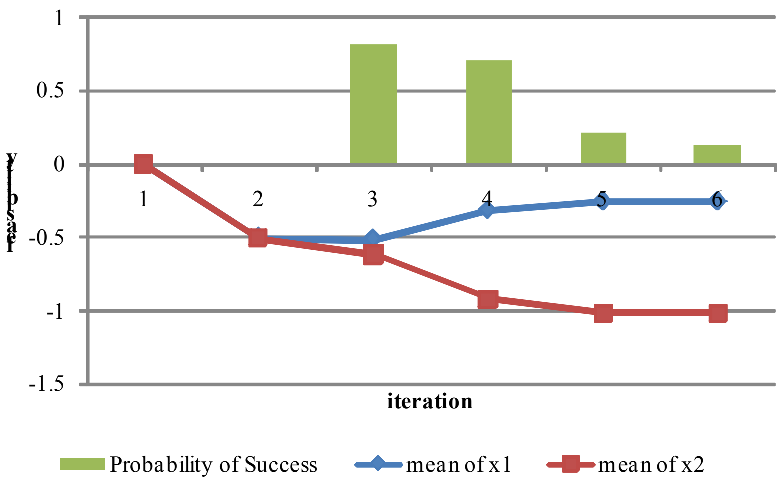

Fig. 4.35 The feasibility of the design space with RI based method

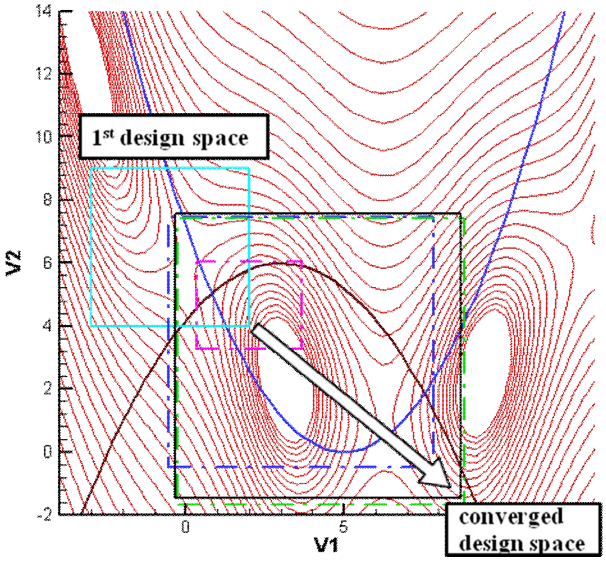

Fig. 4.36 The procedure of automatic rearrangement of the design space with RI based method for Branin function

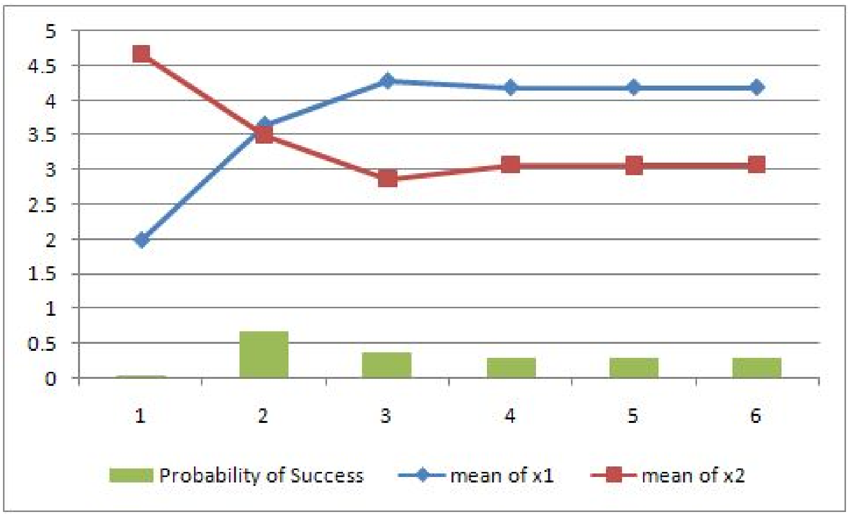

Fig. 4.37 The feasibility of the design space with RI based method for Branin function

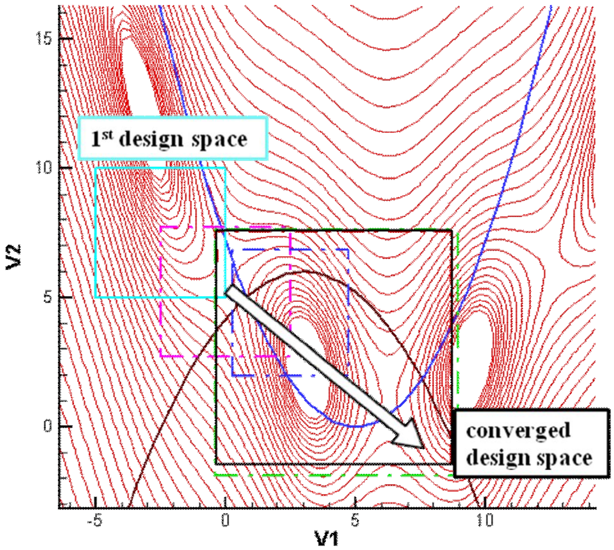

Fig. 4.38 The procedure of automatic rearrangement of the design space with RI based method for Branin function (start on infeasible region)

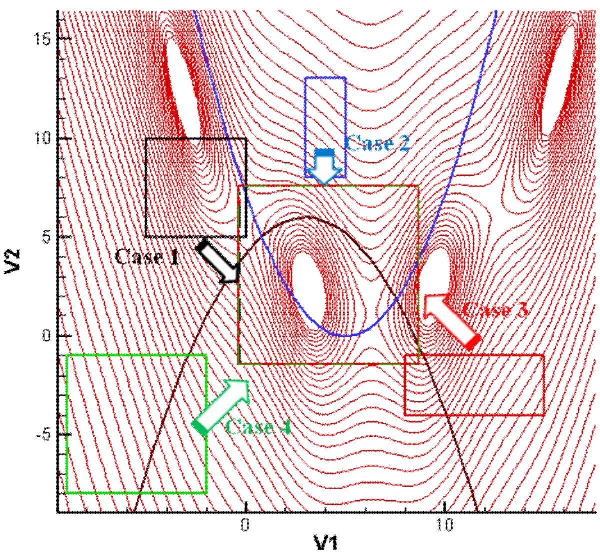

Fig. 4.39 Converged design spaces with respect to starting location

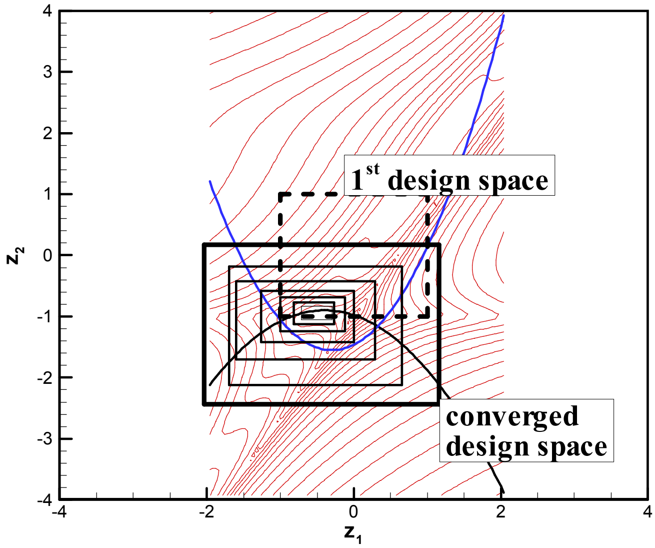

Fig. 4.40 The procedure of automatic rearrangement of the design space

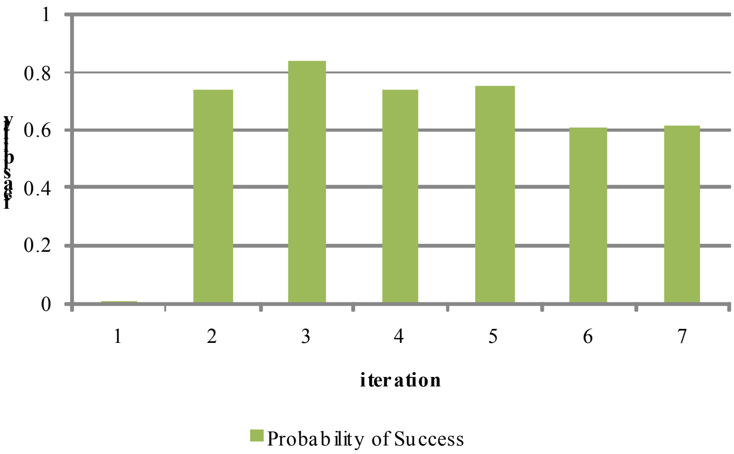

Fig. 4.41 The feasibility of the design space

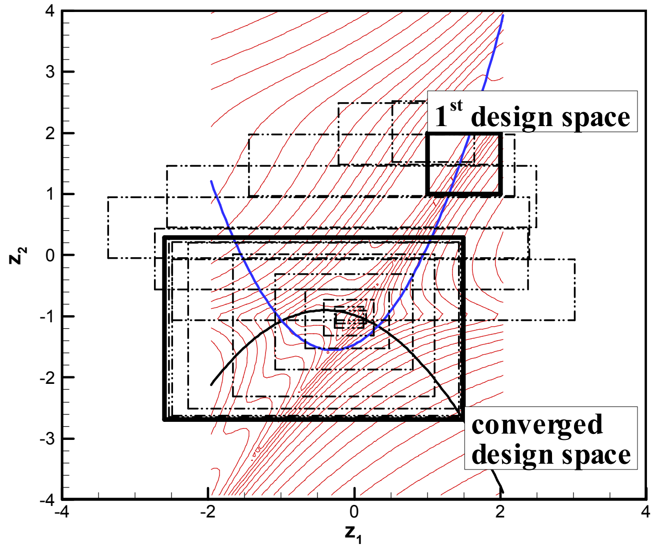

Fig. 4.42 The procedure of automatic rearrangement of the design

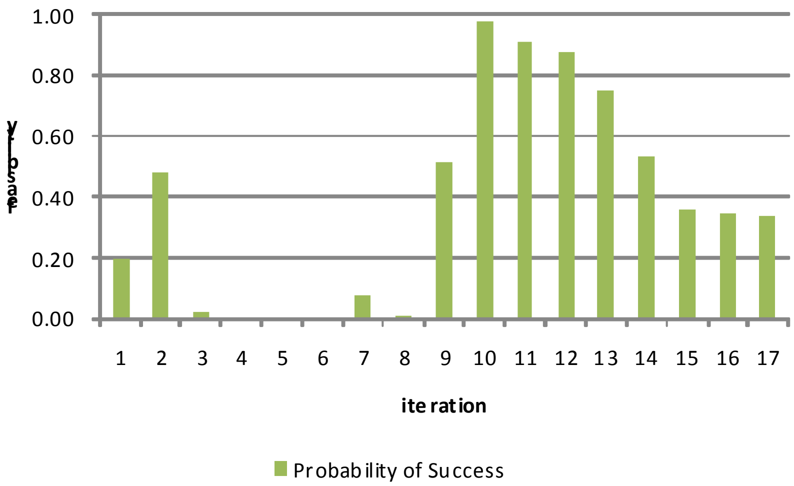

Fig. 4.43 The feasibility of the design space

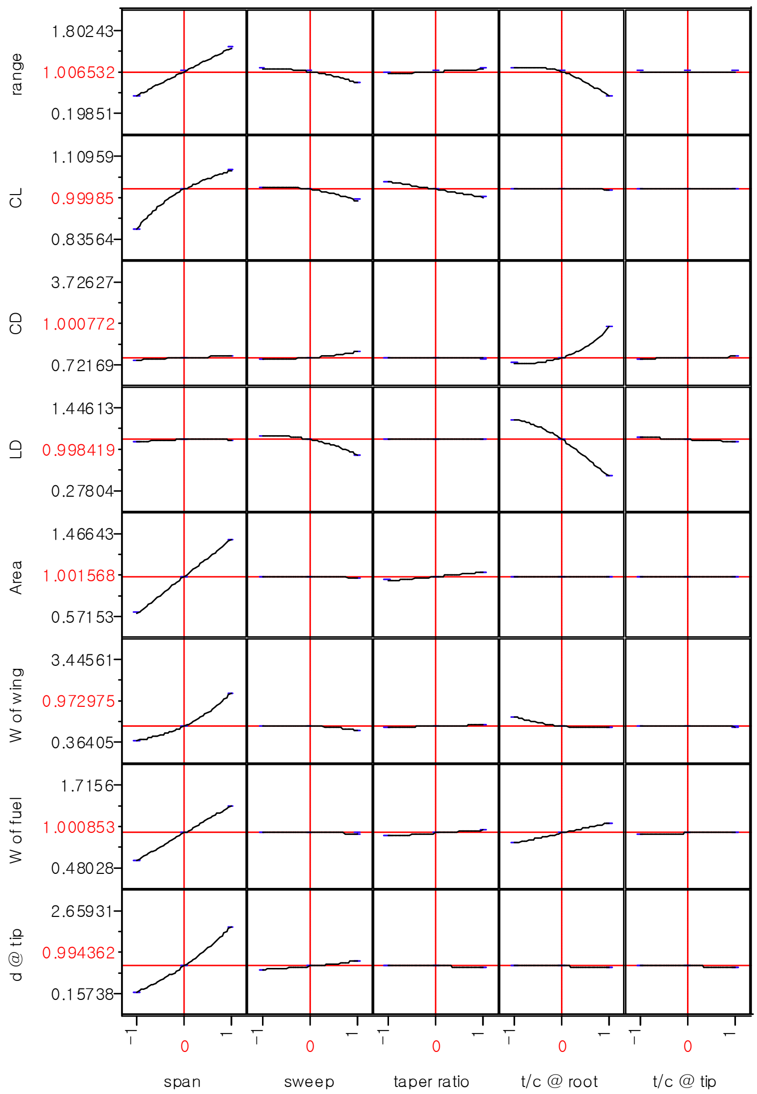

Fig. 4.44 Sensitivity analysis of selected design variables to the objective and constraints functions

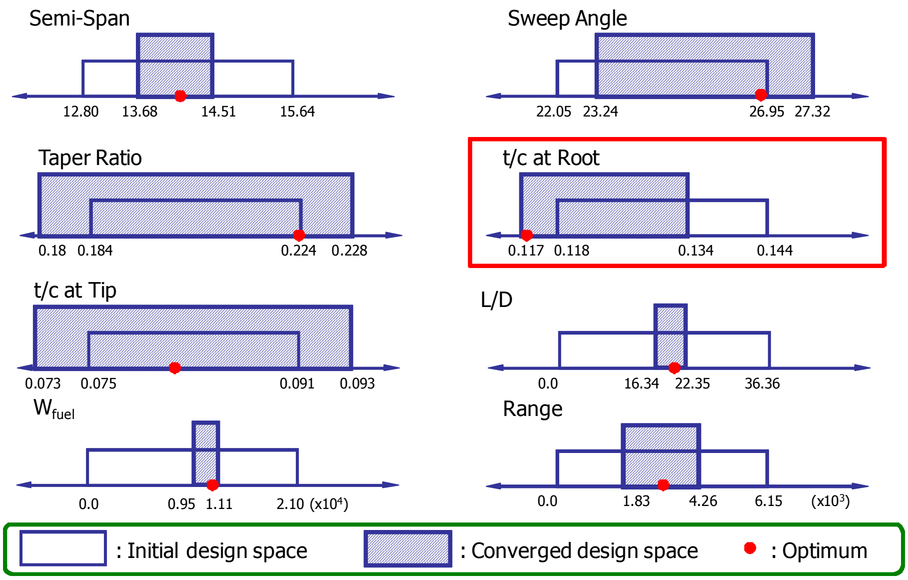

Fig. 4.45 The initial and converged design space and optimal solution in the converged design space

Table 4.13 Design space and POS of the Goldstein function with RI based method (start on feasible region)

	X1	X2	POS(%)
Initial space	(-1, 1)	(-0.5, 1.5)	2.5298
Converged space	(-1.17, 0.63)	(-2.10, 0.12)	14.0962

Table 4.13 Design space and POS of the Goldstein function with RI based method (start on infeasible region)

	X1	X2	POS(%)
Initial space	(0, 1)	(0, 1)	0.
Converged space	(-1.17, 0.66)	(-2.14, 0.12)	13.7216

Table 4.15 Design space and POS of the Branin function with RI based method (start on feasible region)

	X1	X2	POS(%)
Initial space	(-3, 2)	(4, 9)	6.0865
Converged space	(-0.349, 8.711)	(-1.456, 7.565)	30.4354

Table 4.16 Design space and POS of the Branin function with RI based method (start on infeasible region)

	X1	X2	POS(%)
Initial space	(-5, 0)	(5, 10)	0.
Converged space	(-0.348, 8.711)	(-1.456, 7.564)	30.4390

Table 4.17 Comparison of the initial and converged design space with respect to the starting location

Case	Total Iter.	Init. Space	Conv. Space
1	6	-5<x1<0 5<x2<10	-0.348<x1< 8.711 -1.456<x2< 7.564
2	7	3<x1<5 8<x2<13	-0.349<x1< 8.711 -1.456<x2< 7.564
3	7	8<x1<15 -4<x2<-1	-0.349<x1< 8.711 -1.456<x2< 7.565
4	8	-9<x1<-2 -8<x2<-1	-0.349<x1< 8.711 -1.456<x2< 7.564

Table 4.18 the range of the design variables (system and subsystems)

	variables	min.	max.
System	z1 z2	-1 -1	1 1
Subsystem 1.	x1 x2	-1 -1	1 1
Subsystem 2.	x1 y1	-1 -1	1 1

Table 4.19 The range of the design variables (system and subsystems)

	variables	min.	max.
System	z1	1	2
	z2	1	2
Subsystem 1.	x1	1	2
	x2	1	2
Subsystem 2.	x1	1	2
	y1	1	2

Table 4.20 ANOVA results of constructed ANN model.

	RMSE	R2
Range	0.0141982	0.9984
L/D	0.01730317	0.9976
C_L	0.00741811	0.9996
C_D	0.02414505	0.9953
Area	0.0047938	0.9998
W_{wing}	0.01296684	0.9987
W_{fuel}	0.00919147	0.9993
d_{tip}	0.00589646	0.9997

Table 4.21 Results of the design optimization in the initial and converged design space.

	Baseline	Initial Design Space	**Converged Design Space**
Semi-span (m)	14.220	14.190	14.113
Sweep angle (deg)	24.50	25.324	26.218
Taper ratio	0.204	0.210	0.220
t/c root	0.131	0.123	0.118
t/c tip	0.0830	0.0878	0.0845
L/D	18.181	19.014	19.681
W_{fuel} (kg)	10491.592	10704.780	10895.289
Range (km)	3068.022	3208.589	3321.190
Improvement of Range	0 %	4.58%	**8.25%**

4.3 Discussion

In this chapter, the Chebyshev inequality based method and the reliability index based method for the design space exploration and rearrangement have been proposed, and have been applied to a number of the test cases for investigation of the utility.

For the Goldstein function and the Branin function, the initial design spaces of the both proposed methods have converged into the equivalent design space under the same starting condition. However, RI based method requires fewer number of iterations to find the converged design space in the majority of cases. Moreover, RI based method can find the converged design space under the starting condition on the infeasible region. For the aerodynamic-structural multidisciplinary design optimization of the aircraft wing, both methods have successfully converged into the higher feasible design space, also. Even the case of CO of the transonic wing, appropriate design space can be found using the proposed methods.

Since the geometrical information included in the RI based method, more appropriate mean and deviation value of the feasible region can be obtained regardless of the location and size of the initial design space, and it promotes the efficiency and the robustness of the rearrangement process. Though, starting on the infeasible region, unexpected additional iteration is required to rearrange the design space into the feasible region. It is caused by the lack of information of the feasible region at the initial design space. Due to the unclear mean and deviation value of the feasible region, the initial design space must be moved to the feasible direction by the size of the initial design space, and it aggravates the convergence efficiency.

Consequently, it is verified that the proposed methods have the ability and the utility of the systematic rearrangement of the design space.

Chapter 5. Conclusions and Future Works

In this study, design space exploration and rearrangement method to include more feasible region in the design process is suggested. To examine the validity of this method, two design variable function problem with the initial design space which has feasible region and infeasible region is applied to MDF and CO problems. Moreover, this method is applied to CO problem of the aircraft wing which three disciplines such as aerodynamics, structure and performance are combined to show its utility for complex and practical problem. As a result, the following conclusions can be made;

(1) It is confirmed that whole feasible region can be covered with this method by several design space rearrangement process. Reliability index proposed an appropriate mean value as the indicator for searching feasible region. In both MDF and CO application, this method suggested a design space which includes valid feasible region though it did not have any feasible region in the initial design phase.

(2) This approach is expanded into the multi-level application and it can mitigate the difficulty for defining the design space with incomplete information of a system and subsystems (disciplines). Each discipline searches for the design space satisfying its own constraints and the system controls the design space from subsystems' design space. This procedure plays a part in the supplementation of incomplete information of a system and subsystems.

(3) The proposed method in this study offers higher possibility to obtain the global optimum. As appears out of Goldstein and aircraft wing problems, this method is identified to suggest the superior optimum value in the rearranged design space to the one from initial design space as more feasible region is included. In case of practical aircraft wing design problem, the objective function range achieved 8% performance improvement in the converged new design space while 4% performance improvement is shown in the initial design space.

Although accomplished sturdy about the design space exploration and rearrangement, there are numbers of future works as ever.

The most studies are concentrating on the closed and convex type design problems to avoid the complexity of the MDO problem. Though, in the practical design problem, there exist the design problem which has unconnected multiple feasible region. For this case, established study cannot provide the robust and reliable DSE and rearrangement strategy. Hence, proposed method should be extended to consider the unclosed and concave design problems.

And also, total efficiency of the DSE framework should be reconsidered to improve convergence efficiency of the rearrangement process. Appropriate DOE method is required to reduce building time and cost of surrogate model which take the most of calculation time and cost.

Reference

[1] Sobieszczanski-Sobieski, J. and Haftka, R. T., “Multidisciplinary Aerospace Optimization: Survey of Recent Developments,” AIAA Paper 96-0711, Jan. 1996.

[2] Fabrycky, W. J. and Blanchard , B. S., *Life-Cycle Cost and Economic Analysis*, Prentice Hall, Englewood Cliffs, NJ, 1991.

[3] Mavris , D. N., Delaurentis, D. A., Bandte, O. and Hale, M.A., “A Stochastic Approach to Multi-disciplinary Aircraft Analysis and Design,” AIAA Paper, AIAA 98-0912, January 1998.

[4] Arora, J. S., *Introduction to Optimum Design*, McGraw-Hill, 1989.

[5] Giles, M. B. and Drela, M., “Two-Dimensional Transonic Aerodynamic Design Method,” *AIAA Journal*, Vol. 25, No. 9, 1987, pp. 1199-1206.

[6] Henne, P. A., “Inverse Transonic Wing Design Method.” *Journal of Aircraft*, Vol. 18, No. 1, 1981, pp. 121-127.

[7] Takanashi, S., “Iterative Three-Dimensional Transonic Wing Design Using Integral Equations,” *Journal of Aircraft*, Vol. 22, No. 8, 1985, pp. 655-660.

[8] Barger, R. L. and Brooks, C. W., “A Streamline Curvature Method for Design of Supercritical and Subcritical Airfoils,” NASA TN D-7770, 1987.

[9] Campbell, R. L., and Smith, L. A., “A Hybrid Algorithm for Transonic Airfoil and Wing Design,” AIAA Paper, AIAA 87-2552.

[10] Malone, J. B., Vadyak, J. and Sankar, L. N., “Inverse Aerodynamic Design Method for Aircraft Components,” *Journal of Aircraft*, Vol. 24, No. 2, 1987, pp. 8-9.

[11] Malone, J. B., Narramore, J. C. and Sankar, L. N., "Airfoil Design Method using the Navier-Stokes Equations," *Journal of the Aircraft*, Vol. 28, No. 3, 1991, pp. 216-224.

[12] Santos, L. C. and Sankar, L. N., "A Hybrid Inverse Optimization Method for the Aerodynamic Design of Lifting Surfaces," AIAA Paper, AIAA 94-1895.

[13] Van Egmond, J. A., "Numerical Optimization of Target Pressure Distributions for Subsonic and Transonic Airfoils Design," Computational Methods for Aerodynamic Design (Inverse) and Optimization, AGARD 463, Ref. 17, March 1990.

[14] Obayashi, S. and Takanashi, S., "Genetic Optimization of Target Pressure Distributions for Inverse Design Methods," *AIAA Journal*, Vol. 34, No. 5, 1996, pp. 881-886.

[15] Kim, H. J. and Rho, O. H., "Dual-Point Design of Transonic Airfoils Using the Hybrid Inverse Optimization Method," *Journal of Aircraft*, Vol. 34, No. 5, 1997, pp. 612-618.

[16] Kim, H. J. and Rho, O. H., "Aerodynamic Design of Transonic Wings Using the Target Pressure Optimization Approach," *Journal of Aircraft*, Vol. 35, No. 5, 1998, pp. 671-677.

[17] Ahn, T. S., Kim, H. J., Kim, C., and Rho, O. H., "Inverse Design of Transonic Wings Using Wing Planform and Target Pressure Optimization," *Journal of Aircraft*, Vol. 38, No. 4, 2001, pp. 644-652.

[18] Hicks, R. M. and Henne, P. A., "Wing Design by Numerical Optimization," *Journal of Aircraft*, Vol. 15, No. 7, 1978, pp. 407-412.

[19] Jameson, A., Pierce, N. A., and Martinelli, L., "Optimum Aerodynamic Design using the Navier-Stokes Equations," AIAA Paper, AIAA 97-0101.

[20] Reuther, J. J., Jameson, A., Alonso, J. J., Rimlinger, M. J., and Saunders, D., "Constrained Multipoint Aerodynamic Shape Optimization Using an Adjoint Formulation and Parallel Computers, Part 1," *Journal of Aircraft*, Vol. 36, No.1, 1999, pp. 51-60..

[21] Quagliarella, D. and Cioppa, A. D., "Genetic Algorithms applied to the Aerodynamic Design of Transonic Airfoils," AIAA Paper, AIAA 94-1896-CP.

[22] Yamamoto, K. and Inoue, O., "Application of Genetic Algorithm to Aerodynamic Shape Optimization," AIAA Paper, AIAA 95-1650.

[23] Cao, H. V. and Blom, G. A., "Navier-Stokes/Genetic Optimization of Multi-Element Airfoils," AIAA Paper, AIAA 96-2487.

[24] Oyama, A., Obayashi, S., and Nakahashi, K., "Transonic Wing Optimization using Genetic Algorithm," AIAA Paper, AIAA 97-1854.

[25] Ahn, J. K., Kim, H. J., Lee, D. H., and Rho, O. H., "Response Surface Method for Aircraft Design in Transonic Flow," *Journal of Aircraft*, Vol. 38, No. 2, 2001, pp. 231-238.

[26] Yee, K., Kim, Y. and Lee, D. H., "Aerodynamic Shape Optimization of Rotor Airfoils Undergoing Unsteady Motion," AIAA Paper, AIAA 99-3107.

[27] Chen, H.H., Chang, K.C., Tzong, T., and Cebeci, T., "Aeroelastic Analysis of Wing and Wing/Fuselage Configurations," AIAA Paper 98-0907, Jan. 1998.

[28] Newsome, R.W., Berkooz, G., and Bhaskaran, R., "Use of Analytical Flow Sensitivities in Static Aeroelasticity," *AIAA Journal*, Vol. 36, No. 8, 1998, pp. 1537-1540.

[29] Li, G., and Grandhi, R., "Accuracy and Efficiency Improvement of Response Surface Methodology for Multidisciplinary Design Optimization," AIAA Paper 2000-4715, Sept. 2000.

[30] Samareh, J. A., “Multidisciplinary Aerodynamic-Structural Shape Optimization Using Deformation (MASSOUD),” AIAA Paper 2000-4911, Sept. 2000.

[31] Burgee, S., Guinta, A. A., Balalbanov, V., Grossman, B., Mason, W. H., Narducci, R., Haftka, R. T., and Watson, L. T., “A Coarse-Grained Parallel Variable-Complexity Multidisciplinary Optimization Paradigm,” *The International Journal of Supercomputer Applications and High Performance Computing*, Vol. 10, No. 4, 1996, pp. 269-299.

[32] Sevant, N.E., Bloor, M.I.G., and Wilson, M.J., “Cost-Effective Multipoint Design of a Blended HSCT,” AIAA Paper 98-2785, June 1998.

[33] Maute, K., Nikbay, M., and Farhat, C., “Coupled Analytical Sensitivity Analysis and Optimization of Three-Dimensional Nonlinear Aeroelastic Systems,” *AIAA Journal*, Vol. 39, No. 11, 2001, pp. 2051-2061.

[34] Martins, J.R.R.A., Alonso, J.J., and Reuther, J.J., “High-fidelity aerostructural design optimization of a supersonic business jet.” *Journal of Aircraft*, Vol. 41, No. 3, 2004, pp. 523-530.

[35] Geuzaine, P., Brown, G., Harris, C., and Farhat, C., “Aeroelastic Dynamic Analysis of a Full F-16 Configuration for Various Flight Conditions,” *AIAA Journal*, Vol. 41, No. 3, 2003, pp. 363-371.

[36] Nemec, M., and Zingg, D.W., “Multipoint and Multi-Objective Aerodynamic Shape Optimization,” AIAA Journal, Vol. 42, No. 6, 2004, pp. 1057-1065.

[37] Kim, Y., Kim, J., Jeon, Y., Bang, J., Lee, D.H., Kim, Y., and Park, C., “ Multidisciplinary Aerodynamic-Structural Design Optimization of Supersonic Fighter Wing Using Response Surface Methodology,” AIAA Paper 2002-0322, Jan. 2002.

[38] Kim, Y., Lee, D.H., Kim, Y., and Yee, K., “Multidisciplinary Design Optimization of Supersonic Fighter Wing Using Response Surface Methodology,” AIAA Paper 2002-5408, Sept. 2002.

[39] Kim, y., **Jeon**, Y., Lee, D., “Multi-objective and Multidisciplinary design optimzation of supersonic fighter wing,” Journal of Aircraft Vol. 43, No. 3, pp.817~824, May-2006

[40] Balling, R. J., and Sobieszczanski-Sobieski, J., “Optimization of Coupled systems: A Critical Overview of Approaches,” AIAA Journal, Vol. 34, No.1, 1996, pp. 6-17.

[41] Sobieszczanski-Sobieski, J., “Optimization by Decomposition: A Step from Hierarchic to Non- Hierarchic Systems,” NASA TM-101494, NASA CP-3031, part 1, 1989.

[42] Kroo, I., Altus, S., Braun, R., Gage, P. and Sobieski, I., “Multidisciplinary Optimization Methods for Aircraft Preliminary Design.” AIAA Paper 94-4325, Sept. 1994.

[43] Sobieszczanski-Sobieski, J., and Agte, J. S., “Bi-Level Integrated System Synthesis(BLISS),” AIAA Paper 98-4916, Sept. 1998.

[44] Jones, D. R., Perttunen, C. D. and Stuckman, B. E., “Lipschitzian Optimization without the Lipschitz Constant,” *Journal of Optimization Theory and Application*, Vol. 79, No. 1, October 1993, pp. 157-181.

[45] Baker, C. A., Watson, L. T., Grossman, B., Haftka, R. T. and Mason, W. H., “A Study of a Global Design Space Exploration Method for Aerospace Vehicles,” AIAA Paper, AIAA 2000-4763, September 2000.

[46] Sevant, N. E., Bloor, M. I. G. and Wilson, M. J., “Aerodynamic Design of a Flying Wing using Response Surface Methodology,” *Journal of Aircraft*, Vol. 37, No. 4, July-August 2000, pp. 562-569.

[47] Chung, H. and Alonso, J. J., “Comparison of Approximation Models with Merit Functions for Design Optimization,” AIAA Paper, AIAA 2000-4754, September 2000.

[48] Sasena, M. J., Papalambros, P. and Goovaerts, P., “Exploration of Metamodeling Sampling Criteria For Constrained Optimization,” *Engineering Optimization*, Vol. 34, No. 3, 2002, pp. 263-278.

[49] Jeong, S., Murayama, M. and Yamamoto, K., “Efficient Optimization Design Method Using Kriging Model,” *Journal of Aircraft*, Vol. 42, No. 2, March-April 2005, pp. 413-420.

[50] Poirel, D., Dunn, S. and Porter, J., “Flutter-Margin Method Accounting for Modal Parameter Uncertainties,” *Journal of Aircraft*, Vol 42, No. 5, September-October 2005, pp. 1236-1243.

[51] Ahn, J., Kim, S. and Kwon, J., “Reliability-Based Wing Design Optimization Using Trust Region-Sequential Quadratic Programming Framework,” *Journal of Aircraft*, Vol. 42, No. 5, September-October 2005, pp. 1331-1336.

[52] Gao, W., “Reliability-Based Optimization of Active Nonstationary Random Vibration Control,” *AIAA Journal*, Vol. 43, No. 6, June 2005, pp. 1293-1298.

[53] Mullur, A. A. and Messac, A., “Extended Radial Basis Functions: More Flexible and Effective Metamodeling,” *AIAA Journal*, Vol. 43, No. 6, June 2005, pp. 1306-1315.

[54] McCormick, D. J. and Olds, J. R., "Approximation of Probabilistic Distributions Using Selected Discrete Simulations," AIAA Paper, AIAA 2000-4863, September 2000.

[55] Cao, Y., Hussaini, M. Y. and Zang, T. A., "Exploitation of Sensitivity Derivatives for Improving Sampling Methods," *AIAA Journal*, Vol. 42, No. 4, April 2004, pp. 815-822.

[56] Y. Jeon, E. Park, Y. Kim, S. Jun, Y. Ku and D. Lee, Feasibility Improvement of the Design Space Using Probabilistic Method, *42th AIAA Aerospace Sciences Meeting and Exhibit*, 2004, AIAA-2004-0537.

[57] K. Lee, Y. Jeon, K. Kim, D. Lee and K. Lee, Three-Dimensional Micro Propeller Design by Using Efficient Two Step Optimization, *Journal of Fluid Science and Technology*, Vol. 2, No. 2, pp. 334~345, 2007.

[58] Y. Jeon, S. Jun, S. Hong, K. Park, S. Kang and D. Lee, Design Space Exploration and Modification with Reliability Index, *Proceedings of the 2009 KSAS Spring Conference*, pp.543~ 546, April, 2009, KSAS09-1418.

[59] Hirsch, C., Numerical Computation of Internal and External Flows, John Wiley & Sons, New York, 1988.

[60] Anderson, W., Thomas, J. and Van Leer, B., "Comparison of Finite Volume Flux Vector Splittings for the Euler Equations," AIAA Journal, Vol. 12, No. 9, 1986, pp1453-1460.

[61] Roe, P. L., "Approximate Riemann Solvers, Parameter Vectors and Difference Scheme," *Journal of Computational Physics*, Vol. 43, 1981, pp.357-372.

[62] Anderson, W. and Thomas, J., "Comparison of Finite Volume Flux Vector Splitting for the Euler Equations," *AIAA Journal*, Vol. 24, No. 9, 1986, pp.1453-1460.

[63] K., “High Resolution TVD Schemes using Flux Limiters”, *Lectures in Applied Mathematics*, Vol. 22, 1985, pp.289-309.

[64] Jameson, A. and Yoon, S., “Multigrid Solution of the Euler Equations Using Implicit Schemes,” *AIAA Journal*, Vol. 24, No. 11, 1986, pp. 1737-1743.

[65] Jameson, A. and Yoon, S., “Lower-Upper Implicit Schemes with Multiple Grids for the Euler Equations,” *AIAA Journal*, Vol. 25, No. 11, 1987, pp. 929-935.

[66] Turkel, E., Swanson, R. C., Vasta, V. N. and White, J. A., “Multigrid for Hypersonic Viscous Tow- and Three-Dimensional Flows,” AIAA Paper, AIAA 91-1572-CP.

[67] Schmitt, V. and Charpin, F., “Pressure Distribution on the ONERA M6 Wing at Transonic Mach Numbers,” AGARD-AR-138, 1979.

[68] Cook, R. D., Malkus, D. S., and Plesha, M. E., *Concepts and applications of Finite Element Analysis*, 3rd edition, John Wiley & Sons, New York.

[69] Simo, J. C., Fox, D. D. and Rifai, M. S., “On a Stress Resultant Geometrically Exact Shell Model. Part II: The Linear Theory; Computational Aspects,” Computer Methods in Applied Mechanics and Engineering, Cpl. 73, Issue 1, April 1989, pp. 53-92.

[70] Chapra, S. C., Canale, R. P., *Numerical Methods for Engineers*, McGraw-Hill, International editions.

[71] S. Yoon, *Multidisciplinary Optimal Design of a Transport Wing Configuration*, Master Thesis, Seoul National University, Seoul, Republic of Korea, Feb. 1998.

[72] S. Yoon, J. Ahn, and D. Lee, Multidisciplinary Optimal Design of a Transport Wing Configuration, *KSAS journal*, Vol. 27, No. 6, 1999, pp. 128 ~ 138.

[73] Myers, R. H., and Montgomery, D. C., Response Surface Methodology: Process and Product Optimization Using Designed Experiments, John Wiley & Sons, New York, 1995.

[74] M.T. Hagan, H.B. Demuth and M.H. Beale, Neural Network Design, PWS Publishing Company, 1996.

[75] Ang, A. H.-S., Tang, W. H.,, Volume I John Wiley & Sons, Inc., New York, NY, 19Probability Concepts in Engineering Planning and Design84.

초 록

본 연구에서는 확률 통계적 기법을 이용한 설계 공간의 탐색과 재설정에 관한 연구를 수행하였다. 설계 공간의 가용성을 효율적으로 계산하기 위해 근사 모델과 몬테카를로 시뮬레이션 기법을 적용하였다. 제시된 기법을 이용하여 설계 공간의 확률 밀도 함수와 누적 분포 함수, 신뢰성 지수 등의 확률 통계적 수치 값들을 효율적으로 계산하고 설계 성공 확률을 확인하였다. 계산된 설계 공간의 확률 통계적 특성 값들을 기반으로, Chebyshev 부등식과 신뢰성 지수를 이용하여 좀 더 넓은 가용 영역을 포함하는 설계 공간으로의 자동 재설정을 수행하였다.

먼저, 제안된 기법의 검증을 위하여 대수식으로 구성된 엄밀 함수에 대한 설계 공간의 탐색과 재설정을 수행하여 유용성을 검증하였다. 두 가지의 엄밀 함수에 대해 단일 단계 최적화 기법인 다분야 만족 기법 (multi-disciplinary feasible, MDF) 과 다단계 최적화 기법인 협동 최적화(collaborative optimization, CO) 로 정식화를 수행하여 다양한 다분야 통합 최적화 기법에 대한 유용성을 검증하였다. 그 결과로 수렴된 설계 공간은 초기 설계 공간의 외부에 놓여져 포함되지 않았던 가용 영역을 포함한 공간으로 자동 재설정 되었다. 이러한 결과를 바탕으로 제안된 기법을 대표적인 다분야 통합 최적설계 문제인 공력과 구조, 성능 분야를 함께 고려하는 항공기 날개의 다분야 통합 최적화 문제에 적용하였으며, 단일 단계 최적화와 더불어 대표적인 다단계 최적화

기법인 협동 최적화 기법도 적용하였다. 또한, 초기 설계 공간과 수렴된 설계 공간 각각에서의 최적화를 개별적으로 수행하여 그 값들을 비교하여 수렴된 설계 공간의 가용성과 최적해가 초기 설계 공간의 값보다 향상된 값을 지니고 있음을 확인하였다.

이러한 결과를 통해서, 본 논문에서 제시된 확률 통계적 기법을 이용한 설계 공간의 탐색 및 재설정 기법은 다양한 다분야 통합 최적설계 문제에 적용함에 있어 초기 설계 공간에서 제외된 가용 영역까지도 포함한 가용성이 높은 영역으로 설계 공간을 효율적으로 탐색하고 자동적으로 재설정 할 수 있으며, 보다 향상된 최적해를 수렴된 설계 공간에서 도출할 수 있음을 확인하였다.

Key Words : 공력-구조 다분야간 최적 설계, 항공기 날개, Chebyshev 부등 조건, 협동 최적화, 설계 공간 탐색, 설계 공간 재설정, 몬테카를로 시뮬레이션, 신뢰성 지수

학 번 : 2001-30442

성 명 : 전 용 희

감사의 글

오랜 대학원 생활을 마감하며 여러 은사님과 지인들께 감사의 인사를 드립니다. 돌아보면 많은 아쉬움이 남아 있지만 여러 고마운 분들과 함께 할 수 있어서 행복하고 소중한 시간들이 더 많았던 시간이었습니다.

세상의 어느 누구보다도 저를 믿어주시고, 묵묵히 바라봐 주신 부모님께 가장 먼저 감사의 말씀을 올립니다. 부모님의 사랑이 여러모로 부족한 제게는 가장 큰 힘이었음을 이 자리를 빌어 다시 한번 감사 드립니다.

부족하기만 한 제자에게 사랑과 관심으로 지도해 주신 이동호 교수님께 무한한 감사의 말씀을 드립니다. 언제, 어느 곳에서도 교수님의 가르침과 기대에 부응하는 제자가 되겠습니다. 또한 바쁘신 와중에도 박사 학위 심사 위원장을 맡아 주신 이수갑 교수님과 논문 심사에 참여하여 많은 고견과 조언으로 도움을 주신 김종암 교수님, 최동훈 교수님, 이도형 교수님께도 심심한 감사의 말씀을 드립니다. 교수님들의 지도 편달과 조언으로 논문을 잘 마무리 할 수 있었습니다. 또한 여러 일들로 경황없으신 와중에도 기회가 닿을 때 마다 학업과 인생에 대해 항상 고마우신 말씀과 관심으로 격려해주시고 이끌어주신 김규홍 교수님과 유영상 교수님께도 깊은 감사를 드립니다.

연구실에 들어와 여러 가지로 낯설고 미숙했던 제게 연구실의 여러 선후배 동료들과의 생활은 가장 큰 생활의 활력소였으며, 수많은 추억과 좋은 기억들을 가져다 주었습니다. 학문에서나 인생의

선배로서 친절한 도움과 조언을 아끼지 않으셨던 이관중 교수님과 황재호 박사님, 이보성 박사님, 김유신 박사님, 권혁빈 박사님께 감사 드립니다. 연구실 생활의 시작과 함께 부대끼며 동고동락 했던 기학이와 완돈이, 태윤이, 그리고 인생의 선배로써 많은 이야기를 해주신 박용진 소령님과 노주현 박사님께 고마운 마음을 전합니다. 선후배를 떠나 오랜 연구실 생활에서 항상 힘이 되어준 상욱이와 수환이, 상훈이, 형민, 지훈, 상원, 민호, 경현, 승온에게도 고맙다는 말을 전합니다. 그리고 연구실의 맏언니 정화와 막내 선이, 훈일이와 세일이, 준호에게도 감사의 마음을 전하며 좋은 논문과 결과가 있기를 기원합니다. 이 외에도 함께 연구실 생활을 했던 여러 선후배님들께도 감사의 마음을 전합니다. 여러분들의 도움과 지지가 연구실 생활에 큰 힘이 되었습니다.

또한, 연구실 외의 많은 친구들과 지인들의 성원도 큰 힘이 되었습니다. 일일이 감사의 인사를 전해야 하지만 여의치 못하여 마음속으로 감사의 인사를 대신합니다.

저에게 한결 같은 믿음과 지지를 아끼지 않으신 형님과 형수님을 비롯한 가족들과 처가 가족들께도 진심으로 감사 드립니다.

마지막으로 가장 가까이에서 사랑과 믿음으로 언제나 함께 하며 격려해준 사랑하는 아내 연희와 아들 준후에게 고맙고 사랑한다는 말을 전하며 이 논문을 바칩니다.

2012 년 7 월 27 일

전 용 희 드림